

Graphene-based polymer nanocomposites

Citation for published version (APA):

Tkalya, E. (2012). *Graphene-based polymer nanocomposites*. [Phd Thesis 1 (Research TU/e / Graduation TU/e), Chemical Engineering and Chemistry]. Technische Universiteit Eindhoven.
<https://doi.org/10.6100/IR724486>

DOI:

[10.6100/IR724486](https://doi.org/10.6100/IR724486)

Document status and date:

Published: 01/01/2012

Document Version:

Publisher's PDF, also known as Version of Record (includes final page, issue and volume numbers)

Please check the document version of this publication:

- A submitted manuscript is the version of the article upon submission and before peer-review. There can be important differences between the submitted version and the official published version of record. People interested in the research are advised to contact the author for the final version of the publication, or visit the DOI to the publisher's website.
- The final author version and the galley proof are versions of the publication after peer review.
- The final published version features the final layout of the paper including the volume, issue and page numbers.

[Link to publication](#)

General rights

Copyright and moral rights for the publications made accessible in the public portal are retained by the authors and/or other copyright owners and it is a condition of accessing publications that users recognise and abide by the legal requirements associated with these rights.

- Users may download and print one copy of any publication from the public portal for the purpose of private study or research.
- You may not further distribute the material or use it for any profit-making activity or commercial gain
- You may freely distribute the URL identifying the publication in the public portal.

If the publication is distributed under the terms of Article 25fa of the Dutch Copyright Act, indicated by the "Taverne" license above, please follow below link for the End User Agreement:

www.tue.nl/taverne

Take down policy

If you believe that this document breaches copyright please contact us at:

openaccess@tue.nl

providing details and we will investigate your claim.

Graphene-based polymer nanocomposites

PROEFSCHRIFT

ter verkrijging van de graad van doctor aan de
Technische Universiteit Eindhoven, op gezag van de
rector magnificus, prof.dr.ir. C.J. van Duijn, voor een
commissie aangewezen door het College voor
Promoties in het openbaar te verdedigen
op maandag 6 februari 2012 om 16.00 uur

door

Evgeniy Tkalya

geboren te Podolsk, Rusland

Dit proefschrift is goedgekeurd door de promotor:

prof.dr. C.E. Koning

Graphene-based polymer nanocomposites

By Evgeniy Tkalya

Technische Universiteit Eindhoven, 2012.

A catalogue number is available from the Eindhoven University of Technology library.

ISBN: 978-90-386-3082-3

Copyright © 2012, Evgeniy Tkalya

The research results described in this thesis form part of the research program of the Dutch Polymer Institute (DPI, PO Box 902, 5600 AX Eindhoven), project #648.

Cover design: Evgeniy Tkalya.

Printed by Printyourthesis.com

Contents

1. General introduction.....	1
1.1. Polymeric Composites	2
1.2. Graphene	3
1.2.1. Types of graphene edges.....	5
1.2.2. Graphene structural defects.....	6
1.3. Methods of Graphene preparation	9
1.3.1. Mechanical exfoliation.	9
1.3.2. Chemical vapor deposition	10
1.3.3. Epitaxial growth	13
1.3.4. Oxidation and reduction.....	15
1.3.5. Liquid-phase exfoliation of graphite.....	18
1.3.6. Graphite intercalation compounds	20
1.4. Characterization of graphene	21
1.5. Graphene/polymer nanocomposites	22
1.5.1. Solvent processing.....	23
1.5.2. <i>In-situ</i> process.....	24
1.5.3. Melt processing	25
1.6. Outline of the thesis	27
1.7. References	28
2. Latex-based concept for the preparation of graphene-based polymer nanocomposites.....	35
2.1. Introduction.....	36
2.2. Results and discussion	36
2.2.1. Preparation of graphite oxide	36
2.2.2. Reduction of graphite oxide	37
2.2.3. Graphene/polystyrene nanocomposites.....	39

2.3. Conclusions.....	44
2.4. Experimental.....	45
2.5. References.....	48
3. The use of surfactants for dispersing carbon nanotubes and graphene to make conductive nanocomposites.....	49
3.1. Introduction.....	50
3.2. Mechanism of stabilization.....	51
3.3. Dispersion of Graphene/CNTs in polymer matrix using water-based systems	54
3.3.1. Surfactants.....	54
3.3.2. Composites.....	55
3.3.3. Thin transparent films.....	60
3.4. Dispersion of Graphene/CNTs in a polymer matrix using organic solvents	61
3.4.1. Surfactants.....	61
3.4.2. Composites.....	62
3.5. Conclusions and outlook.....	63
3.6. References.....	64
4. Experimental and theoretical study of the influence of the state of dispersion of graphene on the percolation threshold of conductive graphene/polystyrene nanocomposites.....	69
4.1. Introduction.....	70
4.2. Results and discussion.....	70
4.2.1. Characterization of the nanofiller and its dispersions.....	70
4.2.2. Nanocomposites characteristics.....	75
4.2.3. Theoretical predictions.....	77
4.3. Conclusions.....	81
4.4. Experimental.....	82
4.5. References.....	84

5. Dependence of percolation threshold of graphene/polymer nanocomposites on surfactant used for graphene dispersion in the aqueous state of the latex concept.	87
5.1. Introduction.....	88
5.2. Results and discussion.	89
5.2.1. Optimization of the graphene exfoliation conditions.	89
5.2.2. Composite conductivities	94
5.2.3. Lowering percolation threshold using PEDOT:PSS as surfactant	97
5.3. Conclusions.....	107
5.4. Experimental.....	108
5.5. References	110
6. Conductive cellulose-based polymer nanocomposites	113
6.1. Introduction.....	114
6.2. Results and discussion	115
6.2.1. MWCNTs- and cellulose whiskers-based polymer composites.....	116
6.3. Conclusions.....	130
6.4. Experimental.....	131
6.5. References	133
7. Technology assessment	135
7.1. Highlights and industrial application	136
7.2. Summarizing and outlook.....	142
7.3. References	143
8. Summary	145
9. Acknowledgements.....	148
10. List of Publications	151
11. Curriculum Vitae	152

Glossary

AFM	Atomic Force Microscopy
C-AFM	Conductive Atomic Force Microscopy
CMC	Critical micelle concentration
CMG	Chemically modified graphene
CNT	Carbon nanotube
CTAB	Cetyltrimethyl ammoniumbromide
CVD	Chemical vapor deposition
DGU	Density gradient ultracentrifugation
DMA	N,N-Dimethylacetamide
DMAc	Dimethylacetamide
DMEU	1,3-dimethyl-2-imidazolidinone
DMF	N,N-dimethylformamide
DOC	Sodium deoxycholate
EG	Expanded graphite
EMI	Electromagnetic interference
FGIC	Fluorinated graphite intercalation compounds
GA	Gum Arabic
GIC	Graphite intercalation compounds
GO	Graphite oxide
IGEPAL	Polyoxyethylene(40) nonylphenyl ether
ITO	Indium tin oxide
LDS	Lithium dodecyl sulfate
LEEM	Low-energy electron microscopy
MMA	Methyl methacrylate
MWCNT	Multi-walled carbon nanotube
MWD	Molecular weight distribution
NMP	N-Methylpyrrolidone
PA	Polyamide
PANI	Polyaniline
PDMS	Polydimethylsiloxane

PEDOT	Poly(3,4-ethylenedioxythiophene)
PEO	Poly(ethylene oxide)
PET	Polyethylene terephthalate
PMMA	Poly(methyl methacrylate)
PP	Polypropylene
PS	Polystyrene
PSS	Poly(sodium 4-styrene sulphonate)
PVAc	Poly(vinyl acetate)
PVDF	Poly(vinylidene fluoride)
SAN	Poly(styrene-co-acrylonitrile)
SC	Sodium Cholate
SDBS	Sodium dodecylbenzenesulfonate
SDS	Sodium dodecyl sulfate
STM	Scanning Tunneling Microscopy
SWCNT	Single-walled carbon nanotube
TDOC	Sodium taurodeoxycholate
TEM	Transmission Electron Microscopy
TPU	Thermoplastic polyurethane
TRGO	Thermally reduced graphene oxide
Triton X-100	Polyethylene glycol p-(1,1,3,3-tetramethylbutyl)-phenyl ether
TTAB	Tetradecyl trimethyl ammonium bromide
Tween-20	Polyoxyethylene (20) sorbitan monolaurate
Tween-80	Polyoxyethylene (20) sorbitan monooleate
UV-Vis	Ultra-violet visible light
XPS	X-ray photoelectron spectroscopy

Chapter 1

General introduction

ABSTRACT: The chapter gives general information about graphene, namely its structure, properties and methods of preparation, and highlights the methods for the preparation of graphene-based polymer nanocomposites.

1.1. Polymeric Composites

The main reason for the rapid development of polymer composite materials is that the traditional "pure" polymers have largely played out their performance capabilities whereas technology requires materials with new properties and advances. There are a number of advantages polymeric composites have over traditional materials (metals, ceramics, wood, "pure" polymers etc.):

- a unique combination of properties, not typical for other individual materials (strength, strain, thermal, rheological, adhesive, electrical, friction, heat transfer, and other properties);
- the ability to control composites properties by simply changing the composition and preparation conditions. Typically, composite materials are not "champions" with respect to separately considered properties. But with respect to the combination of certain properties they have no equal. By definition composite materials are made by blending two or more chemically dissimilar components with a clear boundary between them. In its structure a composite material can be composed of several phases: a continuous phase (matrix) and one or more dispersed phases, or of two or more (co)continuous phases with possible dispersed phases in each of the continuous phases. Composite material with a continuous phase made of a polymer is called a polymer composite material. In composite materials the dispersion medium (continuous phase) is called the matrix, and the dispersed phase is called the dispersed or filler material.

The main types of polymer composites are:

- Polymers that contain any solid particles or fibers;
- Polymer blends;
- Polymers containing liquid in the form of fillers or plasticizers;
- Polymers containing gas as a filler;^[1]

A nanocomposite is defined as a composite material where at least one of the dimensions of one of its constituents is on the nanometre size scale. Nanocomposites are found in nature, for example in the structure of the abalone shell and bone.^[2] The use of nanoparticle-rich materials long predates the understanding of the physical and chemical nature of these materials. Jose-Yacaman *et al.* investigated the origin of the depth of color and the resistance to acids and bio-corrosion of Maya blue paint, attributing it to a nanoparticle mechanism.^[3] From the mid 1950s nanoscale organo-clays have been used to control flow of polymer solutions (e.g. as paint viscosifiers) or the constitution of gels (e.g. as a thickening substance in cosmetics, keeping the preparations in a homogeneous form).^[2] By the 1970s polymer/clay composites were the topic of textbooks, although the term "nanocomposites" was not in common use. In mechanical terms, nanocomposites differ from

conventional composite materials due to the exceptionally high surface to volume ratio of the reinforcing phase and/or its exceptionally high aspect ratio.^[2] Polymer nanocomposites exhibit substantial property enhancements at much lower filler loadings than polymer composites with conventional micron-scale fillers such as carbon fibers or glass, which can result in a much lower component weight and can simplify processing. A big breakthrough in the field came with the discovery of fullerene or carbon black in 1985, the third carbon allotrope in addition to graphite and diamond.

Another breakthrough came a few years later, in 1991, when Iijima discovered carbon nanotubes (CNT). Almost immediately polymer/CNT nanocomposites attracted considerable attention owing to their unique multi-functional properties such as exceptional mechanical, thermal and electrical properties. A large part of the CNT/polymer based composites exploit CNTs as a conductive filler dispersed into an insulating matrix. Applications range from electronics to aerospace sectors, such as electrostatic dissipation, electromagnetic interference (EMI) shielding, multilayer printed circuits, and transparent conductive coatings.^[4]

1.2. Graphene

Graphene is the name given to a flat monolayer of carbon atoms tightly packed into a two-dimensional (2D) honeycomb lattice, and is a basic building block for graphitic materials of all other dimensionalities (**Figure 1**).

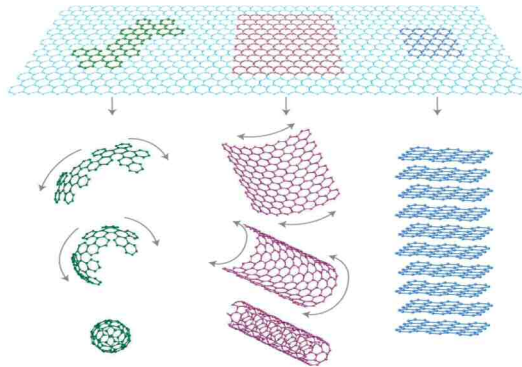


Figure 1. Graphene is a 2D building material for carbon materials of all other dimensionalities. It can be wrapped up into 0D buckyballs, rolled into 1D nanotubes or stacked into 3D graphite.^[5] (Reprinted by permission from Macmillan Publishers Ltd from ref. 5. Copyright 2007)

It can be wrapped up into 0D fullerenes, rolled into 1D nanotubes or stacked into 3D graphite.^[5] Until its discovery it was argued that 2D crystals were thermodynamically unstable and could not exist.^[6,7] The theory of Landau and Peierls stated that thermal fluctuations in low-dimensional crystal lattices should lead to such displacements of atoms that they become comparable to interatomic distances at any finite temperature.^[5] The argument was later supported by experimental observations which demonstrated that the melting point of thin films drops down dramatically with decreasing thickness of the material, and subsequently films become unstable at thicknesses of a few tens of atomic layers. Due to this fact atomically thick monolayers for many years were assumed to exist just as integral parts of 3D structures. Without 3D support 2D structures were supposed not to exist, until 2004, when the common wisdom was flaunted by the experimental discovery of graphene as well as other free-standing 2D atomic crystals, for example, single-layer boron nitride.^[8]

In 2007 Meyer's studies using transmission electron microscopy revealed that suspended graphene sheets are not perfectly flat: they exhibit an intrinsic microscopic roughening such that the surface normal varies by several degrees along the sheet and out-of-plane deformations reach 1 nm (**Figure 2**).^[9]

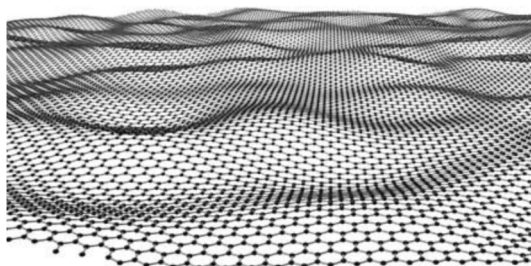


Figure 2. Geometry of graphene platelets.^[9] (Reprinted by permission from Macmillan Publishers Ltd from ref. 9. Copyright 2007)

A graphene single-layer is the strongest material ever measured, exhibiting a Young's modulus of 1 TPa and ultimate strength of 130 GPa.^[10] It has a thermal conductivity of 5000 W/(m³ K), which is more than twice the value of graphite (≈ 2000 W/(m³ K)) and comparable with the upper bound of the highest values reported for SWCNT bundles.^[11] An electrical conductivity of up to 6000 S/cm has been reported for a single graphene layer.^[12] These properties in addition to an extremely high surface area (theoretical limit: 2630 m²/g) and gas impermeability indicate graphene's great potential for improving mechanical, electrical, thermal, and gas barrier properties of polymers.^[13]

The implementation of the huge potential of applications that graphene has, can only become reality if the development of simple and relatively inexpensive methods of producing these material in macroscopic quantities with the desired characteristics is achieved. For several years since the opening of the first method of isolating of graphene based on the mechanical cleavage of graphite layers the efforts of many research groups have been focused on the development of more effective approaches to solve this problem and to design new technological approaches for the isolation and purification of graphene.

1.2.1. Types of graphene edges

Infinite defects-free graphene sheets do not differ from each other. The real graphene platelets differ one from another not only in size but also in the boundaries structure. These differences significantly affect the characteristics of graphene and in particular its electronic properties, meaning it can exhibit either quasi-metallic or semiconducting behavior, depending on the atomic structure of their edges. Cutting a graphene sheet along a straight line produces two typical kinds of peripheral shapes called armchair and zigzag, depending on the axial directions of 30° difference.^[14] There are also intermediate structures for which the angle of chirality is in the range between the specified values.

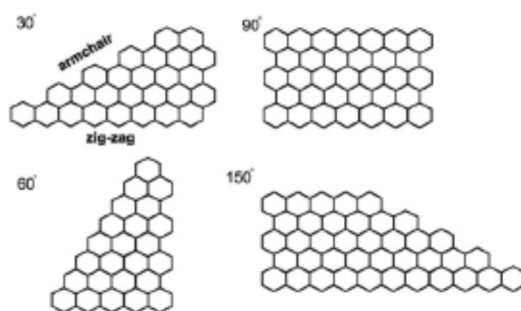


Figure 3. Different types of edges that can be formed by cutting the graphene plane at different angles.^[15] (Reprinted with permission from ref. 15. Copyright 2009 American Chemical Society)

This property of graphene is illustrated in **Figure 3** which shows fragments of graphene samples with different structures of the edges. Raman spectroscopy and Scanning Tunneling Microscopy (STM) can be used to study the quality of the edges in graphene.^[15, 16]

1.2.2. Graphene structural defects

Usually depending on production method and environment conditions the graphene surface possesses structural defects which can affect its electrical, mechanical and transport properties to a large extent. The unique property of graphene is that it can adjust structural lattice defects in reconstructed arrangements. Such a property is not known for any other material. Several experimental studies have demonstrated the occurrence of either native or physically introduced defects in graphene. Transmission electron microscopy (TEM) and STM have been used to obtain images of defective graphene with atomic resolution.^[17, 18] The interpretation of the experimental results was simplified by the fact that the theory of defects in graphene had already been developed to some extent in the context of carbon nanotubes and graphite.^[19-27] Defects can migrate from one place to another which can significantly influence the properties of a defect crystal. The mobility of graphene defects can be immeasurably low or immeasurably high. The migration is governed by an activation barrier which depends on the defect type.^[19]

The most essential types of the structural defects in graphene are: Stone-Wales (SW) defect, single vacancy, multiple vacancy, and adatoms.

Stone-Wales defect occurs when four hexagons are transformed into two pentagons and two heptagons [SW(55-77) defect] by rotating one of the C-C bonds by 90° (**Figure 4**).

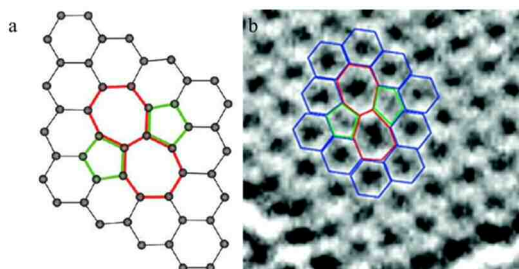


Figure 4. Schematic (a) and experimental (b) TEM images of Stone-Wales defect.^[17] (Reprinted with permission from ref. 17. Copyright 2008 American Chemical Society)

The SW(55-77) defect has a formation energy $E_f \approx 5$ eV.^[28, 29] The high formation energy of the SW defect indicates a negligible equilibrium concentration, at least at typical experimental temperatures below 1000 °C. However, once the defect is formed under nonequilibrium conditions (*e.g.*, rapid quenching from high temperature or under irradiation), the 5 eV barrier for the reverse transformation should warrant its stability at room temperature.^[19] A single vacancy defect corresponds to the

absence of one carbon atom in a hexagonal graphene lattice (**Figure 5**). This defect leads to the saturation of two out of three dangling bonds next to the missing atom, whereas one dangling bond remains because of geometrical reasons. The single vacancy defect has a formation energy $E_f \approx 5$ eV. The migration energy of the defect is about 1.3 eV which allows migration at 100-200 °C. The reconstruction behavior, which is influenced by defect migration, has been experimentally studied for nanotubes whose structure is related to graphene. It was shown that nanotubes reconstruct in-situ under electron irradiation at 200-300 °C remaining the atomic lattice coherent.^[30, 31] When the electron energy is significantly higher than the displacement energy of carbon atom in graphene, irradiation with electrons or ions at room temperature leads to defects formation resulting in holes and amorphization.^[19]

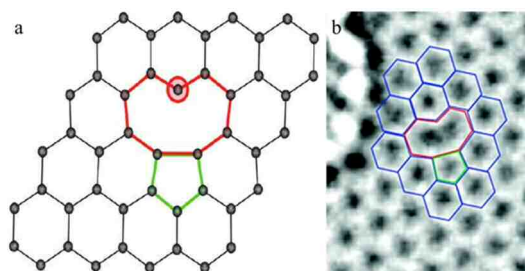


Figure 5. Schematic (a) and experimental (b) TEM images of single vacancy defect.^[17] (Reprinted with permission from ref. 17. Copyright 2008 American Chemical Society)

Multiple vacancies can be created either by removing a few neighboring atoms or by coalescence of two or more single vacancies defects. An even number of missing carbon atoms allows a complete reconstruction, meaning a complete saturation of dangling bonds, whereas an odd number of missing carbon atoms remains an open bond. Therefore structural defects with an even number of vacancies are energetically more favorable over defects with an odd number of vacancies.^[21]

The energetically favored position of the interstitial atoms is the bridge configuration where a new carbon (so-called adatom) atom is located on top of a carbon-carbon bond (**Figure 6**). When interacting with a graphene lattice, the guest carbon atom changes the hybridization of carbon atoms in the layer. In addition to the bridge position, other metastable configurations like the dumbbell configuration can occur.^[32] When two migrating adatoms meet each other and form a dimer, they can be incorporated into the graphene lattice.^[19]

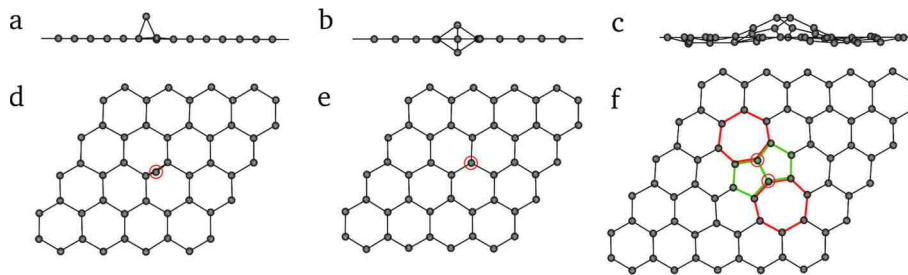


Figure 6. Carbon adatoms: (a, d) single adatom in the bridge; (b, e) single adatom in the dumbbell configuration; (c, f) dimer of two close adatoms.^[19] (Reprinted with permission from ref. 19. Copyright 2011 American Chemical Society)

When a foreign atom incorporates into a graphene network various configurations such as on top of a carbon atom, on top of the center of a hexagon, or in the bridge position, are possible.

One of the most occurred types of defects are edge defects in graphene. As said above, the simplest edge structures are the armchair and the zigzag orientation. They can reconstruct. One of the simplest examples of an edge defect is the removal of one carbon atom from a zigzag edge. This results in one pentagon in the middle of a row of hexagons at the edge. Other edge reconstructions can lead to different combinations of pentagons and heptagons at the edge.^[19, 33]

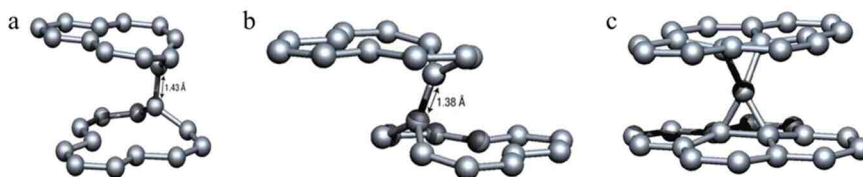


Figure 7. Interlayer defect structures in a graphene bilayer: (a,b) interlayer double vacancy with different bond length; (d) the 4-fold coordinated bridge atom.^[34] (Reprinted by permission from Macmillan Publishers Ltd from ref. 34. Copyright 2003)

Defects between neighboring graphene single layers, for instance in a bilayer, are also quite important. Although defects can exist in both layers independently, it was found that interstitial atoms when located between two graphene layers tend to form crosslinks between the atomic layers.^[34, 35] Some of such defect configurations are shown in **Figure 7**.

1.3. Methods of Graphene preparation

1.3.1. Mechanical exfoliation.

In 2004 Novoselov and Geim reported separated single graphene layer obtained by mechanical cleavage of graphite. 5 μm -deep mesas on top of the highly-oriented graphite platelets were prepared by dry etching followed by pressing against photoresist spun over glass substrate. After attaching to the photoresist layer the mesas were cleaved off from the rest of graphite surface. Then using scotch tape graphite was pilled off from the mesas following by releasing flakes left in the photoresist in acetone. Si wafer was dipped in the solution to capture the graphene flakes.^[36] Mechanical cleavage allows to obtain 10 μm wide and 100 μm long single graphene layers possessing a regular structure. The main problem of this method of graphene sheets production is their identification. Micromechanical cleavage results in a significant amount of fragments which are graphene flakes containing a number of layers, from one to hundreds. The share of single layer samples in this conglomerate is relatively small, so that the main difficulty of this method of synthesis is associated with the detection of a single layer of graphene.

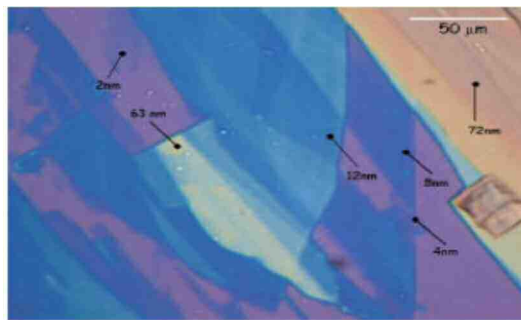


Figure 8. Optical photo in white light of graphitic films of various thickness.^[36] (From ref. 36. Reprinted with permission of the American Association for the Advancement of Science (AAAS))

To identify such objects is very difficult using methods of observation based on scanning probe microscopy which can not determine the number of layers of a multilayer structure. The crucial factor in the considerable progress in obtaining and identifying a graphene single layer was the use of an optical microscope (**Figure 8**). Observations show that a graphene single layer placed on a substrate of silicon, coated with a thin layer of SiO_2 , creates an interference pattern, which is the clear evidence

for the existence of graphene. The ability to obtain such a picture is very sensitive to the thickness of the SiO₂ layer and to the purity of its surface. To illustrate this, the use of a substrate with an oxide layer thickness of 315 nm instead of 300 led to complete disappearance of the interference pattern.^[5, 8, 36]

1.3.2. Chemical vapor deposition

The method of chemical vapor deposition (CVD) is widely used for the synthesis of carbon nanostructures. For example, since 1970s this method has been effectively used for producing carbon filaments which are the basis of a composite material with outstanding mechanical properties.^[37] The CVD of is one of the most common methods for obtaining CNTs on a macroscopic scale.^[38] It is based on the thermocatalytic decomposition of gaseous hydrocarbons on the surface of some metals which leads to the formation of various carbon nanostructures.^[39] An example of the successful use of CVD for the synthesis of graphene is the work of Kim et al., where the nickel substrate of 300 nm thickness acts as a catalyst.^[40] Thin layers of nickel of thickness less than 300 nm were deposited on SiO₂/Si substrates using an electron-beam evaporator, and the samples were then heated to 1000 °C inside a quartz tube under an argon atmosphere. After flowing the reaction gas mixtures (CH₄:H₂:Ar = 50:65:200 standard cubic centimeters per minute), the samples were rapidly cooled to room temperature. The experiments showed that such a rapid cooling is an important factor preventing the agglomeration of graphene sheets in an undesired multilayer structure and promoting the separation of these sheets from the substrate for further use.

It was found that the average number of graphene layers and the coverage of the substrate are determined by the thickness of the nickel film and the duration of the growth process. Thus, the film synthesized within 7 minutes on a nickel substrate of 300 nm thickness contained predominantly two-layer flakes of graphene. Analysis of images obtained by AFM indicated a bumpy surface structure of the graphene sheets. An aqueous iron (III) chloride (FeCl₃) solution (1 M) was used as an oxidizing etchant to remove the nickel layers. This process allowed to perform the etching of the substrate without additional gassing or precipitation. After a few minutes of such an etching process the graphene film easily separated from the substrate and floated on the surface of the solution. After transfer to the substrate the remaining nickel films were removed using hydrofluoric acid. Also a dry-transfer process of the graphene films can be used. In this method first a polydimethylsiloxane (PDMS) stamp is pressed against the graphene film grown on the nickel substrate. After removal of the nickel substrate by etching using FeCl₃ the graphene film becomes attached to the PDMS

substrate. By varying the shape of the nickel substrate graphene films of different sizes and shapes can be prepared and transferred to an arbitrary substrate (**Figure 9**).

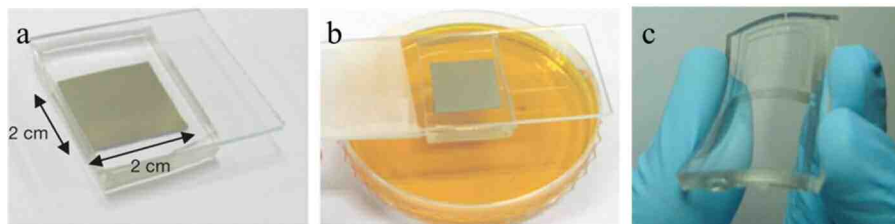


Figure 9. (a) and (b) The dry-transfer method based on a PDMS stamp. After attaching the PDMS substrate to the graphene (a), the underlying nickel layer is etched and removed using FeCl_3 solution (b); (c) graphene films on the PDMS substrates.^[40] (Reprinted by permission from Macmillan Publishers Ltd from ref. 40. Copyright 2009)

Further efforts towards improving the CVD method for obtaining graphene sheets resulted in a significant increase in the size of the synthesized samples. For example, Li et al. reported about single-layer graphene sheets with a transverse size of about 1 cm, which is much higher than achieved earlier. In this method graphene was grown on the copper foil of 25 microns thickness at 1000 °C in a stream of methane and hydrogen.^[41] The resulting graphene film of 1 x 1 cm area (**Figure 10**) was investigated using optical, transmission and scanning electron microscopes, as well as by Raman spectroscopy. The results of the measurements showed that the films obtained exhibit usually a continuous structure and contain mostly single-layer graphene, which is sometimes interlaced by two- and three-layered structures. According to the estimations based on Raman measurements, the obtained graphene film is composed of more than 95 % of a single graphene layer. The estimated proportion of double-layered graphene covers 3-4% of the area, so the amount of graphene consisting of more than two layers does not exceed 1%.^[41]

It was found that graphene growth on Cu is self-limited; growth that proceeded for more than 60 min yielded a similar structure to growth runs performed for ~10 min. For growth times much less than 10 min, the Cu surface is not fully covered. The growth of graphene on Cu foils of varying thickness (12.5, 25, and 50 μm) also yielded similar graphene structures with regions of double and triple flakes, but neither discontinuous monolayer graphene for thinner Cu foils nor continuous multilayered graphene for thicker Cu foils, as one could have expected based on the precipitation mechanism. These observations allow to conclude that graphene is growing by a surface-catalyzed process, rather than by a precipitation process, as has been reported by others for Ni.^[40, 42, 43]

Monolayer graphene formation caused by surface segregation or surface adsorption of carbon has also been observed on transition metals such as Ni and Co at elevated temperatures.^[44-46] However, when the metal substrates were cooled down to room temperature, thick graphite films were obtained because of precipitation of excess C from these metals, in which the solubility of C is relatively high.

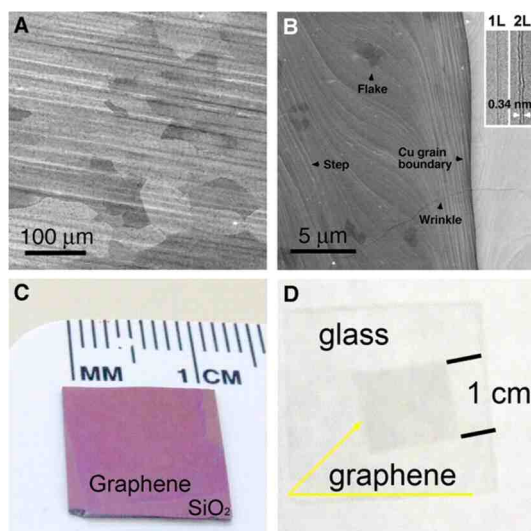


Figure 10. (a) SEM image of graphene on a copper foil with a growth time of 30 min. (b) High-resolution SEM image showing a Cu grain boundary and steps, two- and three-layered graphene flakes, and graphene wrinkles. Inset in (b) shows TEM images of folded graphene edges. 1L, one layer; 2L, two layers. (c and d) Graphene films transferred onto a SiO₂/Si substrate and a glass plate, respectively.^[41] (From ref. 41. Reprinted with permission of the American Association for the Advancement of Science (AAAS))

Bae and coworkers were able to increase the size of the graphene sheet up to 75 cm in the diagonal.^[47] Synthesis of graphene sheets was carried out by CVD in a cylindrical reactor with a diameter of 20 cm. Copper foil of 75 cm in the diagonal used as a substrate was rolled into a cylinder. In order to provide a uniform temperature distribution along the substrate surface a quartz tube of 18.75 cm diameter was inserted inside the foil cylinder. At first the sample was treated with hydrogen for 30 min at 1000 °C and 90 mTorr which resulted in increase of the grains size in the copper foil structure from a few microns to 100 microns, since it was found that the copper foils with larger grain size yield higher-quality graphene films. Graphene synthesis was carried out at the same temperature for 30 minutes by flowing a mixture of CH₄ and H₂ at a 3:1 ratio through the reactor at 460 mTorr followed by rapid cooling in the stream of hydrogen at 90 mTorr to room temperature.

Subsequent separation of the graphene sheet from the copper substrate was carried out in several stages: adhesion of polymer supports (polyethylene terephthalate) to the graphene on the copper foil; etching of the copper layers; release of the graphene layers and transfer onto a target substrate. In the adhesion step, the graphene film, grown on a copper foil, was attached to a thin polymer film coated with an adhesive layer by passing between two rollers. In the subsequent step, the copper layers were removed by electrochemical reaction with aqueous 0.1 M ammonium persulphate solution $(\text{NH}_4)_2\text{S}_2\text{O}_8$.^[48] Finally, the graphene films were transferred from the polymer support onto a target substrate by removing the adhesive force holding the graphene films. When using thermal release, the graphene films were detached from the tapes and released to counter-substrates by thermal treatment (**Figure 11**).^[48-50]

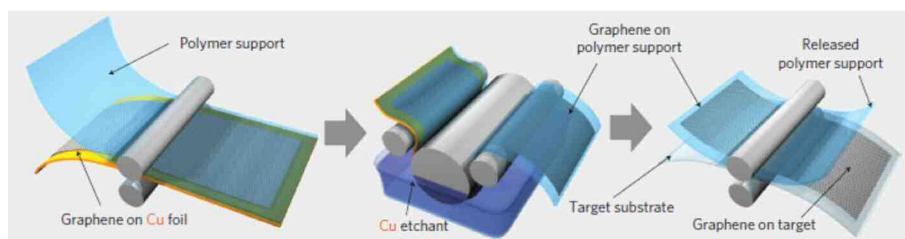


Figure 11. Schematic of the roll-based production of graphene films grown on a copper foil. The process includes adhesion of polymer supports, copper etching (rinsing) and dry transfer-printing on a target substrate.^[47] (Reprinted by permission from Macmillan Publishers Ltd from ref. 47. Copyright 2010)

Raman spectroscopy showed that the obtained graphene films have mostly a single layer structure.

1.3.3. Epitaxial growth

Another effective approach for the synthesis of graphene is based on the thermal decomposition of silicon carbide which results in the epitaxial growth of graphene film on the surface of a SiC crystal.^[5,51-53] The advantage of this approach is that the size of the synthesized sample can be comparable to the size of the original SiC crystal if the crystal is of a good quality. In addition to that, to study the electrical properties of graphene it should be placed on an insulating substrate, hence a considerable advantage of this method is that insulating SiC substrates can be used so that transfer to another insulator is not required in contrast to the situations when the sample is produced on a metallic substrate. However, the large-scale structural quality is limited by the lack of continuity and

uniformity of the grown film.^[54, 55] On the Si-terminated basal plane, vacuum annealing leads to small graphene domains typically 30–100 nm in diameter, whereas on the C-terminated face, larger domains (~200 nm) of multilayered, rotationally disordered graphene can be produced.^[54] The small-grain structure is due to morphological changes of the surface in the course of high-temperature annealing. Moreover, decomposition of SiC is not a self-limiting process and, as a result, regions of different film thicknesses coexist, as was shown by low-energy electron microscopy (LEEM).^[54, 55] Emtsev et al. were able to achieve a significant improvement in the degree of homogeneity of the graphene films obtained by thermal decomposition of silicon carbide.^[53] The starting material used in the experiment was a highly orientated 6H-SiC wafer. Before the thermal treatment leading to the formation of graphene films, the samples were etched in hydrogen at atmospheric pressure and $T = 1550$ °C for 15 min to remove surface polishing damage. Graphene growth was carried out in a vertical cold-wall reactor comprising a double-walled, water-cooled quartz tube and a graphite susceptor in a slow flow of argon. Heating and cooling rates were 2–3 °C per second. The typical annealing time was 15 min. A wide range of annealing temperatures from 1500 to 2000 °C and reactor gas pressures from 10 to 900 mbar were tested. The authors showed that the growth of epitaxial graphene on SiC in an argon atmosphere close to atmospheric pressure provides morphologically superior graphene layers in comparison with vacuum graphitization. The key factor in achieving an improved growth is the significantly higher annealing temperature of 1650 °C that is attainable for graphene formation under argon at a pressure of 900 mbar as compared with 1280 °C in high vacuum. Graphene formation is the result of Si evaporation from the substrate. For a given temperature, the presence of a high pressure of argon leads to a reduced Si evaporation rate because the silicon atoms desorbing from the surface have a finite probability of being reflected back to the surface by collision with Ar atoms. The significantly higher growth temperature thus attained results in an enhancement of surface diffusion such that the restructuring of the surface is completed before graphene is formed. Ultimately, this leads to the markedly improved surface morphology.^[53]

In addition to SiC substrate graphene synthesis by epitaxy on transition metals has also been considered.^[56-61] Sutter and coworkers used ruthenium as a substrate for graphene growth. The authors made use of the temperature-dependent solubility of interstitial carbon in transition metals to achieve the controlled layer-by-layer growth of large graphene domains on Ru. At high temperature, C is absorbed into the Ru bulk. Slow cooling from 1150 °C to 825 °C lowers the interstitial C solubility by a factor of 6, driving significant amounts of C to the surface. The result is an array of lens-shaped islands of macroscopic size (>100 μm) covering the entire Ru substrate.^[56]

1.3.4. Oxidation and reduction

1.3.4.1. Graphene oxide

Since it was first prepared in the nineteenth century, graphite oxide has been mainly produced by the Staudenmaier, Brodie and Hummers methods.^[62-66] All three methods involve oxidation of graphite in the presence of strong acids and oxidants. The level of the oxidation can be varied on the basis of the method applied, the reaction conditions and the precursor graphite used. The structure of graphene oxide has been the subject of theoretical and experimental study. The Lerf-Klinowski model is believed to be the most likely description of GO structure.^[67-82]

Solid-state ¹³C NMR spectroscopy of graphite oxide and recently of ¹³C-labelled graphite oxide favors the model shown in **Figure 12**; the sp²-bonded carbon network of graphite is strongly disrupted and a significant fraction of this carbon network is bonded to hydroxyl groups or participates in epoxide groups.^[62, 71, 72, 81] Minor components of carboxylic or carbonyl groups are thought to populate the edges of the layers in graphite oxide.

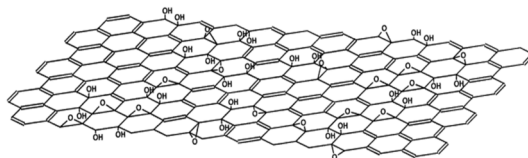


Figure 12. Proposed chemical structure of graphene oxide.^[72] (Reprinted from ref. 72. Copyright 1998 with permission from Elsevier)

Graphite oxide thus consists of a layered structure of graphene oxide sheets that are strongly hydrophilic such that intercalation of water molecules between the layers readily occurs. The inter-layer distance between the graphene oxide sheets increases reversibly from 6 to 10 Å with increasing relative humidity.^[83] Graphite oxide can be completely exfoliated to produce aqueous colloidal suspensions of graphene oxide sheets by simple sonication and by stirring the water/graphite oxide mixture for a sufficiently long time.^[62] The measurement of the surface charge (zeta potential) of graphene oxide sheets shows that they have negative charges when dispersed in water. This suggests that electrostatic repulsion between negatively charged graphene oxide sheets could generate a stable aqueous suspension of them.^[84]

1.3.4.2. Chemical reduction of graphene oxide

Although oxidation of graphene or graphite can generate homogeneous colloidal suspensions, the resulting material is electrically insulating owing to the disruption of the 'graphitic' network. On the other hand, the reduction of the graphene oxide by chemical methods, using reductants such as hydrazine, dimethylhydrazine, hydroquinone and NaBH_4 , has produced electrically conducting material.^[62, 85-91] The reduction of an aqueous graphene oxide suspension by hydrazine has resulted in agglomerated graphene-based nanosheets, and, when dried, in a black powder (**Figure 13**) that is electrically conductive with a powder conductivity $\sim 2 \times 10^2 \text{ S m}^{-1}$. Elemental analysis (atomic C/O ratio, ~ 10) of the reduced graphene oxides revealed the existence of a significant amount of oxygen, indicating that reduced graphene oxide is not the same as pristine graphene. Theoretical calculations of the reduction of graphene oxide (the model used for graphene oxide had the graphene decorated with hydroxyl and epoxide groups) suggest that reduction below 6.25% of the area of the graphene oxide (C/O = 16 in atomic ratio) may be difficult in terms of removing the remaining hydroxyl groups.^[68]

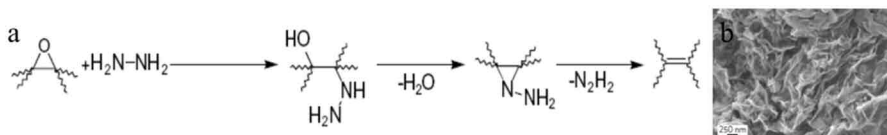


Figure 13. (a) Proposed mechanism for reduction of graphene oxide by hydrazine; (b) A scanning electron microscope image of aggregated graphene oxide sheets chemically reduced with hydrazine monohydrate.^[85] (Reprinted from ref. 85. Copyright 2007 with permission from Elsevier)

Homogeneous colloidal suspensions of electrically conducting reduced graphene oxide have been produced by chemical reduction with dimethyl-hydrazine or hydrazine in the presence of either polymer or surfactant.^[88, 92] The reduction of an aqueous suspension containing a mixture of graphene oxide sheets and poly(sodium 4-styrene sulphonate) (PSS) afforded an aqueous black suspension of reduced graphene oxide sheets coated by the PSS.^[92] The reduction of isocyanate-modified graphene oxide in the presence of polystyrene generated a suspension of reduced graphene oxide sheets in DMF.^[88]

Reduction of sodium dodecylbenzenesulfonate (SDBS)-wrapped graphene oxide with hydrazine and then its chemical modification with aryl diazonium salt produced SDBS-wrapped chemically modified graphene (CMG) that was dispersible in DMF, $\text{N,N}'$ -dimethylacetamide and NMP at

concentrations up to 1 mg/ml.^[86] Colloidal suspensions of modified graphenes decorated with small organic molecules or nanoparticles have also been reported. Xu and coworkers functionalized the reduced graphene oxide sheets using pyrenebutyric acid. The aqueous graphene oxide suspension was reduced using hydrazine in the presence of pyrenebutyric acid, yielding a black aqueous colloidal suspension (0.1 mg/ml) of reduced graphene oxide sheets covered by pyrenebutyric acid. Its paper-like material, prepared by filtration, showed electrical conductivity of 200 S/m.^[93] A suspension at concentration of 0.48 mg/ml of gold-nanoparticle-modified graphene sheets in THF was produced by the reaction of NaBH₄ and octadecylamine-modified graphene oxide followed by the addition of AuCl₄⁻ to the suspension.^[91] The gold nanoparticles (diameter, ~5-11 nm) were anchored to the modified graphene sheets.

A few methods for creating colloidal suspensions of graphene sheets without the help of stabilizers or surfactants have been reported. An aqueous suspension (0.5 mg/ml) of reduced graphene oxide sheets under basic conditions (pH 10) was described by Li and coworkers.^[84] The graphene oxide was reduced by hydrazine, and excess hydrazine was removed by dialysis. It was suggested that shifting the pH to 10 converts neutral carboxylic groups to negatively charged carboxylate groups, so that when the interior of the graphene oxide sheets are reduced by hydrazine, the negatively charged particles do not agglomerate.

1.3.4.3. Thermal reduction of graphene oxide

Thermally reduced graphene oxide (TRGO) can be produced by rapid heating of dry GO under inert gas and at high temperature.^[67, 94-96] Heating GO in an inert environment at 1000 °C for 30 s leads to reduction and exfoliation of GO, producing TRGO sheets. Exfoliation takes place when the pressure, generated by the gas (CO₂) evolved due to the decomposition of the epoxy and hydroxyl sites of GO (see figure 12) exceeds the van der Waals forces holding the graphene oxide sheets together. About 30% weight loss is associated with the decomposition of the oxygen groups and evaporation of water.^[95] The exfoliation leads to a volume expansion of 100-300 times producing very low-bulk-density TRGO. Because of the structural defects caused by the loss of CO₂, these sheets are highly wrinkled as shown in **Figure 14**.^[67]

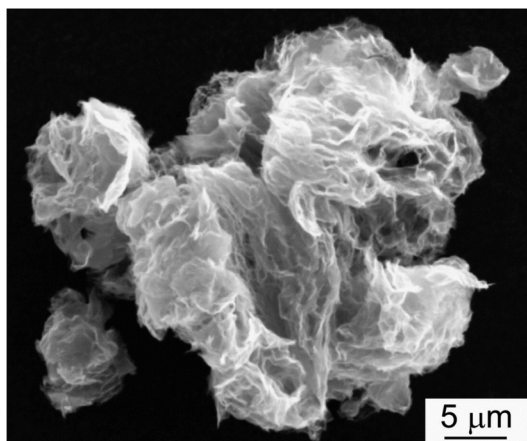


Figure 14. SEM image of dry, as-produced TRGO powder. The sheets are highly agglomerated, and the particles have a fluffy morphology.^[67] (Reprinted with permission from ref. 67. Copyright 2007 American Chemical Society)

80% of the TRGO sheets are single layers with an average size of about 500 nm, independent of the starting GO size.^[95] The advantage of the thermal reduction methods is the ability to produce chemically modified graphene sheets without the need for dispersion in a solvent. TRGO has a C/O ratio of about 10/1 compared to 2/1 for GO.^[13, 67] This ratio has been increased up to 660/1 through heat treatment at higher temperature (1500 °C) or for longer time.^[97] TRGO sheets have a high surface area, 1700 m²/g, as measured in methylene blue and can be well dispersed in organic solvents such as N,N-dimethylformamide (DMF) and tetrahydrofuran. The thermal reduction also leads to restoration of the electrical conductivity with reported electrical conductivity of a compacted film with density 0.3 g/(cm³) ranging between 10 and 20 S/cm, compared to 6000 S/cm for defect-free single graphene sheets.^[13, 94]

1.3.5. Liquid-phase exfoliation of graphite

One of the most efficient ways to exfoliate graphite into individual sheets of graphene is based on the use of surfactants when exfoliating in water or on the use of organic solvents whose surface energy matches the surface energy of graphene when exfoliating in organic media. Such an approach utilizes a layered structure of crystalline graphite, which gives a possibility for the atoms or molecules of different nature to penetrate into the space between the layers. This increases the distance between the layers and thus reduces the interaction energy between them. As a result it opens a way to separate graphite layers by sonication. Such an approach utilizing sonication had

resulted before in sufficient exfoliation of carbon nanotubes bundles in a small number of solvents such as N-Methylpyrrolidone (NMP).^[98-102] Such exfoliation occurs because the strong interaction between solvent and nanotube sidewall means that the energetic penalty for exfoliation and subsequent solvation becomes small.^[103] Coleman and coworkers exfoliated graphite in NMP by a long bath sonication treatment, followed by centrifugation to remove non-exfoliated graphite particles, resulting in a black homogeneous suspension of graphene flakes in the solvent.^[103, 104] This procedure was repeated for three other solvents known to successfully disperse nanotubes: N,N-Dimethylacetamide (DMA), gamma-butyrolactone (GBL) and 1,3-dimethyl-2-imidazolidinone (DMEU).^[103] Characterization of the suspensions revealed the presence of defect- and oxide-free mono- and bilayer graphene flakes as well as multilayer structures.

Since water has a surface energy that is much too high to work on its own as an exfoliant for graphene utilization of surfactants is required. Exfoliation of graphite resulting in thin graphene sheets can occur in water in the presence of surfactants such as sodium dodecylbenzene sulfonate (SDBS) and sodium cholate (SC) under similar conditions as described above for organic solvents.^[105, 106] Green et al exfoliated graphite in SC/water solution applying horn sonication and density gradient ultracentrifugation (DGU) to isolate graphene sheets with controlled thickness.^[107] It resulted in stable graphene dispersions with graphene concentrations of 90 µg/ml. Lotya et al. exfoliated graphite by bath sonication in water/surfactant solution followed by centrifugation, resulting in graphene dispersions in water at concentration up 0.3 mg/ml.^[106] Depending on the sonication and centrifugation time different concentrations of graphene sheets can be obtained. Transmission electron microscopy showed the dispersed phase to consist of small graphitic flakes. More than 40% of these flakes had <5 layers with ~3% of flakes consisting of monolayers. Free-standing films prepared out of graphene/SC dispersions by vacuum filtration exhibit an electrical conductivity of 7000 S/m before annealing which is comparable to films made from reduced graphene oxide. The mean conductivity rises to 17500 S/m after annealing at 500 °C for 2 h under argon/hydrogen atmosphere.

The methods discussed above have been very successful and have led to a number of advances including the preparation of polymer-graphene composites, facile production methods for transparent conductors, and sorting of graphene by layer number. However, these methods still face some problems. For example, when processing graphene from surfactant dispersions, it can be difficult to remove residual surfactant. Alternatively, the best solvents tend to be nonvolatile, causing problems with processing. This can make it difficult to remove solvents when processing graphene into films or

composites.^[108] In particular, it is virtually impossible to deposit individual flakes from solvent-exfoliated graphene, as aggregation tends to occur during the slow solvent evaporation. While graphene dispersions in high boiling point solvents have been transferred into low boiling point solvents by solvent exchange, it would be preferable to have a method which allows direct exfoliation of graphite to give stable dispersions of graphene in low boiling point solvents.^[108, 109] O'Neill and coworkers were able to identify such low boiling point solvents and optimize the dispersion conditions which resulted in stable graphene dispersions obtained in chloroform, acetone and isopropanol. Depending on the preparation conditions, which include low energy bath sonication and centrifugation, dispersions with graphene concentration as high as 0.5 mg/ml can be obtained.^[108]

1.3.6. Graphite intercalation compounds

Many exfoliated graphite fillers are derived from graphite intercalation compounds (GIC) which are compounds of graphite with atoms or molecules of alkali metals or mineral acids intercalated between the carbon layers.^[110-113] The intercalation increases the interlayer spacing of graphite, weakening the interlayer interactions and facilitating the exfoliation of the GIC.^[114] Varying structural arrangements of the intercalant are possible, such as alternating layers of graphene and intercalant (referred to as firststage GICs), as well as multiple (two to five) adjacent graphene layers between intercalant layers (higher-stage GICs).^[115] It is the former arrangement, however, which is preferred for the complete exfoliation of these materials into monolayer platelets.^[111] Intercalation of graphite by a mixture of sulfuric and nitric acid produces a higher-stage GIC that can be exfoliated by rapid heating or microwave treatment of the dried down powder, producing a material commonly referred to as expanded graphite (EG).^[113, 115] EG retains a layered structure but has a slightly increased interlayer spacing relative to graphite, consisting of thin platelets (30-100 nm) which are loosely stacked.^[113] Notably, an acid treatment may also oxidize the platelets, but to a far lesser degree than GO.^[115, 116] EG itself has been investigated as a composite filler, although its effectiveness in enhancing properties compared with GO-derived fillers is limited by its layered structure and relatively low specific surface area, generally less than 40 m²/g.^[117-120] Recently, a thinner form (~10 nm) of EG known as graphite nanoplatelets (GNP) was produced by either microwave radiation of acid-intercalated graphite followed by pulverization using ball milling or ultrasonication, or by thermal expansion of fluorinated graphite intercalation compounds (FGIC).^[121-123] Lee et al prepared GNP from the FGIC C₂F·nClF₃ containing the inorganic volatile intercalating agent ClF₃. The composition of FGIC in mass percentages was C 44, F 44, Cl 12. The main difference in preparation methods

between GIC and FGIC is the thermal decomposition of GIC and FGIC. In the case of GICs $C \cdot xR$, expansion of the matrix occurs only as a result of the rapid increase in the vapor pressure of the volatile intercalated substance R (the regime of thermal shock). In the case of the FGIC $C_2F_nClF_3$, expansion of the graphite layers occurs as a result of both the rapid increase in the vapor pressure of the volatile intercalated substance and the formation of gaseous fluorocarbons (mainly CF_4) and other gaseous products by interaction between the matrix and intercalant. This severe expansion process not only makes a large number of defects in the exfoliated graphite but also gives material properties essential for easy dispersion. Dispersion of the material in water with the aid of SDBS gave sheets with a thickness of down to 5 nm.^[123] Smaller platelet thicknesses have been obtained by re-intercalation of EG or co-intercalation of GIC with organic molecules prior to exfoliation. For instance, mixing potassium with EG yielded a stoichiometric first-stage GIC (KC_8), which was reported to be exfoliated into GNPs with thicknesses as low as 2 nm upon reaction with water or alcohols, along with sonication.^[111, 115] To make high-quality graphene sheets, Li et al started by first exfoliating expandable graphite by brief (60 s) heating to 1000 °C. Then graphite was reintercalated with oleum (fuming sulphuric acid with 20% free SO_3), and tetrabutylammonium hydroxide (TBA, 40% solution in water) was inserted into the oleum-intercalated graphite in *N,N*-dimethylformamide (DMF). The TBA-inserted oleum-intercalated graphite was then sonicated in a DMF solution of 1,2-distearoyl-sn-glycero-3-phosphoethanolamine-*N*-[methoxy(polyethyleneglycol)-5000] for 60 min to form a homogeneous suspension. Centrifugation was used to remove large pieces of material from the supernatant. This method resulted in large amounts of graphene sheets suspended in DMF and can be transferrable to other solvents including water and organic solvents.^[116]

1.4. Characterization of graphene

It is important to verify that the preparation methods described above do in fact produce graphene since properties of the nanofiller are important for its application, for instance for the preparation of the polymer composites. The usual methods include optical microscopy, SEM, TEM, AFM, Raman spectroscopy, X-ray diffraction and XPS.

X-ray diffraction is used to demonstrate that graphite has been intercalated. For example, the sharp reflection at $2\theta = 26.3^\circ$ (Cu $K\alpha$ radiation, X-ray wavelength = 0.154 nm) in graphite shifts to 14.1° - 14.9° in graphite oxide. However, X-ray diffraction disappears as the sheets of GO exfoliate into single sheets.^[13, 67, 95]

Surface area has been used as an indicator of degree of exfoliation. Since theoretically the specific surface area is inversely proportional to the thickness of disk-like particles, well-exfoliated sheets will have a higher surface area. The surface area can be determined by N₂ or methylene blue adsorption.^[13, 67, 95] However, Schniepp et al. noted that N₂ adsorption measurements were highly dependent on the compressibility of TRGO.^[13, 95]

The identification of graphene sheets, down to one layer in thickness, can be realized through optical microscopy via the color contrast caused by the light interference effect on the SiO₂ substrate, which is modulated by the graphene layer.^[124, 125]

AFM is an effective way for the characterization of graphene. Though graphene is very thin, it can give the morphological information using AFM. From the step height of graphene on the substrate, it is possible to estimate the number of graphene layers in the sheet. Due to the differences in tip attraction/repulsion between the insulating substrate and graphene it is hard to measure the theoretical thickness of 0.34 nm which results in a typical thickness ranging from 0.6 to 1.0 nm for single layers.^[126] Also folded or wrinkled sheets as well as adsorbed solvents or moisture can complicate the measurements.^[13, 67, 85, 95]

SEM can give qualitative insight into the three-dimensional structure of graphene sheets.^[67]

TEM can observe the morphology of graphene as well as determine lateral size and count a number of graphene layers quite accurately. In addition to that electron diffraction patterns can clearly differentiate single from bilayer sheets.^[9] High-resolution TEM (HR-TEM) can identify atomic bonds on functionalized sheets (C-OH vs C-O-C) and atomistic defects.^[75]

Standard elemental analysis is applied to estimate the degree of oxidation of graphene oxide.

X-ray photoelectron spectroscopy can determine an amount of oxygen on the graphene surface as well as identify the types of the bonds.

Raman spectroscopy can provide a quick and effective way for structure and quality characterization of graphene. It can quantify the transformation of sp³-hybridized carbons back to sp² on reduction of GO and indicate the presence of disordered stacking in graphite samples. The transformation of sp³ to sp² restores electrical conductivity; thus, conductivity is also a valuable qualitative measure of the conversion of graphene oxide to graphene.^[13, 85]

1.5. Graphene/polymer nanocomposites

Graphene which is used for the preparation of graphene-based polymer nanocomposites is mainly produced via either chemical reduction or thermal reduction of graphite oxide due to the

advantage of these methods of graphene production over the others with respect to the scale on which graphene can be prepared. Most of graphene/polymer nanocomposites have been developed utilizing three strategies: 1) solvent processing; 2) *in-situ* polymerization and 3) melt processing.^[127]

1.5.1. Solvent processing

The method consists of three steps: dispersion in a suitable solvent by, for example, ultrasonication, addition of the polymer, and removal of the solvent by evaporation or distillation.

Stankovich et al. treated graphite oxide with organic isocyanates.^[88] The isocyanate treatment reduced the hydrophilic character of graphene oxide sheets by forming amide and carbamate ester bonds to the carboxyl and hydroxyl groups of graphite oxide, respectively. As a result, such isocyanate-derivatized graphite oxides no longer exfoliate in water but readily form stable dispersions in polar aprotic solvents DMF, consisting of completely exfoliated, functionalized individual graphene oxide sheets with thickness ~ 1 nm. The nanocomposites prepared by solution-phase mixing of the exfoliated phenyl isocyanate-treated graphite oxide sheets with polystyrene, followed by their chemical reduction exhibited a percolation threshold of 0.1 vol % and ultimate conductivity of 1 S/m.^[88]

Ansari and coworkers dispersed both TRGO and graphene, produced by exfoliation of graphite by tip-sonication in DMF by sonication, followed by adding poly(vinylidene fluoride) (PVDF).^[128] The composite solutions were then coagulated by adding water and the precipitated composites were dried in vacuum. Samples were prepared by compression molding. The TRGO-filled PVDF nanocomposites showed percolation around 2 wt % compared to 5 wt % for the graphene produced directly from graphite-filled composites. The lower percolation threshold was attributed to the higher aspect ratio of TRGO compared to the graphene produced directly from graphite, which leads to easy connectivity and better conductivity.^[128]

Nanocomposite films of a TRGO and poly(ethylene oxide) (PEO) were cast from the physical blend of an aqueous TRGO dispersion assisted by PSS and an aqueous PEO solution and exhibited a percolation threshold at about 1.5 wt % and a conductivity of 1 S/m at 4 wt % loading of graphene.^[129]

Pang et al. utilized a water/ethanol-assisted dispersion process under ultrasonication to disperse the graphene obtained via chemical reduction of GO and to coat the conductive filler on the surface of ultra-high molecular weight polyethylene (UHMWPE) particles.^[130] During mixing, GO was reduced to graphene with hydrazine. On evaporation of the solvents, only UHMWPE particles covered with

layers of graphene remained. The graphene-coated UHMWPE particles were subsequently compression-molded into boards at 200 °C for electrical conductivity measurements. The obtained segregated structure with graphene as conductive filler and UHMWPE as matrix exhibited a very low percolation threshold, namely ca. 0.070 vol.%, in the resultant composites.^[130]

Graphene/waterborne polyurethane nanocomposites were prepared by adding graphene dispersed in acetone to the pre-synthesized polymer dissolved in water. The percolation threshold of the composites occurred at about 2 wt % and the exhibited conductivity values are higher than those of CNTs/waterborne polyurethane nanocomposites at the same loading of nanofiller.^[131]

Poly(vinylalcohol)/reduced graphite oxide nanocomposites were synthesized by reducing graphite oxide in the presence of the final polymer matrix material and coagulating the system with 2-propanol. It was observed that some interactions occur between the polymer and the reduced graphite oxide layers, mainly by hydrogen bonding. The electrical conductivity achieved at concentrations beyond 7.5 wt % of reduced graphite oxide was as high as 10 S/m, whereas a percolation threshold occurred between 0.5 and 1 wt%.^[132]

Due to the simplicity of this solvent processing method for graphene/polymer nanocomposites preparation, it is expected that graphene/polymer composites will continue to be developed using this methodology.

1.5.2. *In-situ* process

In this strategy, the graphene sheets are usually mixed with monomers or pre-polymers, sometimes in the presence of a solvent, and then the polymerization reaction proceeds by adjusting parameters such as temperature and time.^[127]

Graphene/thermoplastic polyurethane (TPU) nanocomposites were prepared in DMF via in situ synthesis of TPU in the presence of TRGO using chain extension reactions involving surface functional groups. The percolation threshold of in-situ polymerized composites was found to be slightly greater than that of the same composites prepared by solution mixing, both being between 0.3 and 0.5 vol %. The origin of the difference is that covalently-grafted TPU chains on the TRGO surface may hinder direct contacts between platelets, and in addition reduce the effective particle aspect ratios.^[133]

It was demonstrated that poly(ethylene oxide) (PEO) can be easily intercalated into the GO gallery.^[134] Jang et al. prepared GO/poly(methyl methacrylate) (PMMA) nanocomposites by a method utilizing macroazoinitiator (MAI). The MAI, which has a PEO segment, was intercalated

between the lamellae of GO to induce the inter-gallery radical polymerization of methyl methacrylate (MMA) and exfoliate the GO platelets. The prepared GO/PMMA nanocomposites were crushed into powder and dried at 65 °C under vacuum conditions for 24 h to remove low molecular weight components followed by compression molding at 190 °C and a pressure of 22 MPa. The measured conductivity of the composites reached as much as 10^{-3} S/m at 4.2 wt % loading of GO.^[135] So although no special GO reduction step was used the composites were slightly conductive. This is due to thermal induced reduction.

In addition to the solvent processing method graphene/waterborne polyurethane nanocomposites could be prepared by *in-situ* polymerization of diisocyanate with polycaprolactone diol and poly(tetramethylene glycol).^[136] The percolation threshold occurred at 2 wt % which is comparable to that achieved for the waterborne polyurethane nanocomposites prepared by solvent processing.^[131]

Liang and coworkers prepared completely exfoliated partially reduced graphene-based sheets in water.^[137] An epoxy/hardener (4:1 weight ratio, in acetone) solution was added to the suspension of partially reduced graphene-based sheets and then sonicated and stirred for hours. After that, the mixture was poured into suitable molds to let the solvent evaporate completely at 60 °C. All the samples were cut into slabs and were then annealed at 250 °C for 2 h to fully reduce the partially reduced graphene-based sheets and increase the conductivity. The percolation threshold was found to occur at 0.1 wt % and the ultimate conductivity achieved was 0.1 S/m.^[137]

1.5.3. Melt processing

Melt processing is much more commercially attractive than the other two methods, as both solvent processing and in-situ polymerization process are less versatile and environmentally friendly. This strategy involves the direct inclusion of the graphene sheets into the melted polymer using a twin-screw extruder and adjusting parameters such as screw speed, temperature and time.^[127] The drawbacks of this procedure are the low bulk density of thermally exfoliated graphene that makes extruder feeding a troublesome task and the lower degree of dispersion compared to solvent blending.^[133] This reduced dispersion degree can then result in poorer properties, implying higher percolation thresholds and lower conductivities. On the other hand this approach provides manufacturers many degrees of freedom with regard to the selection of polymer grades and choice of the graphene content.^[138]

Kim et al. used this method to prepare graphene/TPU nanocomposites. TRGO platelets were fed into a twin-screw extruder at 180 °C and blended under dry N₂ for 6 min. Melt-blended samples were

further processed into ~0.1 mm thick films by hot pressing (140 kPa for 2 min) at 180 °C. The percolation threshold of the composites occurred at a loading of graphene slightly higher than 0.5 vol %, which is higher than the value for the same composites prepared by the in-situ process.^[133]

Zhang et al. successfully dispersed TRGO in polyethylene terephthalate (PET) by melt compounding at 285 °C using a Brabender mixer.^[138] Compounding was performed with an initial screw speed of 50 rpm/min for 4 min, after which the screw speed was raised to 100 rpm/min within 1 min and the compounding was conducted at this speed for 5 min. Graphene nanosheets were homogeneously dispersed in the PET matrix with almost no large agglomerates observed. The good dispersion of graphene sheets should be due to the good interaction between the oxygen- and hydroxyl-functional groups present on the surface of graphene and the polar carboxyl and ester groups of PET. The electrical conductivity quickly rises to 7.4×10^{-2} S/m from 2.0×10^{-13} with a slight increase in content from 0.47 to 1.2 vol.%. With only 3.0 vol.% graphene, the conductivity approaches to 2.11 S/m. On the contrary, PET/graphite composites show a higher percolation threshold of 2.4 vol % and a broad percolation transition within a range of graphite content from 2.4 to 5.8 vol %. The conductivity of PET/pristine graphite composite with 7.1 vol % of graphite is only 2.45×10^{-4} S/m.^[138]

Steurer et al. used the solvent processing and melt processing techniques for preparation of nanocomposites with the following polymer matrixes: poly(propylene), polycarbonate, polyamide 6, and poly(styrene-co-acrylonitrile) SAN.^[139] Because of the low bulk density of TRGO, solution blends of TRGO with the polymer were prepared to obtain homogenous polymer/filler compound. These premixed compounds were first dried and then melt compounded in a minicompounder. The following solvents were used: acetone for SAN/TRGO, dichloromethane for PC/TRGO, both at room temperature, and boiling xylene for iPP/TRGO. In the case of PA6, the filler was dispersed in acetone and then polyamide powder was added. The polymers and their corresponding nanocomposites were processed using a twin screw minicompounder with a mixing chamber volume of 5 ml. All the samples were compounded at 100 rpm for three minutes. The melt mixing temperature was 210 °C for SAN and iPP, 250 °C for PA6 and 280 °C for PC. The percolation thresholds occurred at 4 wt %, 2.5 wt %, 5 wt % and 7.5 wt % for SAN, PC, iPP and PA6, respectively. In the case of PC and iPP matrixes the percolation thresholds are the same as those obtained for MWCNT-based composites utilizing these polymers, whereas for graphene/SAN and graphene/PA6 nanocomposites the obtained percolation thresholds are significantly lower than that obtained for the MWCNT-based nanocomposites using the same polymers as the matrix material.^[139]

In this work we utilized the environmentally friendly latex-technology for the preparation of graphene-based polymer nanocomposites. The concept is explained in chapter 2.

1.6. Outline of the thesis

Polymer nanocomposites based on carbon black and carbon nanotubes have been used for improved mechanical, thermal, electrical, and gas barrier properties of polymers.^[140, 141] The discovery of graphene with its combination of extraordinary physical properties and ability to be dispersed in various polymer matrices has created a new class of polymer nanocomposites.^[13] The goal of the work described in this thesis was to develop graphene-based polymer nanocomposites with different levels of nanofiller loading using the latex technology, to optimise the electrical properties of graphene-based nanocomposites and to establish if such nanocomposites can compete with CNT-based polymer nanocomposites in terms of conductivity.

Chapter 2 describes preparation of the polystyrene nanocomposites based on graphene prepared via oxidation of graphite with subsequent exfoliation and chemical reduction of graphite oxide.

Chapter 3 covers and discusses the main approaches recently used to produce CNTs/graphene dispersions and conductive CNTs/graphene-based polymer composites with the help of surfactants. The main focus is given to water-based systems.

Chapter 4 studies the effect of the dispersion state of graphene as a factor influencing the electrical percolation threshold of graphene/polystyrene nanocomposites.

Chapter 5 compares the ability of some conventional surfactants such as sodium dodecylbenzene sulfonate (SDBS), sodium cholate (SC), sodium poly (styrene sulfonate) (PSS) and Tween-80 to disperse graphene in water. Percolation thresholds and ultimate conductivity values of the composites based on graphene dispersed in the presence of these surfactants are compared. An influence of utilizing conductive surfactants for graphene dispersion in water on percolation threshold and conductivity of the corresponding nanocomposites is discussed.

Chapter 6 deals with the systems consisting of a nanofiller and a conductive surfactant. For evaluation of the contribution of these two components to the overall conductivity of the composites one of them, *i.e.* the CNTs, is replaced with a non-conductive analogue with a similar aspect ratio, *i.e.* cellulose whiskers.

Chapter 7 gives an overview and presents a technological assessment of the work described in the thesis. Different aspects of upscaling of this work are addressed.

1.7. References

- [1] <http://p-km.ru>.
- [2] <http://en.wikipedia.org/wiki/Nanocomposite>
- [3] M. JoseYacaman, L. Rendon, J. Arenas, M. C. S. Puche, *Science* **1996**, 273, 223.
- [4] N. Grossiord, *PhD thesis* **2007**, Eindhoven, the Netherlands.
- [5] A. K. Geim, K. S. Novoselov, *Nature Materials* **2007**, 6, 183.
- [6] L. D. Landau, *Phys. Z. Sowjetunion* **1937**, 11, 26.
- [7] R. E. Peierls, *Ann. I. H. Poincare* **1935**, 5, 177.
- [8] K. S. Novoselov, D. Jiang, F. Schedin, T. J. Booth, V. V. Khotkevich, S. V. Morozov, A. K. Geim, *Proceedings of the National Academy of Sciences of the United States of America* **2005**, 102, 10451.
- [9] J. C. Meyer, A. K. Geim, M. I. Katsnelson, K. S. Novoselov, T. J. Booth, S. Roth, *Nature* **2007**, 446, 60.
- [10] C. Lee, X. D. Wei, J. W. Kysar, J. Hone, *Science* **2008**, 321, 385.
- [11] A. A. Balandin, S. Ghosh, W. Z. Bao, I. Calizo, D. Teweldebrhan, F. Miao, C. N. Lau, *Nano Letters* **2008**, 8, 902.
- [12] X. Du, I. Skachko, A. Barker, E. Y. Andrei, *Nature Nanotechnology* **2008**, 3, 491.
- [13] H. Kim, A. A. Abdala, C. W. Macosko, *Macromolecules* **2010**, 43, 6515.
- [14] Fujita, *J. Phys. Soc. Japan* **1996**, 65.
- [15] L. M. Malard, M. A. Pimenta, G. Dresselhaus, M. S. Dresselhaus, *Physics Reports-Review Section of Physics Letters* **2009**, 473, 51.
- [16] Y. Kobayashi, K. Fukui, T. Enoki, K. Kusakabe, Y. Kaburagi, *Physical Review B* **2005**, 71, 193406.
- [17] J. C. Meyer, C. Kisielowski, R. Erni, M. D. Rossell, M. F. Crommie, A. Zettl, *Nano Letters* **2008**, 8, 3582.
- [18] L. Tapaszto, G. Dobrik, P. Nemes-Incze, G. Vertesy, P. Lambin, L. P. Biro, *Physical Review B* **2008**, 78, 233407.
- [19] F. Banhart, J. Kotakoski, A. V. Krasheninnikov, *Acs Nano* **2011**, 5, 26.
- [20] A. J. Lu, B. C. Pan, *Physical Review Letters* **2004**, 92, 105504.
- [21] J. Kotakoski, A. V. Krasheninnikov, K. Nordlund, *Physical Review B* **2006**, 74, 245420.
- [22] Y. Miyamoto, S. Berber, M. Yoon, A. Rubio, D. Tomanek, *Chemical Physics Letters* **2004**, 392, 209.
- [23] A. V. Krasheninnikov, P. O. Lehtinen, A. S. Foster, R. M. Nieminen, *Chemical Physics Letters* **2006**, 418, 132.
- [24] J. Rossato, R. J. Baierle, A. Fazzio, R. Mota, *Nano Letters* **2005**, 5, 197.
- [25] A. A. El-Barbary, R. H. Telling, C. P. Ewels, M. I. Heggie, P. R. Briddon, *Physical Review B* **2003**, 68, 144107.
- [26] C. P. Ewels, R. H. Telling, A. A. El-Barbary, M. I. Heggie, P. R. Briddon, *Physical Review Letters* **2003**, 91, 025505.
- [27] A. V. Krasheninnikov, V. F. Elesin, *Surface Science* **2000**, 454, 519.

- [28] J. Ma, D. Alfe, A. Michaelides, E. Wang, *Physical Review B* **2009**, *80*, 033407.
- [29] L. Li, S. Reich, J. Robertson, *Physical Review B* **2005**, *72*, 184109.
- [30] K. Urita, K. Suenaga, T. Sugai, H. Shinohara, S. Iijima, *Physical Review Letters* **2005**, *94*, 155502.
- [31] F. Banhart, T. Fuller, P. Redlich, P. M. Ajayan, *Chemical Physics Letters* **1997**, *269*, 349.
- [32] L. Tsetseris, S. T. Pantelides, *Carbon* **2009**, *47*, 901.
- [33] P. Koskinen, S. Malola, H. Hakkinen, *Physical Review Letters* **2008**, *101*, 115502.
- [34] R. H. Telling, C. P. Ewels, A. A. El-Barbary, M. I. Heggie, *Nature Materials* **2003**, *2*, 333.
- [35] G. Teobaldi, H. Ohnishi, K. Tanimura, A. L. Shluger, *Carbon* **2010**, *48*, 4145.
- [36] K. S. Novoselov, A. K. Geim, S. V. Morozov, D. Jiang, Y. Zhang, S. V. Dubonos, I. V. Grigorieva, A. A. Firsov, *Science* **2004**, *306*, 666.
- [37] M. Zhang, J. H. Zhao, Z. Wu, B. Q. Wei, J. Liang, D. H. Wu, L. M. Cao, Y. F. Xu, W. K. Wang, *Journal of Materials Science Letters* **1998**, *17*, 2109.
- [38] G. Che, B. B. Lakshmi, C. R. Martin, E. R. Fisher, R. S. Ruoff, *Chemistry of Materials* **1998**, *10*, 260.
- [39] I. M. I. A.V. Eletsii, A.A. Knizhnik, D.N. Krasikov, *Phys. Usp.* **2011**, *54*, 233.
- [40] K. S. Kim, Y. Zhao, H. Jang, S. Y. Lee, J. M. Kim, K. S. Kim, J. H. Ahn, P. Kim, J. Y. Choi, B. H. Hong, *Nature* **2009**, *457*, 706.
- [41] X. S. Li, W. W. Cai, J. H. An, S. Kim, J. Nah, D. X. Yang, R. Piner, A. Velamakanni, I. Jung, E. Tutuc, S. K. Banerjee, L. Colombo, R. S. Ruoff, *Science* **2009**, *324*, 1312.
- [42] Q. K. Yu, J. Lian, S. Siriponglert, H. Li, Y. P. Chen, S. S. Pei, *Applied Physics Letters* **2008**, *93*.
- [43] A. Reina, X. T. Jia, J. Ho, D. Nezich, H. B. Son, V. Bulovic, M. S. Dresselhaus, J. Kong, *Nano Letters* **2009**, *9*, 30.
- [44] M. Eizenberg, J. M. Blakely, *Surface Science* **1979**, *82*, 228.
- [45] M. Eizenberg, J. M. Blakely, *Journal of Chemical Physics* **1979**, *71*, 3467.
- [46] J. C. Hamilton, J. M. Blakely, *Surface Science* **1980**, *91*, 199.
- [47] S. Bae, H. Kim, Y. Lee, X. F. Xu, J. S. Park, Y. Zheng, J. Balakrishnan, T. Lei, H. R. Kim, Y. I. Song, Y. J. Kim, K. S. Kim, B. Ozyilmaz, J. H. Ahn, B. H. Hong, S. Iijima, *Nature Nanotechnology* **2010**, *5*, 574.
- [48] K. Jo; Gyoo-Chul (Gyeonggi-do, Chae; Gee-Sung (Incheon, KR), Hwang; Yong-Sup (Gyeonggi-do, KR), Kwon; Oh-Nam (Chungcheonnang-do, KR), Lee; Kyoung-Mook (Seoul, KR), Baek; Kui-Jong (Chungcheongnam-do, KR), Rhee; Tai-Hyung (Chungcheonnang-do, KR), *U.S. Patent 6881879* **2005**.
- [49] Y. Lee, S. Bae, H. Jang, S. Jang, S. E. Zhu, S. H. Sim, Y. I. Song, B. H. Hong, J. H. Ahn, *Nano Letters* **2010**, *10*, 490.
- [50] J. D. Caldwell, T. J. Anderson, J. C. Culbertson, G. G. Jernigan, K. D. Hobart, F. J. Kub, M. J. Tadjer, J. L. Tedesco, J. K. Hite, M. A. Mastro, R. L. Myers-Ward, C. R. Eddy, P. M. Campbell, D. K. Gaskill, *Acs Nano* **2010**, *4*, 1108.

- [51] C. Berger, Z. M. Song, T. B. Li, X. B. Li, A. Y. Ogbazghi, R. Feng, Z. T. Dai, A. N. Marchenkov, E. H. Conrad, P. N. First, W. A. de Heer, *Journal of Physical Chemistry B* **2004**, *108*, 19912.
- [52] C. Berger, Z. M. Song, X. B. Li, X. S. Wu, N. Brown, C. Naud, D. Mayou, T. B. Li, J. Hass, A. N. Marchenkov, E. H. Conrad, P. N. First, W. A. de Heer, *Science* **2006**, *312*, 1191.
- [53] K. V. Emtsev, A. Bostwick, K. Horn, J. Jobst, G. L. Kellogg, L. Ley, J. L. McChesney, T. Ohta, S. A. Reshanov, J. Rohrl, E. Rotenberg, A. K. Schmid, D. Waldmann, H. B. Weber, T. Seyller, *Nature Materials* **2009**, *8*, 203.
- [54] J. Hass, R. Feng, T. Li, X. Li, Z. Zong, W. A. de Heer, P. N. First, E. H. Conrad, C. A. Jeffrey, C. Berger, *Applied Physics Letters* **2006**, *89*.
- [55] H. Hibino, H. Kageshima, F. Maeda, M. Nagase, Y. Kobayashi, H. Yamaguchi, *Physical Review B* **2008**, *77*, 075413
- [56] P. W. Sutter, J. I. Flege, E. A. Sutter, *Nature Materials* **2008**, *7*, 406.
- [57] A. T. N'Diaye, S. Bleikamp, P. J. Feibelman, T. Michely, *Physical Review Letters* **2006**, *97*, 215501.
- [58] J. Coraux, A. T. N'Diaye, C. Busse, T. Michely, *Nano Letters* **2008**, *8*, 565.
- [59] S. Marchini, S. Gunther, J. Wintterlin, *Physical Review B* **2007**, *76*, 075429.
- [60] A. L. Vazquez de Parga, F. Calleja, B. Borca, M. C. G. Passeggi, J. J. Hinarejos, F. Guinea, R. Miranda, *Phys Rev Lett* **2008**, *100*, 056807.
- [61] Y. Pan, D. X. Shi, H. J. Gao, *Chinese Physics* **2007**, *16*, 3151.
- [62] S. Park, R. S. Ruoff, *Nature Nanotechnology* **2009**, *4*, 217.
- [63] B. C. Brodie, *Ann. Chim. Phys.* **1860**, *59*.
- [64] C. Schafhaeutl, *Phil. Mag.* **1840**, *16*, 570.
- [65] L. Staudenmaier, *Ber. Deut. Chem. Ges.* **1898**, *31*.
- [66] W. S. Hummers, R. E. Offeman, *Journal of the American Chemical Society* **1958**, *80*, 1339.
- [67] M. J. McAllister, J. L. Li, D. H. Adamson, H. C. Schniepp, A. A. Abdala, J. Liu, M. Herrera-Alonso, D. L. Milius, R. Car, R. K. Prud'homme, I. A. Aksay, *Chemistry of Materials* **2007**, *19*, 4396.
- [68] D. W. Boukhvalov, M. I. Katsnelson, *Journal of the American Chemical Society* **2008**, *130*, 10697.
- [69] R. Lahaye, H. K. Jeong, C. Y. Park, Y. H. Lee, *Physical Review B* **2009**, *79*, 125435.
- [70] J. T. Paci, T. Belytschko, G. C. Schatz, *Journal of Physical Chemistry C* **2007**, *111*, 18099.
- [71] A. Lerf, H. Y. He, M. Forster, J. Klinowski, *Journal of Physical Chemistry B* **1998**, *102*, 4477.
- [72] H. Y. He, J. Klinowski, M. Forster, A. Lerf, *Chemical Physics Letters* **1998**, *287*, 53.
- [73] M. Mermoux, Y. Chabre, A. Rousseau, *Carbon* **1991**, *29*, 469.

- [74] A. Clauss, R. Plass, H. P. Boehm, U. Hofmann, *Zeitschrift Fur Anorganische Und Allgemeine Chemie* **1957**, *291*, 205.
- [75] K. A. Mkhoyan, A. W. Contryman, J. Silcox, D. A. Stewart, G. Eda, C. Mattevi, S. Miller, M. Chhowalla, *Nano Letters* **2009**, *9*, 1058.
- [76] W. H. Zhang, V. Carravetta, Z. Y. Li, Y. Luo, J. L. Yang, *Journal of Chemical Physics* **2009**, *131*.
- [77] W. Gao, L. B. Alemany, L. J. Ci, P. M. Ajayan, *Nature Chemistry* **2009**, *1*, 403.
- [78] H. K. Jeong, Y. P. Lee, R. Lahaye, M. H. Park, K. H. An, I. J. Kim, C. W. Yang, C. Y. Park, R. S. Ruoff, Y. H. Lee, *Journal of the American Chemical Society* **2008**, *130*, 1362.
- [79] T. Nakajima, A. Mabuchi, R. Hagiwara, *Carbon* **1988**, *26*, 357.
- [80] W. Scholz, H. P. Boehm, *Zeitschrift Fur Anorganische Und Allgemeine Chemie* **1969**, *369*, 327.
- [81] W. W. Cai, R. D. Piner, F. J. Stadermann, S. Park, M. A. Shaibat, Y. Ishii, D. X. Yang, A. Velamakanni, S. J. An, M. Stoller, J. H. An, D. M. Chen, R. S. Ruoff, *Science* **2008**, *321*, 1815.
- [82] T. Szabo, O. Berkesi, P. Forgo, K. Josepovits, Y. Sanakis, D. Petridis, I. Dekany, *Chemistry of Materials* **2006**, *18*, 2740.
- [83] A. Buchsteiner, A. Lerf, J. Pieper, *Journal of Physical Chemistry B* **2006**, *110*, 22328.
- [84] D. Li, M. B. Muller, S. Gilje, R. B. Kaner, G. G. Wallace, *Nature Nanotechnology* **2008**, *3*, 101.
- [85] S. Stankovich, D. A. Dikin, R. D. Piner, K. A. Kohlhaas, A. Kleinhammes, Y. Jia, Y. Wu, S. T. Nguyen, R. S. Ruoff, *Carbon* **2007**, *45*, 1558.
- [86] J. R. Lomeda, C. D. Doyle, D. V. Kosynkin, W. F. Hwang, J. M. Tour, *Journal of the American Chemical Society* **2008**, *130*, 16201.
- [87] V. C. Tung, M. J. Allen, Y. Yang, R. B. Kaner, *Nature Nanotechnology* **2009**, *4*, 25.
- [88] S. Stankovich, D. A. Dikin, G. H. B. Dommett, K. M. Kohlhaas, E. J. Zimney, E. A. Stach, R. D. Piner, S. T. Nguyen, R. S. Ruoff, *Nature* **2006**, *442*, 282.
- [89] G. X. Wang, J. Yang, J. Park, X. L. Gou, B. Wang, H. Liu, J. Yao, *Journal of Physical Chemistry C* **2008**, *112*, 8192.
- [90] Y. Si, E. T. Samulski, *Nano Letters* **2008**, *8*, 1679.
- [91] R. Muszynski, B. Seger, P. V. Kamat, *Journal of Physical Chemistry C* **2008**, *112*, 5263.
- [92] S. Stankovich, R. D. Piner, X. Q. Chen, N. Q. Wu, S. T. Nguyen, R. S. Ruoff, *Journal of Materials Chemistry* **2006**, *16*, 155.
- [93] Y. X. Xu, H. Bai, G. W. Lu, C. Li, G. Q. Shi, *Journal of the American Chemical Society* **2008**, *130*, 5856.
- [94] R. K. Prudhomme, I. A. Aksay, D. Adamson, A. Abdala, R. K., *U.S. Patent 20070092432* **2007**.

- [95] H. C. Schniepp, J. L. Li, M. J. McAllister, H. Sai, M. Herrera-Alonso, D. H. Adamson, R. K. Prudhomme, R. Car, D. A. Saville, I. A. Aksay, *Journal of Physical Chemistry B* **2006**, *110*, 8535.
- [96] P. Steurer, R. Wissert, R. Thomann, R. Mulhaupt, *Macromolecular Rapid Communications* **2009**, *30*, 316.
- [97] I. A. Aksay, S. Korkut, D. L. Milius, R. K. Prudhomme, *W.O. Patent 2009/134492 A2* **2009**.
- [98] C. A. Furtado, U. J. Kim, H. R. Gutierrez, L. Pan, E. C. Dickey, P. C. Eklund, *Journal of the American Chemical Society* **2004**, *126*, 6095.
- [99] S. Giordani, S. D. Bergin, V. Nicolosi, S. Lebedkin, M. M. Kappes, W. J. Blau, J. N. Coleman, *Journal of Physical Chemistry B* **2006**, *110*, 15708.
- [100] B. J. Landi, H. J. Ruf, J. J. Worman, R. P. Raffaele, *Journal of Physical Chemistry B* **2004**, *108*, 17089.
- [101] T. Hasan, V. Scardaci, P. H. Tan, A. G. Rozhin, W. I. Milne, A. C. Ferrari, *Journal of Physical Chemistry C* **2007**, *111*, 12594.
- [102] S. D. Bergin, V. Nicolosi, S. Giordani, A. de Gromard, L. Carpenter, W. J. Blau, J. N. Coleman, *Nanotechnology* **2007**, *18*.
- [103] Y. Hernandez, V. Nicolosi, M. Lotya, F. M. Blighe, Z. Y. Sun, S. De, I. T. McGovern, B. Holland, M. Byrne, Y. K. Gun'ko, J. J. Boland, P. Niraj, G. Duesberg, S. Krishnamurthy, R. Goodhue, J. Hutchison, V. Scardaci, A. C. Ferrari, J. N. Coleman, *Nature Nanotechnology* **2008**, *3*, 563.
- [104] U. Khan, A. O'Neill, M. Lotya, S. De, J. N. Coleman, *Small* **2010**, *6*, 864.
- [105] M. Lotya, Y. Hernandez, P. J. King, R. J. Smith, V. Nicolosi, L. S. Karlsson, F. M. Blighe, S. De, Z. M. Wang, I. T. McGovern, G. S. Duesberg, J. N. Coleman, *Journal of the American Chemical Society* **2009**, *131*, 3611.
- [106] M. Lotya, P. J. King, U. Khan, S. De, J. N. Coleman, *Acs Nano* **2010**, *4*, 3155.
- [107] A. A. Green, M. C. Hersam, *Nano Letters* **2009**, *9*, 4031.
- [108] A. O'Neill, U. Khan, P. N. Nirmalraj, J. Boland, J. N. Coleman, *Journal of Physical Chemistry C* **2011**, *115*, 5422.
- [109] X. Y. Zhang, A. C. Coleman, N. Katsonis, W. R. Browne, B. J. van Wees, B. L. Feringa, *Chemical Communications* **2010**, *46*, 7539.
- [110] M. S. Dresselhaus, G. Dresselhaus, *Advances in Physics* **1981**, *30*, 139.
- [111] L. M. Viculis, J. J. Mack, O. M. Mayer, H. T. Hahn, R. B. Kaner, *Journal of Materials Chemistry* **2005**, *15*, 974.
- [112] K. E. Carr, *Carbon* **1970**, *8*, 155.
- [113] G. H. Chen, D. J. Wu, W. U. Weng, C. L. Wu, *Carbon* **2003**, *41*, 619.
- [114] B. Z. Jang, A. Zhamu, *Journal of Materials Science* **2008**, *43*, 5092.
- [115] J. R. Potts, D. R. Dreyer, C. W. Bielawski, R. S. Ruoff, *Polymer* **2011**, *52*, 5.
- [116] X. L. Li, G. Y. Zhang, X. D. Bai, X. M. Sun, X. R. Wang, E. Wang, H. J. Dai, *Nature Nanotechnology* **2008**, *3*, 538.

- [117] P. Potschke, M. Abdel-Goad, S. Pegel, D. Jehnichen, J. E. Mark, D. H. Zhou, G. Heinrich, *Journal of Macromolecular Science Part a-Pure and Applied Chemistry* **2010**, *47*, 12.
- [118] A. Yasmin, J. J. Luo, I. M. Daniel, *Composites Science and Technology* **2006**, *66*, 1182.
- [119] W. Zheng, X. H. Lu, S. C. Wong, *Journal of Applied Polymer Science* **2004**, *91*, 2781.
- [120] A. Celzard, J. F. Mareche, G. Furdin, S. Puricelli, *Journal of Physics D-Applied Physics* **2000**, *33*, 3094.
- [121] Fukushima, *Ph.D thesis, Michigan State University* **2003**.
- [122] K. Kalaitzidou, H. Fukushima, L. T. Drzal, *Composites Science and Technology* **2007**, *67*, 2045.
- [123] J. H. Lee, D. W. Shin, V. G. Makotchenko, A. S. Nazarov, V. E. Fedorov, Y. H. Kim, J. Y. Choi, J. M. Kim, J. B. Yoo, *Advanced Materials* **2009**, *21*, 4383.
- [124] L. B. Gao, W. C. Ren, F. Li, H. M. Cheng, *Acs Nano* **2008**, *2*, 1625.
- [125] Z. H. Ni, H. M. Wang, J. Kasim, H. M. Fan, T. Yu, Y. H. Wu, Y. P. Feng, Z. X. Shen, *Nano Letters* **2007**, *7*, 2758.
- [126] L.-X. Dong, Q. Chen, *Front. Mater. Sci. China* **2010**, *4*, 45.
- [127] R. Verdejo, M. M. Bernal, L. J. Romasanta, M. A. Lopez-Manchado, *Journal of Materials Chemistry* **2010**, *21*, 3301.
- [128] S. Ansari, E. P. Giannelis, *Journal of Polymer Science Part B-Polymer Physics* **2009**, *47*, 888.
- [129] H. B. Lee, A. V. Raghu, K. S. Yoon, H. M. Jeong, *Journal of Macromolecular Science Part B-Physics* **2010**, *49*, 802.
- [130] H. Pang, T. Chen, G. Zhang, B. Zeng, Z.-M. Li, *Materials Letters* **2010**, *64*, 2226.
- [131] A. V. Raghu, Y. R. Lee, H. M. Jeong, C. M. Shin, *Macromolecular Chemistry and Physics* **2008**, *209*, 2487.
- [132] H. Javier Salavagione, G. Martinez, M. A. Gomez, *Journal of Materials Chemistry* **2009**, *19*, 5027.
- [133] H. Kim, Y. Miura, C. W. Macosko, *Chemistry of Materials* **2010**, *22*, 3441.
- [134] Y. Matsuo, K. Tahara, Y. Sugie, *Carbon* **1996**, *34*, 672.
- [135] J. Y. Jang, M. S. Kim, H. M. Jeong, C. M. Shin, *Composites Science and Technology* **2009**, *69*, 186.
- [136] Y. R. Lee, A. V. Raghu, H. M. Jeong, B. K. Kim, *Macromolecular Chemistry and Physics* **2009**, *210*, 1247.
- [137] J. Liang, Y. Wang, Y. Huang, Y. Ma, Z. Liu, F. Cai, C. Zhang, H. Gao, Y. Chen, *Carbon* **2009**, *47*, 922.
- [138] H.-B. Zhang, W.-G. Zheng, Q. Yan, Y. Yang, J.-W. Wang, Z.-H. Lu, G.-Y. Ji, Z.-Z. Yu, *Polymer* **2010**, *51*, 1191.
- [139] P. Steurer, R. Wissert, R. Thomann, R. Muelhaupt, *Macromolecular Rapid Communications* **2009**, *30*, 316.
- [140] J. C. Huang, *Advances in Polymer Technology* **2002**, *21*, 299.

- [141] M. Moniruzzaman, K. I. Winey, *Macromolecules* **2006**, *39*, 5194.

Chapter 2

Latex-based concept for the preparation of graphene-based polymer nanocomposites

ABSTRACT. The latex technology concept was applied for the preparation of graphene/polystyrene nanocomposites. Aqueous dispersions of graphene were obtained via oxidation and exfoliation of graphite and subsequent reduction in the presence of poly(sodium 4-styrene sulfonate) (PSS) acting as a surfactant. The quality of the prepared nanofillers was characterized by atomic force microscopy (AFM). Different amounts of aqueous graphene dispersions were then mixed with polystyrene (PS) latex and composites are prepared by freeze-drying and subsequent compression molding. The final bulk and local conductivities of the composites were respectively measured by a four-point method and by means of conductive AFM (C-AFM) analysis. The morphology of the conductive nanocomposites was studied with charge contrast scanning electron microscopy imaging (SEM). The percolation threshold for conduction was found to be below 1 wt% of graphene in the composites, and a maximum conductivity of about 15 S/m could be achieved for 1.6-2 wt% nanofiller.

This chapter has been published: E. Tkalya, M. Ghislandi, A. Alekseev, C. Koning, J. Loos, *Journal of Materials Chemistry* **2010**, *20*, 3035.

2.1. Introduction

Various methods have been developed in recent years to efficiently disperse individual graphene platelets in a polymer matrix. Direct mixing of the graphene and the polymer, with or without the help of a solvent, has proven to be efficient and appears to be the easiest and least laborious way to achieve this goal. On the other hand, in the case of utilizing carbon nanotubes as a conductive filler for conductive polymer nanocomposites latex-based methods showed their versatility resulting in low percolation thresholds and high ultimate conductivities.^[1-4] The basic concept consists of the generation of a stable, mixed colloidal system containing both a suspension of individual graphene sheets stabilized by surfactant molecules in water and polymer latex particles, also stabilized by surfactants. After the removal of water, the resulting powder can be processed by e.g. compression molding into a desired shape, preserving in most cases the dispersion and exfoliation of the filler in the polymer matrix. The advantages of this technique are obvious: it is easy, versatile, reproducible and reliable. This approach allows nanocomposite production with a relatively homogeneous dispersion of the nanofiller in the polymer matrix, low percolation thresholds and high conductivity levels. It is very flexible with respect to the choice of the polymer matrix: it can be applied to any polymer that can either be synthesized by emulsion polymerization, or brought into a polymer latex form in an artificial way. It does not require the use of toxic and inflammable solvents and is safe and environmentally friendly. In this study, graphene/polystyrene nanocomposites were fabricated using latex technology and characterized with respect to morphology and conductivity properties. Graphene was prepared via oxidation of graphite by Hummers' method followed by reduction of the water-soluble graphite (GO) platelets with hydrazine hydrate in the presence of surfactant to prevent aggregation of the resulting graphene platelets.

2.2. Results and discussion

2.2.1. Preparation of graphite oxide

Graphite oxide produced by Hummers method (see experimental part) has a layered structure.^[5] It was readily exfoliated in water by a gentle sonication process at a concentration of 1 mg/ml. Most of the graphite oxide platelets analyzed exhibit a thickness below 1 nm, corresponding to 2-3 atomic layers, which clearly indicates the successful exfoliation driven by sonication (**Figure 1**). There is always a compromise between the sonication time and the final graphene surface area and surface/thickness ratio, which is obtained after reduction of the graphite oxide.

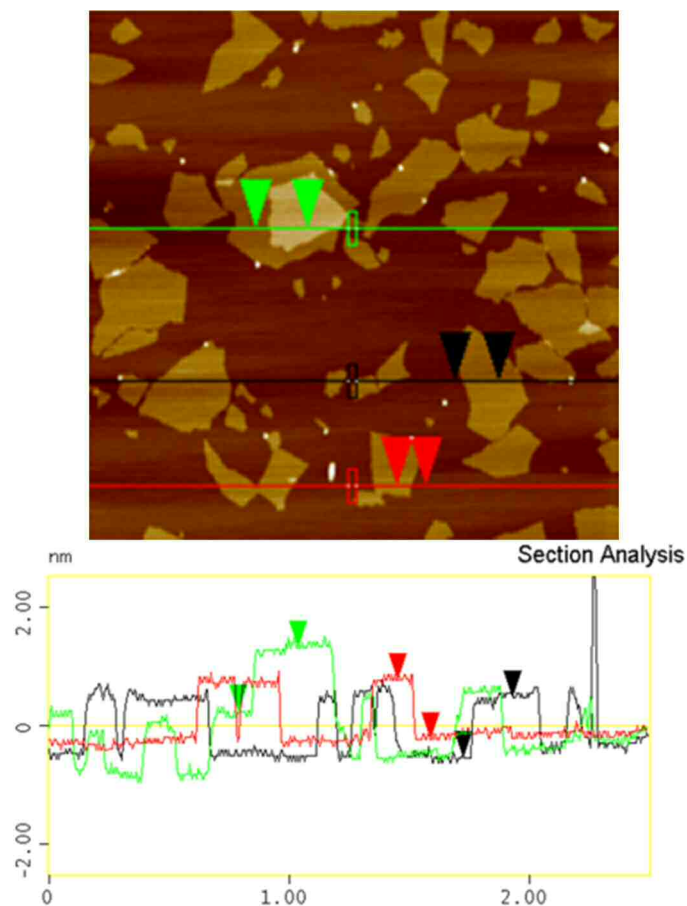


Figure 1. Tapping mode AFM analysis of graphite oxide sheets after sonication, showing platelets surface topography and average thickness.

The optimum sonication time in order to prevent extensive breaking and destruction of the sheets, but still providing good exfoliation, was found to be 12-15 min. The average surface area of the graphite oxide platelets ranged from 1 to 3 μm^2 .

2.2.2. Reduction of graphite oxide

Reduction of graphite oxide with hydrazine at 120 °C in the presence of poly(sodium styrene sulfonate) PSS resulted in a stable dispersion of graphene nanoplatelets in water. After filtering, the graphene covered with PSS could be easily redispersed in water (1 mg/ml) by a second ultrasound treatment, remaining stable for a few days, after which some sedimentation

occurred. Elemental analysis showed that the graphene/PSS ratio after filtering was 70/30 (wt /wt). The reduction of graphite oxide was carried out for 72 hours, since electrical measurements of 'buckypapers' (graphene/PSS films prepared by vacuum filtration) indicated differences in conductivity depending on reduction time, probably due to different degrees of oxygen removal and reformation of double bonds. The maximum conductivity (5500 S/m) was achieved for 72h reduction time, after which no increase was observed anymore. We also employed X-ray photoelectron spectroscopy (XPS) to analyze the GO and GO that had been reduced for 72 hours (**Figure 2**). The spectrum of GO clearly indicates a considerable degree of oxidation with components which correspond to carbon atoms in different oxygen functionalities: C–O bonds, C=O and O–C=O. Although the XPS spectra of the graphite oxide reduced for 72 hours (Figure 2b) also exhibit the same oxygen functionalities that have been assigned for graphite oxide, the peak intensities of these components in the reduced samples are much lower than those for the graphite oxide, indicating considerable, though incomplete, de-oxygenation by the reduction process. One can see that the reduction enhances the amount of C–C and graphitic carbon (C_g) over time, which gives rise to conductivity.

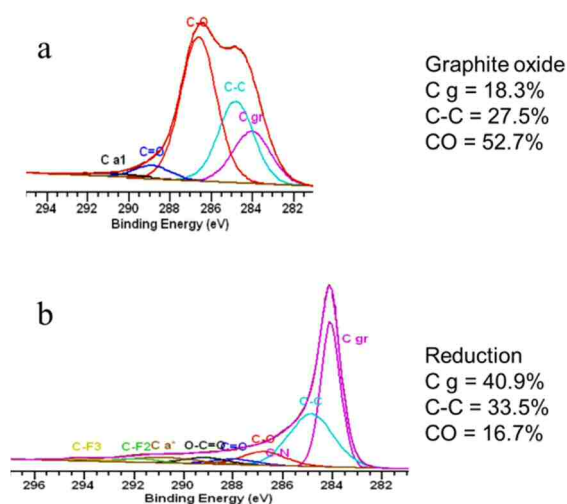


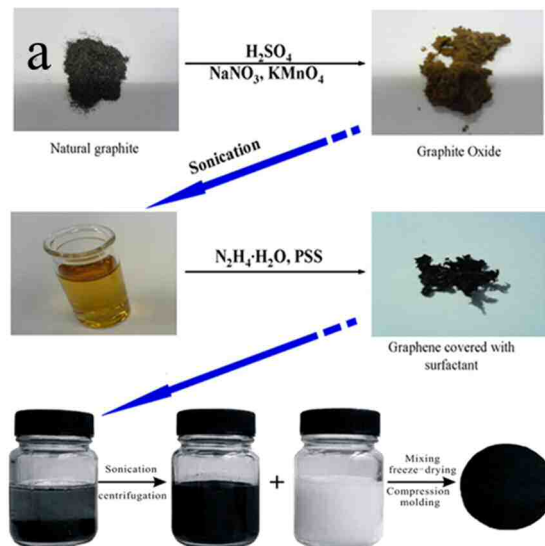
Figure 2. XPS data: (a) graphite oxide; (b) graphite oxide reduced during 72 hours.

The sonication process, which drives the redispersion of graphene/PSS aggregates, can easily be monitored by UV-Vis spectroscopy. The maximum achievable exfoliation (which does not

mean that 100 % of platelets are effectively exfoliated) corresponds to the maximum achievable UV-Vis absorbance of the filler dispersion. The reasoning behind this statement is that individualized and very thin graphene sheets exhibit a UV-Vis absorption spectrum whereas bundled or stacked sheets don't. The absorbance increases continuously with increasing sonication energy-input. Time and energy provided for maximum exfoliation of graphene/PSS vary usually from 30 minutes to 1 hour, which corresponds to 30,000-60,000 J, respectively.

2.2.3. Graphene/polystyrene nanocomposites

After the maximum obtainable exfoliation was achieved, the dispersion of graphene/PSS was mixed with polystyrene latex, followed by freeze-drying and compression molding, resulting in a composite film. For clarity, the entire process is illustrated in **Figure 3a**. We analyzed graphene used for the preparation of the nanocomposites with Transmission Electron Microscopy (TEM). In the figure 3b one can see well-exfoliated graphene flakes in the presence of PS latex particles. The flakes are hardly visible, which confirms that exfoliation was successful. When performing TEM we didn't observe any agglomerations of graphene sheets.



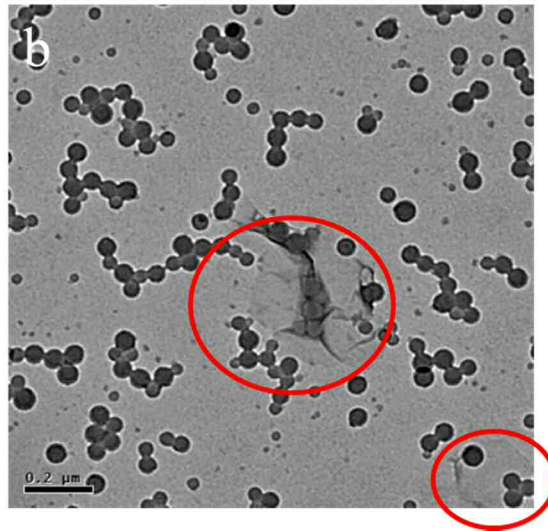


Figure 3. (a) Schematic description of the multi-step process for preparation of graphene/polymer composites using latex technology; (b) TEM of aqueous dispersion of graphene sheets stabilized with PSS and mixed with PS latex particles.

The electrical conductivity of the nanocomposites as a function of the nanofiller content is shown in **Figure 4**. At low graphene concentrations, as long as no conductive network of nanoplatelets is formed in the PS matrix, the conductivity of the nanocomposites remains very close to the conductivity value of the pure insulating PS matrix.

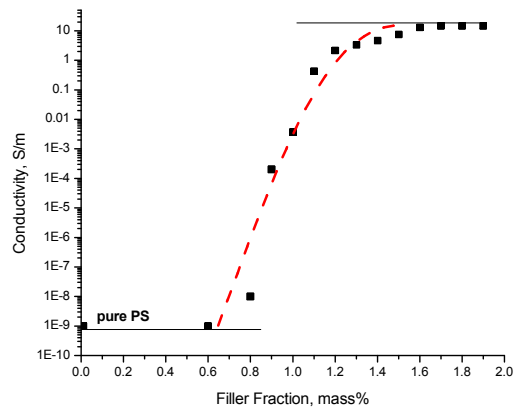


Figure 4. Electrical conductivity of graphene/PS composites as a function of graphene weight fraction.

The composites exhibit a conductivity percolation threshold when the filler content is still below 0.8 wt%. At concentrations between 0.9 and 1.2 wt% the conductivity increases drastically up to 2 S/m. At higher graphene loadings of about 2 wt%, the conductivity level is ca. 15 S/m, which is, to the best of our knowledge, the highest value measured for graphene/PS nanocomposites with low graphene loadings. MWD (molecular weight distribution) of the matrix material can strongly affect the percolation threshold of a nanofiller within PS matrix. For instance for carbon nanotubes, a significant decrease in the percolation threshold was observed upon the introduction of low molecular weight polymer, the shift being most pronounced for higher amounts of low molar mass polymer. The origin of this affect can be twofold: changes in MWD leads to rheological changes of the melt (i.e. decrease in melt viscosity) and low molecular weight polymer may replace surfactant from the carbon nanotubes surface (thereby changing the inter-tube distances and/or electrical conduction across junctions).^[6] In this work high molecular weight PS latex was used with M_w 944 kg/mol.

Table 1 compares conductive properties of graphene/ nanotubes nanocomposites obtained via latex technology, using PS latex with same MWD and the same processing conditions.

Nanofiller	Graphene	SWCNT	MWCNT (Long)	MWCNT
Percolation threshold, wt%	0.6	0.4 ^[7]	0.15 ^[8]	1.5 ^[9]
Ultimate conductivity, S/m	15	20 ^[7]	1000 ^[8]	13 ^[9]

Table 1. Conductive properties of nanocomposites produced via latex technology.

For the final application of graphene in nanocomposites, detailed knowledge on platelets dispersion and organization in the polymer matrix is most important to understand the properties and performance of the nanocomposites. To obtain this information, we have applied various microscopic techniques.

Figure 5 shows a charge contrast SEM image of the surface of a graphene/PS composite film with a graphene concentration of 1.9 wt%.

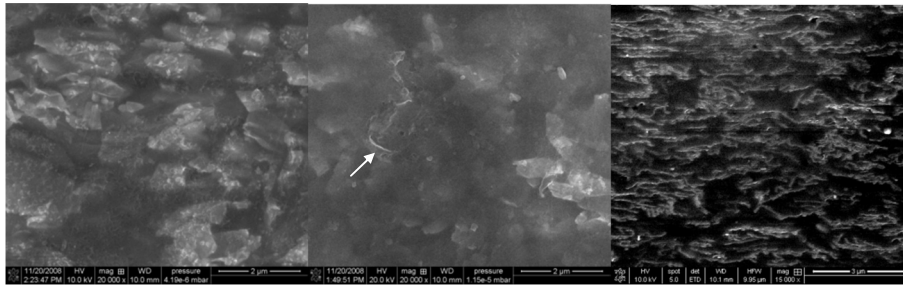


Figure 5. High-resolution SEM charge contrast showing fairly straight and bended graphene sheets. The filler concentration is 1.9 wt%. Attention should be paid to curved lateral cross section sheets (marked by arrow), and to the different brightness of the graphene. Scale bar is 2 μ m in both images.

Besides a more or less dark background, bright areas are visible, which represent graphene sheets distributed in the polymer matrix. Because of the different capability for charge transport of the conductive graphene and the insulating polymer matrix, the secondary electron yield is enriched at the location of the graphene, which results in the contrast between the graphene network and the polymer matrix.^[4]

Therefore, using charge contrast imaging at high acceleration voltage, we are able to gain representative information on the three-dimensional organization of a conductive network of graphene sheets in a polymer matrix. The brightness variations visible in the SEM charge contrast images can be related to the position of the graphene in the sample: high brightness means a position of the sheets at or near the surface, whereas sheets located deep in the nanocomposite appear darker.^[10]

The local organization of graphene sheets in the conductive Gr/PS nanocomposites and their conductivity distribution has been also analyzed with nanometer resolution by means of conductive atomic force microscopy (C-AFM). Using a conductive AFM probe, in our case a gold-coated silicon tip, the local electrical conductivity can be measured at exactly the same area of the specimen subsequent to the topography and phase contrast imaging. The C-AFM tip measures the current throughout the volume of the nanocomposite specimen at a given voltage which is running via the graphene network to the ground contacts. Only platelets that are

connected with the ground contacts can be monitored, and the observed differences in current are determined by the intra-network graphene junctions with highest resistivity. Graphene contributing to sub-networks without connection to the ground contacts show no current. In this way, a current distribution image is obtained and the conductive platelets can be distinguished from the insulating polymer matrix. **Figure 6** shows that most of the bright (white) areas corresponding to graphene in the cross-section topographic image (left) feet with the higher current level seen on the right mapping, indicating the presence of conductive pathways. The analyses of several images show that these networks were observed mainly in the central region of the cross-sections if compared to the edges.

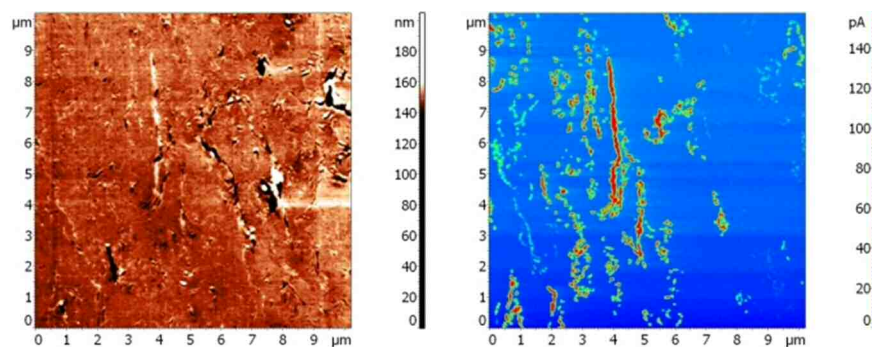


Figure 6. C-AFM images of the PS/graphene samples containing 1.9 wt% graphene obtained in topography (left), and as electrical current distribution image (right), showing the graphene platelets that are connected with the ground electrode.

There have been few reports utilizing in-situ thermal reduction of graphite oxide, i.e. during polymerization of monomers for composite preparation in the presense of GO at high temperatures. [11-13] Liu et al. prepared polyester/reduced graphene oxide composites via in-situ polymerization at elevated temperature of terephthalic acid and ethylene glycol containing well-dispersed GO. The composites exhibited maximum conductivity of 0.5 S/m.[12] Here, as a special and very easy way of preparing conductive PS-based nanocomposites, we mixed well-dispersed GO (without any surfactant present) with PS latex and after freeze-drying prepared composite films by compression molding at 180 °C. This high temperature molding step can partially reduce the GO. The conductivity curve is presented in **Figure 7**. As one can see the reduced GO platelets in the composites percolate at 0.7 wt % of graphene oxide loading and a conductivity of 0.3 S/m is achieved at 3.5 wt %. This percolation threshold is lower that that obtained for the composites utilizing graphene obtained by

chemical reduction of GO. This can be attributed to the higher aspect ratio of in-situ reduced GO sheets in comparison to graphene platelets used for the preparation of graphene/PS composites described earlier in this chapter due to the fact that for dispersion of GO in water just gentle sonication is required whereas when GO is reduced chemically and then mixed with the PS latex additional sonication step has to be applied to redisperse graphene platelets after filtration (see experimental part).

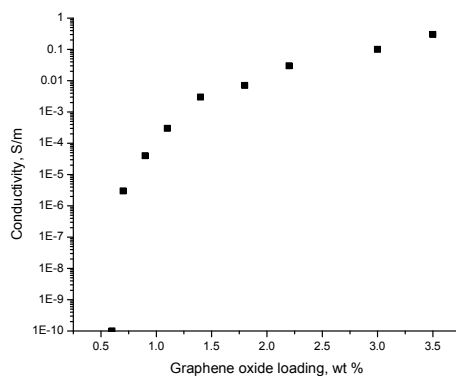


Figure 7. Electrical conductivity of in-situ reduced GO/PS composites as a function of GO weight fraction.

The additional sonication step can break graphene sheets and reduce their aspect ratio, thereby enhancing the percolation threshold. The conductivity achieved for the composites based on in-situ reduced GO is much lower than that achieved for the composites based on the chemically reduced GO. This is attributed to the incomplete reduction of the in-situ reduced GO. To prove that the conductivity does not come from GO we prepared a bucky-paper out of GO and measured its conductivity which we found to be only 1×10^{-6} S/m. Thus it can be assumed that higher conductivity values can be obtained by using the in-situ reduction process provided that the polymer used as a matrix can stand higher processing temperatures.

2.3. Conclusions

For the first time highly conductive graphene/PS nanocomposites with a low percolation threshold have been prepared by latex technology.

The study demonstrates that it is possible to apply latex technology for the preparation of graphene-based nanocomposites. PSS-covered graphene platelets were successfully prepared via a known oxidation/reduction method and dispersed in water by means of sonication. PSS stabilizes the platelets and prevents their aggregation, but at the same time, because of its bulkiness and non-conductive character, probably limits the electron transport at the graphene junctions in the final nanocomposites.

AFM shows that the thickness of the oxidized graphite platelets is around 1 nanometer, indicating approximately 2-3 graphene layers. Relatively well-dispersed graphene sheets in a PS matrix could be visualized using a high charge contrast scanning electron microscopy imaging technique. Probably due to the application of the relatively new latex technology the distribution and homogeneity of the graphene filler inside the polymer could be improved in comparison to other standard nanocomposite manufacturing techniques.

The final conductivities of the graphene/PS nanocomposites, obtained by both four point and local current measurement techniques, reveal interestingly high values up to 15 S/m, which can be achieved for low nanofiller loadings (1.6-2 wt%). A pronounced percolation threshold exhibiting a quite low value around 0.8-0.9 wt% was observed for the produced PS/graphene nanocomposites.

We have also demonstrated that conductive polymer composites can be prepared by thermal reduction of GO in the final step of the "latex technology", namely during compression molding. This makes preparation of graphene-based polymer composites very easy, since the laborious and time consuming chemical reduction of GO in a separate step is skipped. An additional advantage of this method is that a dispersion of graphene oxide in water is very stable over time and can be kept for months, whereas a dispersion of graphene/PSS sedimentates after a few weeks due to reaggregation of graphene platelets.

2.4. Experimental

Chemicals

Sodium dodecyl sulfate (SDS) (90%, Merck), sodium carbonate (SCa) (99%, Aldrich), sodium peroxodisulfate (SPS) (90%, Merck) and poly(sodium 4-styrene sulfonate) (PSS) (Aldrich, Mw 70000 g/mol) were used as received. Styrene (99%, Merck) was passed over an inhibitor remover column. The inhibitor-free monomers were kept under refrigeration for later use. Water used in all reactions was double de-ionized water obtained from a purification system. SP-2 graphite from Bay Carbon was used as filler.

Preparation and characterization of PS latex

PS latex was synthesized via conventional free radical emulsion polymerization. The reaction was performed at 70° C with an impeller speed of 400 rpm. The reactor was charged with the following: styrene (252 g), SDS (26 g, 0.09 mol), SCa (0.7 g, 6.6 mmol) and H₂O (712.2 g). The reaction mixture was degassed, by purging with argon, for 30 min. A solution of SPS (0.45 g, 1.9 mmol) in H₂O (10 g) was also degassed. The reaction was started upon the introduction of the initiator solution, and the reaction time was roughly 1 hour. The average particle size determined by dynamic light scattering was 90 nm. Size exclusion chromatography analysis showed Mn, Mw and PDI values of 495 kg/mol, 944 kg/mol and 1.9, respectively.

Graphene/PS composites processing

Graphene was synthesized via oxidation of graphite (Hummers method) , followed by ultrasonication and subsequent reduction following the method described by Stankovich et al.^[5, 14] The oxidation of graphite to graphite oxide was accomplished by treating graphite with essentially a water-free mixture of concentrated sulfuric acid, sodium nitrate and potassium permanganate. The entire process requires about three hours for completion. The obtained graphite oxide was exfoliated in order to generate graphene oxide sheets by tip sonication with a horn sonicator Sonic Vibracell VC750 with a cylindrical tip (13 mm end cap diameter). The frequency was fixed at (20+/- 2.0) kHz with an amplitude of 30%. The sheets were reduced for 72 h with hydrazine at 120 °C in the presence of a ten-fold excess (wt/wt) of PSS. After its preparation, graphene covered with PSS was filtered off and dried under vacuum. The final PSS content (30%) was determined by elemental analysis. The product was then redispersed in water by a 40 minutes sonication process and then mixed with PS latex, the mixture was frozen in liquid nitrogen for several minutes and the frozen water was removed with a Christ Alpha 2–4 freeze dryer operated at 0.2 mbar and 20 °C overnight. The resulting composite powder was compression molded into films for 20 min at 180 ° C between Teflon sheets with a Collin Press 300G.

When preparing nanocomposites based on graphene oxide reduced in-situ graphene oxide (without surfactant) was mixed with PS latex followed by freeze-drying and compression molding as described above.

UV–Vis spectroscopic measurements

UV–Vis absorption spectra were recorded with a Hewlett–Packard 8453 spectrometer

operating between 200 and 1100 nm, following a procedure described in literature for carbon nanotube dispersions. Small sample volumes (about 30 μl each, thus the sonicated volume under investigation is almost unchanged during the whole experiment) were taken regularly during the second sonicating process of the reduced graphene loaded with PSS and diluted, resulting in a graphene concentration of 0.03 mg/ml.

Electrical conductivity measurements

The electrical conductivity was measured using a standard four-point method. Parallel contact lines 1 cm in length and with a 1 cm interval were drawn with conductive-silver paint (Fluka) on the composite film, and all conductivity measurements were performed at room temperature with a Keithley 6512 programmable electrometer. For each sample, conductivity data represent the average value of 10 consecutive measurements.

Scanning Electron Microscopy Analyses

The images of Gr/PS composite films were obtained with a Quanta 3D FEG (Fei Co.) equipped with a field emission electron source. High vacuum conditions were applied and a secondary electron detector was used for image acquisition. No additional sample treatment, such as surface etching or coating with a conductive layer, has been applied before surface scanning. Standard acquisition conditions for charge contrast imaging were used.^[4]

Atomic force microscopy (AFM) Investigations

AFM characterization of graphite oxide platelets was performed with a Nanoscope 3A instrument (Veeco) operated in normal tapping mode. The substrate used for filler deposition was mica. The conductive AFM (C-AFM) measurements on composites cross sections were performed by an NTEGRA Tomo (NT-MDT Co.). The device is a combination of a microtome EM UC6-NT (Leica) and an SPM measuring head. Such design allows for alternate microtome cutting and SPM measurements of the sample block-face.^[15] The local current measurements were performed in C-AFM mode with a gold-coated silicon cantilever NSC36/Cr-Au (Micromash). The sample was electrically connected to a grounded holder; a bias of 2 V was applied.

2.5. References

- [1] A. Dufresne, M. Paillet, J. L. Putaux, R. Canet, F. Carmona, P. Delhaes, S. Cui, *Journal of Materials Science* **2002**, *37*, 3915.
- [2] J. C. Grunlan, A. R. Mehrabi, M. V. Bannon, J. L. Bahr, *Advanced Materials* **2004**, *16*, 150.
- [3] O. Regev, P. N. B. ElKati, J. Loos, C. E. Koning, *Advanced Materials* **2004**, *16*, 248.
- [4] J. Loos, A. Alexeev, N. Grossiord, C. E. Koning, O. Regev, *Ultramicroscopy* **2005**, *104*, 160.
- [5] W. S. Hummers, R. E. Offeman, *Journal of the American Chemical Society* **1958**, *80*, 1339.
- [6] M. C. Hermant, N. M. B. Smeets, R. C. F. van Hal, J. Meuldijk, H. P. A. Heuts, B. Klumperman, A. M. van Herk, C. E. Koning, *E-Polymers* **2009**, *022*, 1.
- [7] M. C. Hermant, B. Klumperman, A. V. Kyrlyuk, P. van der Schoot, C. E. Koning, *Soft Matter* **2009**, *5*, 878.
- [8] N. Grossiord, J. Loos, L. van Laake, M. Maugey, C. Zakri, C. E. Koning, A. J. Hart, *Advanced Functional Materials* **2008**, *18*, 3226.
- [9] J. Yu, K. Lu, E. Sourty, N. Grossiord, C. E. Koning, J. Loos, *Carbon* **2007**, *45*, 2897.
- [10] M. Ouyang, J. L. Huang, C. L. Cheung, C. M. Lieber, *Science* **2001**, *292*, 702.
- [11] D. Chen, H. Zhu, T. Liu, *Acs Applied Materials & Interfaces* **2010**, *2*, 3702.
- [12] K. Liu, L. Chen, Y. Chen, J. Wu, W. Zhang, F. Chen, Q. Fu, *Journal of Materials Chemistry* **2011**, *21*, 8612.
- [13] Z. Xu, C. Gao, *Macromolecules* **2010**, *43*, 6716.
- [14] S. Stankovich, R. D. Piner, X. Q. Chen, N. Q. Wu, S. T. Nguyen, R. S. Ruoff, *Journal of Materials Chemistry* **2006**, *16*, 155.
- [15] A. Alekseev, A. Efimov, K. B. Lu, J. Loos, *Advanced Materials* **2009**, *21*, 4915.

Chapter 3

The use of surfactants for dispersing carbon nanotubes and graphene to make conductive nanocomposites.

ABSTRACT: Applications of composites based on carbon nanotubes and graphene require their exfoliation and dispersion in a polymer matrix. One of the main approaches to disperse and exfoliate carbon nanotubes and graphene is based on the use of surfactants. Here we review the surfactants utilized for dispersing carbon nanotubes and graphene, the mechanisms of filler stabilization and the methods for composites preparation based on the use of surfactants to get conductive polymer composites with minimum nanofiller loading.

3.1. Introduction

In the field of conductive polymer nanocomposites researchers are usually aiming at a controlled and low percolation threshold and a satisfactory overall conductivity combined with enhanced mechanical properties. Tuning these properties is always a challenge, as many parameters are involved and play a role in the system, starting from the selection of the components (filler, polymer matrix plus optional surfactant), passing through the optimum ratio filler/matrix or filler/surfactant/matrix and finishing with one of the known methods used for obtaining a good nanofiller dispersion and processing of the composite.

A great deal of attention has been given to the use of carbon nanotubes (CNTs), and more recently to graphene, in composite materials to harness their exceptional mechanical and electrical properties.^[1-3] A large part of graphene/CNTs polymer composites exploits these fillers, dispersed in an insulating matrix, to provide a conductive path for applications ranging from electronics to automotive and aerospace sectors, such as electrostatic dissipation, multilayer printed circuits, and transparent conductive coatings.^[4-7] The aims are to develop easily processable materials for future applications in which metals and/or semiconductors are currently preferred.

Important points when using CNTs or graphene in nanocomposites are the dispersion of the filler in a polymer matrix as well as the quality of the filler–matrix interface; the bottleneck is that as-produced fillers tend to be held together in bundles/agglomerates by very strong van der Waals interactions and/or entanglements.

Various methods have been developed in recent years to efficiently disperse individual CNTs in a polymer matrix. Direct mixing of the CNTs and the polymer, with or without the help of a solvent, has proven to be efficient and appears to be the easiest and least laborious way to achieve this goal.^[8, 9] On the other hand, the dispersion of the nanotubes in a polymer matrix is often rather inhomogeneous, even sometimes with formation of millimeter-scale inhomogeneities. However, the existence of a certain amount of agglomerates can be a key factor in considerable lowering the value of the percolation threshold and increasing the conductivity.^[10-13] Modifying either the nanofiller surface itself or the polymer matrix by functionalization improves the quality of the interface between two components of the nanocomposite by enhancing the interfacial interactions, but this approach has some drawbacks. In one possible case, the interaction of the filler with the polymer is realized by covalent binding, and in another case, by means of $\pi - \pi$ stacking. Both approaches lead to disturbances of the π -electrons delocalization of the graphene/CNTs surfaces, which results in a

significant deterioration of its electrical properties. Another main approach to incorporate a nanofiller into a polymer matrix is based on the use of a third component, i.e. a surfactant.

In this review the main approaches recently used to produce graphene/CNTs dispersions and conductive CNTs/graphene-based polymer composites with the help of surfactants are discussed and highlighted in terms of importance according to the authors. The main focus is given to water-based systems.

The methods for nanocomposite production inspired by the strategy utilizing surfactants are mainly based on the so-called latex-technology, although in-situ emulsion polymerization and spraying of surfactant-aided exfoliated nanofiller on polymer powder followed by dispersion in xylene and solution-casting have been also utilized.^[14-16] The basic concept consists of the generation of a stable, mixed colloidal system containing both a suspension of individual CNTs/graphene sheets stabilized by surfactant molecules in water and polymer latex particles, also stabilized by surfactants. After the removal of water, the resulting powder can be processed by e.g. compression molding into a desired shape, preserving in most cases the dispersion and exfoliation of the filler in the polymer matrix. The advantages of this technique are obvious: it is easy, versatile, reproducible, and reliable. This approach allows composite production with a relatively homogeneous dispersion of the nanofiller into the polymer matrix, low percolation thresholds and good conductivity levels. It is very flexible with respect to the choice of the polymer matrix: it can be applied to any polymer that can either be synthesized by emulsion polymerization, or brought into a polymer latex form in an artificial way. It does not require the use of toxic and inflammable solvents and is safe and environmentally friendly. Furthermore, since the CNT walls are not chemically modified, their properties are preserved. A drawback is that the mechanical properties of the nanocomposite deteriorate because of the high amount of surfactant necessary for the particles stabilization and realizing that the surfactant remains present in the final polymer nanocomposite. The tensile strength and modulus after processing are below the values for the neat polymers, but this seems to be not a major problem if one focuses on electrical properties.

3.2. Mechanism of stabilization

In a typical dispersion procedure, horn or bath sonication for a determined period of time debundles CNTs or exfoliates graphene platelets into individual tubes or sheets and/or thin bundles respectively, which subsequently are stabilized by the surfactant by steric and/or electrostatic repulsions. During sonication, the mechanical energy provided overcomes the van der Waals

interactions between the CNTs bundles or graphene platelets leading to filler exfoliation, whereas at the same time surfactant molecules adsorb onto the surface of the filler.^[17]

Colloidal particles stabilization mechanism is described by the Derjaguin-Landau-Verwey-Overbeek (DLVO) theory and usually relies on the presence of a surface charge which can be due to deprotonation of surface groups or adsorption of ions from the solvent to the surface of the colloid. The surface charge attracts a diffuse layer of counter-ions from the solvent forming an electric double layer which has a diffuse nature due to Brownian motion. It results in a creation of an effective surface charge which in turn results in Coulomb repulsion between nearby charged colloidal particles.^[18, 19] This can be applied to CNTs and graphene, introducing a temporary and removable surface charge, by allowing surfactant molecules to adsorb onto the filler surface via their hydrophobic tails. Usually an ion becomes dissociated from the hydrophilic head groups and acts as a counter-ion. The adsorbed molecular ions then interact with water.^[20] The magnitude and sign of the effective charge is associated with the double layer through the zeta potential ζ . This is the electrostatic potential at the edge of the layer of bound tail groups.^[20, 21] When dispersing CNTs the surfactant concentration generally needs to be above the critical micelle concentration (CMC) and the surfactant concentration also needs to exceed the CNTs concentration.^[22-27] The latter condition is not always justified when dispersing graphene as some surfactants perform better at concentrations below the CMC and not exceeding the graphene concentration.^[28] The dispersion quality improves as the filler concentration decreases.^[24] The dispersion quality and degree of the exfoliation/individualization of CNTs and graphene scale with ζ . Interestingly, that in contrast to CNTs for graphene this occurs within two separated groups of ionic surfactants: the sulfids (sodium dodecylbenzene sulfonate (SDBS), sodium dodecyl sulfate (SDS), lithium dodecyl sulfate (LDS)); and other ionic surfactants. As ζ represents the electrostatic potential at the edge of the layers of bound ions, one can imagine that ζ can be increased by maximizing the surface charge in this layer.^[21, 22] This tempts one to predict that low molecular surfactants, that pack tightly on the CNTs and graphene surface, are ideal.^[21, 22] Non-ionic surfactants used for CNTs and graphene dispersions have a hydrophobic tail and a long hydrophilic part. For these surfactants the stabilization mechanism tends to be based on steric effects. However additional stabilization factors were found for non-ionic surfactants, i.e. based on the presence of acid groups and ether linkages interacting with water and on the presence of a negative ζ values due to adsorbed impurities.^[21]

Surfactant adsorption at interfaces has been widely studied because of its importance. SDS is one of the most frequently used surfactants. Various configurations of SDS molecules on the surface,

e.g. of the CNTs, can be envisioned. O'Connell et al. proposed a perpendicular orientation of SDS molecules to the surface of nanotubes (**Figure 1**).^[29] However, other studies showed that both anionic and cationic surfactants, strongly aligning along the graphite symmetry axis, self-assemble into so-called half-cylinder structures on a graphite surface, in that case the hydrophobic part is adsorbed on the graphite by Van der Waals interactions following the carbon network and the hydrophilic part of the surfactant is oriented towards the aqueous phase.^[30, 31] Similar half-cylinder structures perpendicular to the tube axis were found on the surface of CNTs when utilizing ionic surfactants for their dispersion (**Figure 1**).^[32] Unlike ionic surfactants, Triton X-100, a non-ionic surfactant with a polyoxyethylene chain linked to an aromatic ring, is physically adsorbed on the surface of the CNTs through π -stacking interactions, leading to a full coating of the tube without any structural organization.^[32]

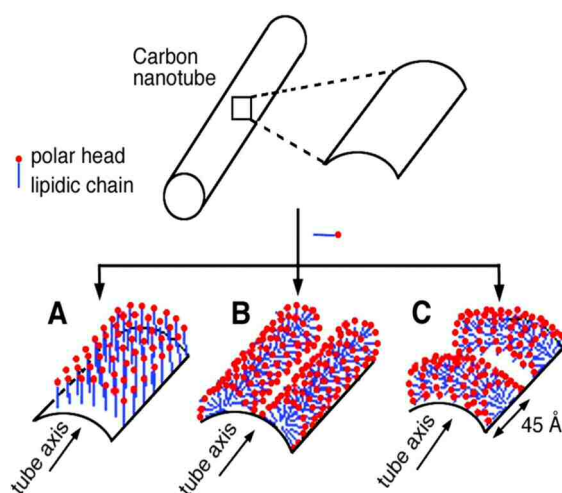


Figure 1. Different possible organizations of the SDS molecules on the surface of a CNT. (a) The SDS molecules adsorb perpendicular to the surface of the nanotube, forming a monolayer. (b) The SDS molecules organize into half-cylinders oriented parallel to the tube axis. (c) The SDS molecules form half-cylinders oriented perpendicular to the tube axis.^[32] (From ref. 32. Reprinted with permission of the American Association for the Advancement of Science (AAAS))

3.3. Dispersion of Graphene/CNTs in polymer matrix using water-based systems

3.3.1. Surfactants

A variety of common ionic surfactants such as SDBS, SDS, LDS, tetradecyl trimethyl ammonium bromide (TTAB) and sodium cholate (SC) have been shown to have the ability to stabilize exfoliated CNTs. The dispersion quality of these surfactant-CNTs dispersions varies as SDS > LDS > SDBS > TTAB > SC.^[22] SDS and SDBS are mainly used to decrease the aggregative tendency of CNTs in water. Among the non-ionic surfactants Triton X-100, Tween-80, Tween-60, Tween-20 were found to efficiently disperse CNTs in water.^[33, 34] Non-ionic surfactants lack the advantage of Coulomb repulsion to prevent CNTs from aggregating. Therefore, in this case the main factor determining the dispersability of carbon nanofillers in water is the presence of long and/or branched disordered polar chains, typically poly(ethylene glycol) chains. This results in a general trend of increasing efficiency with increasing molecular weight of the surfactant.^[33] The presence of an unsaturated carbon bond will provide a further advantage. This is due to the π -electronic affinity of the surfactant toward the CNTs benzene rings.^[35] According to the so-called “unzipping” mechanism the surfactant molecules intrude in the small spaces between individual tubes or sheets in the bundle and prevent them from re-aggregating.^[17] Accordingly, surfactants with too bulky hydrophobic groups less easily penetrate into the inter-tube or inter-platelet region, and show reduced debundling efficiency.^[34]

Mainly ultrasonication is applied for CNTs exfoliation, although gentle stirring was utilized for CNTs dispersion as well.^[33] The obvious disadvantage of the stirring procedure is that it takes a long time in comparison to the more efficient sonication procedures. Grossiord et al. mixed 0.5 wt % bundled single-walled carbon nanotubes (SWCNTs) with 20 mL of an aqueous solution containing 1 wt % of SDS. The resulting mixture was then tip-sonicated under mild conditions, i.e., at a power of 20 W. A total amount of energy of 100000 J and 5000 J was needed for complete exfoliation of HiPCO and Carbolex SWCNTs, respectively. This result implies that HiPCO CNTs exhibit stronger van der Waals attractions when bundled than the Carbolex CNTs. This difference in behavior might stem from the fact that Carbolex CNTs contain more amorphous carbon and/or catalyst impurities. These impurities can be present between the CNTs in the bundles, decreasing the contact area between CNTs in comparison with “cleaner” CNTs.^[26] Bergin et al. obtained debundled HiPCO

SWNTs at a concentration as high as 0.28 mg/ml by 1 hour bath sonication of CNTs in 5 mg/ml SDBS water solution.^[24]

Graphene, depending on the exfoliation procedure, can be dispersed with the aid of a range of surfactants. When obtained via liquid phase exfoliation of graphite in water graphene can be obtained and dispersed with the following surfactants: SDS, SDBS, LDS, cetyltrimethyl ammoniumbromide (CTAB), TTAB, SC, sodium deoxycholate (DOC), sodium taurodeoxycholate (TDOC), IGEPAL CO-890, Triton X-100, Tween 20 and Tween 80.^[21] Lotya et al. produced stable graphene dispersions of concentrations up to 0.3 mg/ml by 400 hours bath sonication of graphite in water in the presence of SC at a concentration of 0.1 mg/ml, which is below the CMC.^[28] When exfoliating graphite via an oxidation/reduction procedure with the aid of hydrazine, poly(sodium 4-styrene sulfonate) (PSS) of 70000 g/mol molecular mass is used, whereas it was shown that SDS and Triton X-100 do not prevent graphene reaggregation.^[36, 37] At first graphite is oxidized to graphite oxide and stirred to produce graphene oxide (GO). GO is reduced by hydrazine hydrate in the presence of PSS at a PSS:GO ratio of 10:1 followed, first, by filtration to remove the excess of PSS and, second, by tip-sonication to redisperse the PSS-covered graphene platelets and piles in water.^[36]

Conductive polymeric surfactants can be utilized to decrease the contact resistivity between the CNTs or graphene platelets in the final polymer nanocomposite. Poly(3,4-ethylenedioxythiophene)/poly(styrene sulfonate), also known as PEDOT/PSS, has successfully been used for dispersing CNTs in water. For complete exfoliation and for obtaining a stable aqueous dispersion of the CNTs a minimum PEDOT/PSS:CNTs ratio of 4:1 is required.^[38]

3.3.2. Composites

The first known reported latex-based process to disperse multi-walled carbon nanotubes (MWCNTs) into a polymer matrix has been described by Dufresne et al.^[39] MWCNTs dispersions were obtained by sonication of purified MWCNTs in an aqueous SDS solution. After a centrifugation step, the resulting supernatant was mixed with latex obtained by the copolymerization of styrene (35wt %) and butylacrylate (65 wt %). Films were made by casting in a mold and storing the mixture at a temperature allowing both the water to evaporate and the polymer particles to aggregate and to form a thin polymer film. The conductivity behavior was found to be characteristic for a very anisotropic behavior of the conducting filler network, with a percolation threshold at around 2.5 wt % and a maximum conductivity of about 1 S/m.

Another similar method was reported by Grunlan et al., in which poly(vinyl acetate) (PVAc) latex was used as a matrix. Untreated SWCNTs produced via the HiPCO process were exfoliated by sonication.^[40] Gum Arabic (GA) was used as a stabilizing agent. Once stabilized, the SWCNT dispersion was mixed with a PVAc emulsion to create a stable mixed colloidal system leading to conductive composites after drying. The percolation threshold measured was about 0.04 wt % with maximum conductivity around 30 S/m at 4 wt % of SWCNT loading. According to Grunlan et al. latex-based filler-polymer composites are expected to have a lower percolation threshold than similar composites of which the preparation method is based on polymer solutions or melts. Polymer solutions and melts are fundamentally different to emulsions due to their liquid-like ability to envelop added filler. During drying or cooling of a melt-based system, the CNTs or graphene sheets can freely organize themselves resulting in a relatively homogeneous conductive network and elevated percolation threshold. On the other hand a polymer emulsion consists of microscopic solid polymer particles suspended in water prior to film formation. The solid particles create excluded volume and essentially push the filler particles into the interstitial space between them. This mechanism dramatically reduces the space available for the CNTs or graphene to form conductive networks, which can result in a significantly reduced percolation threshold. In the presence of CNTs or graphene a “segregated network” evolves due to the inability of the filler to penetrate the polymer particles (Figure 2).^[40]

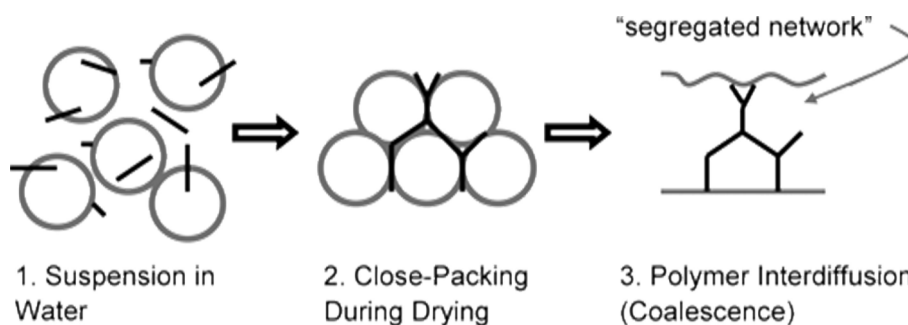


Figure 2. Schematic illustration of the drying process for SWCNTs-filled polymer emulsion. Initially the CNTs and polymer particles are uniformly suspended in water (1). Once most of the water has evaporated, the polymer particles assume a close-packed configuration with the CNTs occupying the interstitial space (2). Finally, the polymer particles will interdiffuse (i.e., coalesce) to form a coherent film, locking the SWCNTs within a segregated network.^[40] (From ref. 40. Copyright Wiley-VCH Verlag GmbH&Co. KGaA. Reproduced with permission)

Very similar to the described latex-based method the so-called latex technology was applied to make conductive polymer nanocomposites based on water-dispersed nanofillers and other polymer matrixes.^[14, 37, 41] Regev et al. compared percolation thresholds of polystyrene (PS)- and poly (methyl methacrylate) (PMMA)-based composites containing SWCNTs first dispersed in water with the aid of SDS and GA. SWCNTs were dispersed with the aid of the mentioned surfactants by tip-sonication and then mixed with a polymer latex prepared by emulsion polymerization followed by freeze-drying and subsequent compression molding, giving finally a composite film (**Figure 3**).^[42] Percolation for SDS-dispersed SWCNTs occurred at 0.28 wt % exhibiting a conductivity of 1 S/m just above 1 wt % loading and showing no significant difference in behavior between the composites based on PS and PMMA latexes.

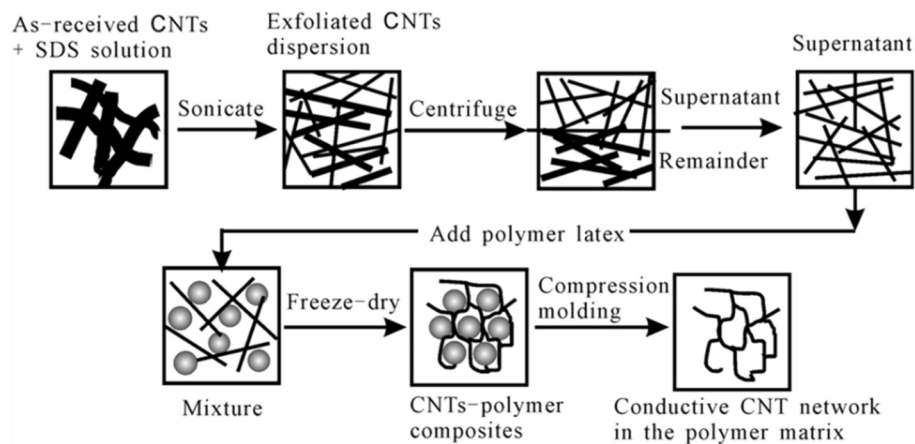


Figure 3 – Schematic description of the multi-step process for preparation of CNT/polymer composites by using latex technology.^[43] (Reprinted from ref. 43. Copyright 2007 with permission from Elsevier)

For GA-dispersed CNTs the percolation threshold occurred further above 1 wt % which can be attributed to the high molecular weight and bulkiness of GA (250 kD), which could induce local steric hindrance and concomitant contact resistance to the percolating conductive CNTs network.^[14] It was also found that changing the processing conditions, such as enhancing the temperature and the time of compression molding, lowers the percolation threshold and raises the conductivity of the nanocomposite by pushing the system towards its equilibrium state. As long as sufficiently high temperatures are used and enough time is given to the system to reach its equilibrium, the particle size of the polymer latex is expected to have a limited impact on the electrical conductivity of the

nanocomposite.^[23] The difference with the concept described by Grunlan is that no shear is applied in his system, whereas the concept used by Regev et al. introduced some shear during the melt-processing step, which results in dynamic percolation and in a system with enhanced electrical properties.^[40] Most probably this shear causes some aggregation of the perfectly dispersed nanofillers which seems to be required for the formation of contacts.

The influence of the characteristics of the CNTs on electrical conductivity of the polymer-based composites prepared via latex technology was studied. MWCNTs of different aspect ratio, namely 400 nm and 1200 nm length on average respectively and a similar 10 nm diameter, were utilized for the production of PS composites. Short CNTs were dispersed by tip-sonication with the aid of SDS at a weight ratio CNTs:SDS of 1:2, whereas for the exfoliation of long CNTs a weight ratio CNTs:surfactant of 1:7.5 was required. The longer MWCNTs had a much more perfect surface quality than the shorter ones. It was demonstrated that composites containing longer MWCNTs exhibited a lower percolation threshold and a much higher ultimate conductivity than the corresponding PS composites based on the shorter CNTs, namely 0.15 wt % vs 0.85 wt % and 10^3 S/m vs 1 S/m respectively.^[44] The difference in the ultimate conductivity can be attributed to the difference in structural quality between the two types of CNTs and to the higher length, which results in a lower contact resistivity, whereas the difference in percolation thresholds is due to the difference in the aspect ratio. It should be noted that the composites containing the long MWCNTs have a very high conductivity despite the high weight ratio SDS:CNTs.

Hermant et al. showed by the applying the latex concept that the molecular weight distribution (MWD) of the matrix material can strongly affect the percolation threshold of CNTs within both PMMA and PS matrixes. This indicates that the influence of low molar mass matrix material is important for different types of matrixes, and most probably can be generalized to other matrices. For both SWCNTs and MWCNTs dispersed in either of the matrixes, a significant decrease in the percolation threshold was observed upon the introduction of low molecular weight polymer, the shift being most pronounced for higher amounts of low molar mass polymer. A critical minimum loading of low molecular weight polymer introduced in the matrix by synthesizing a low molecular weight distribution next to a high molecular weight distribution of the polymer during emulsion polymerization is required to obtain a maximum reduction corresponding to a completely equilibrated network structure. The origin of this effect can be twofold: changes in MWD lead to rheological changes of the melt (i.e. a decrease in melt viscosity which facilitates the reorganization and the required aggregation) and the low molecular weight polymer may replace SDS from the CNTs surface (thereby changing the inter-

tube distances and/or electrical conduction across junctions). The minimal changes in the ultimate conductivity suggest that the tunneling behavior across inter-tube junctions is similar in all systems. Rheological changes can influence the extent to which the CNTs reach an equilibrium conformation during the processing stages of the composite preparation. Whether this equilibrium conformation is more or less aggregated than the initial dispersion state is not really proven, but it can definitely be said that allowing the composite to reach this state can be beneficial when trying to minimize the percolation threshold value.^[45]

Barraza and co-workers prepared SWCNT-PS and SWCNT-styrene-co-isoprene copolymer nanocomposites by using an original method based on mini-emulsion technology. SWCNTs were first exfoliated in water by sonication with the aid of the cationic surfactant cetyltrimethylammonium bromide (CTAB).^[15] The initiator (AIBN), previously dissolved in ethanol, was then added to the resulting SWCNT suspension. The above mentioned mixture was added under stirring to a mixture of solvent (hexadecane)/catalyst (PS-AlCl₃ acid complex)/monomer (styrene or mixture of styrene-co-isopropene). After an additional sonication step to obtain an emulsion, polymerization was finally carried out. A layer of polymer adsorbed on the surface of the CNTs bundles contributes to a better dispersion of the SWNTs in the polymer matrix. On the other hand, this layer minimizes the maximum conductivity value reached. Nevertheless, the resistivity decrease induced by the incorporation of SWNTs into the polymer matrix remains significant (from 10¹⁶ Ω/cm for the unmodified PS to 10⁶ Ω/cm for the SWNT-PS composite with 8.5 wt % of CNTs). The percolation threshold occurs between 4 and 8 wt % of CNTs.

Graphene produced out of graphite via the oxidation/reduction method in the presence of PSS has been also used as a filler for PS nanocomposites. The production of graphene was carried out in the presence of a ten-fold excess of PSS followed by filtration, which decreased the amount of PSS in the system resulting in a graphene/PSS dispersion with a PSS content of 40 wt %. The percolation threshold occurred at 0.9 wt % of graphene loading and a maximum conductivity of 15 S/m was measured for this system.^[37] Use of the conductive surfactant PEDOT:PSS for the preparation of stable SWCNTs dispersions decreases the percolation threshold of the PS composites and increases the ultimate conductivity for the same type of CNTs in comparison with conventional surfactants like SDS. CNTs were dispersed in water using an excess of PEDOT/PSS. It was found that for the optimal exfoliation of the CNTs a PEDOT/PSS:CNTs ratio of 4:1 is required. The percolation threshold occurred as low as 0.2 wt % of the SWCNTs loading. An ultimate conductivity of 500 S/m was reached.^[38] Recently Kyrylyuk et al. showed that the percolation threshold can be substantially

lowered by adding small quantities of conductive polymer latex to the CNTs/polymer latex system. Mixing colloidal particles of different sizes and shapes (in this case spherical latex particles and rod-like nanotubes) introduces competing length scales that can strongly influence the formation of the system-spanning networks that are needed to produce electrically conductive composites.^[46] Mixtures of SDS-stabilized SWCNTs, PS and PEDOT/PSS latexes were freeze dried and the resulting powder was compression molded to form the composite. The interplay between the different species in the dispersions leads to synergetic or antagonistic percolation, depending on the ease of charge transport between the various conductive components.

3.3.3. Thin transparent films

Recently in the field of transparent electrodes and conductive coatings, graphene and CNTs appeared as promising substitutes for indium tin oxide (ITO). Different approaches have been proposed in order to produce thin, transparent and highly conductive films. In general, most of them utilize water-based solutions of CNTs/graphene dispersed with the help of surfactants and/or conductive polymers as primary stage before casting or spin coating the films.

Attempts of creating free standing transparent films of pure graphene/CNTs have also been reported.^[47, 48] Ultrasonication of graphite for 140 min in the presence of surfactant such as SC, followed by centrifugation and filtration, yields transparent films with a conductivity up to 1.5×10^4 S/m. Similar results were obtained for SWCNTs/water systems sonicated in the presence of SDS and spray-coated on a glass substrate. The balance between the final conductivity values and the transparency still needs to be optimized in order to be able to apply these systems commercially in efficient way. Probably the presence of remaining surfactant is still an issue hindering conductivity in this case.

Similar methods were used for dispersing nanofillers in water and posterior mixing with polymer substrates. According to Paul et al. spraying of SWCNTs dispersions onto polyethylene terephthalate (PET) substrates yields highly transparent films with superior conductive properties as compared to similar films obtained via dip coating process.^[49] SDS in this case proved to be more efficient than SDBS and Triton X-100 in terms of the final conductivity of the composite.

The largest area dealing with thin transparent conductive films is related to the use of conductive polymers, i.e. PEDOT/PSS. The latter system is largely used for conductive coatings and more specifically as a thin layer covering ITO in polymer solar cells. Ergo, the idea of substituting ITO with transparent films of polymer nanocomposites of graphene/CNTs has recently been largely explored.

The advantage of this system is that PEDOT/PSS is commercially available as a water-based latex system, where the PSS polymer acts as surfactant, enabling the dispersion of the hydrophobic PEDOT particles. However, PSS is the doping agent for PEDOT, required for obtaining conductivity. The two aqueous dispersions of the PEDOT/PSS and the carbon nanofillers simply are mixed together. SDS was reported to be used for dispersing SWCNTs prior to mixing with PEDOT:PSS.^[50, 51] Still the final electrical resistance of the nanocomposite film surface is higher than that observed for ITO, but some other properties such as processability and flexibility of these nanocomposites polymer substrates make this approach promising. Similar results were obtained using a graphene/SDBS dispersion, which was prepared by SDBS-assisted exfoliation of graphite oxide and in-situ chemical reduction to graphene.^[6] Spin-coating of the mixed solution of surfactant-stabilized graphene and PEDOT/PSS yields a graphene composite electrode without the need for high temperature annealing and with a conductivity comparable to ITO systems. The technique shows great application potential in low-cost, energy-saving and high throughput manufacturing of optoelectronic devices.

3.4. Dispersion of Graphene/CNTs in a polymer matrix using organic solvents

3.4.1. Surfactants

Compared to water-soluble systems, thus far only limited research work has been carried out with surfactant-assisted dispersions in organic solvents. As opposed to aqueous solutions, hydrophobic carbon nanotubes are expected to be wetted by organic solvents and therefore to less self-assemble in bundles and ropes. However, carbon nanotubes were shown to exhibit a sufficient dispersibility only in a limited number of solvents, namely, dimethylformamide (DMF), dimethyl acetamide (DMAc), N-methyl-pyrrolidone (NMP), and chloroform.^[52, 53] Graphene has been successfully exfoliated in DMF, NMP, and cyclohexanone. The problem with these solvents is their high boiling points which requires high temperature for removing the solvent during processing. However, recently graphene exfoliation and dispersion in low boiling solvents such as chloroform, acetone and isopropanol was also demonstrated.^[54]

Most of the reported approaches using surfactants and organic solvents are directed to the improvements of thermo-mechanical properties.

Pristine MCWNTs were shown to form large agglomerates in polypropylene-decalin solution.^[35] Although surface functionalization of carbon nanotubes somewhat improved their dispersibility, additional surfactant assistance was required to obtain individual nanotubes. Within the Span (sorbitan) group of surfactants the state of dispersion was enhanced as the degree of tail unsaturation increased, reaching a maximum of three C=C bonds per tail in the case of Span-85 (sorbitan trioleate). This finding supports the assumption that attractive interactions are formed between CNT/graphene sheets and unsaturated bonds of surfactant molecules.

Physical association of polymers with carbon nanotubes surfaces was shown to enhance the dispersion of CNTs not only in water (as discussed before) but also in organic solvents.^[55] One of the mechanisms suggested is “wrapping”, which is believed to rely on specific interactions between a given polymer and the tubes.^[56] For example, the reversible association of SWNTs with linear polymers, namely polyvinyl pyrrolidone (PVP) and polystyrene sulfonate (PSS), in water was identified as being thermodynamically driven by the elimination of a hydrophobic interface between the tubes and the aqueous medium.^[56] A very different, kinetic mechanism suggests that a long-ranged entropic repulsion between polymer-decorated tubes acts as a barrier that prevents the tubes from approaching one another.^[57] Non-covalent modification of SWCNTs by encasing the tubes within micelles of cross-linked copolymer polystyrene-*block*-polyacrylic acid (PS-*b*-PAA) was demonstrated.^[55] CNTs were first ultrasonicated in a DMF solution of the copolymer and micellization of the amphiphile was induced by adding water to the nanotube suspension. Finally, the PAA blocks of the micellar shells were permanently cross-linked by adding a diamine linker. This encapsulation was shown to enhance the dispersion of SWCNTs in a variety of polar and nonpolar solvents.

A relatively new class of surfactants, i.e. gemini surfactants, were employed to achieve homogeneous and stable dispersions of CNTs in toluene. Gemini surfactants form a class of surfactants consisting of at least two hydrophobic chains and two hydrophilic moieties connected by a spacer group. Despite its rather complicated structure, a gemini surfactant has attractive properties such as a low CMC and a high surface or interfacial activity.^[58]

In addition to polymers conventional anionic surfactants such as SDBS have been utilized in systems containing organic solvents.^[59]

3.4.2. Composites

Sun et al. prepared PS composites based on CNTs dispersed in toluene with the aid of 6,6'-(butane-1,4-diylbis(oxy))bis(3-nonylbenzenesulfonic acid).^[58] Its molecular structure was designed to

meet the following requirements for a PS/CNT system and a solution mixing process: 1) two phenyl rings are introduced since their $\pi - \pi$ interaction with CNTs improves the ability of the CNTs dispersion and stabilization and, in addition, the interaction with the phenyl rings of PS is also favorable; 2) the butyl group in the spacer helps to increase the solubility in toluene (also a good solvent of PS) and the hydrophobicity; 3) the long alkyl chains are favorable for increasing the hydrophobic interaction and miscibility with PS. Note that the alkyl chain length can be neither too short (the extent of increase of the hydrophobic interaction and the miscibility is not enough), nor too long (the thermal stability may be deteriorated). The conductivity of the composites was shown to reach 4 S/m to which, the surfactant also proved to contribute a little. A PS composite containing only surfactant exhibits a conductivity up to 0.006 S/m.^[58]

Deng et al. carried out in-situ polymerizations to produce CNTs-Polyaniline (PANI) composites.^[59] Under continuous stirring in nitrogen atmosphere, chemicals are incorporated in the following order: first the surfactant (SDBS) in solvent (dimethylbenzene) and water, followed by the addition of the CNTs. The monomer (aniline) is then added, and finally the initiator (ammonium peroxydisulfate) is dissolved in a small amount of water to start the reaction. The observed conductive network of CNTs is partly due to the formation of crystalline PANI-chain bridges between the CNTs, which act as additional conductive pathways in the amorphous PANI matrix. The incorporation of 10 wt% of CNTs into the PANI matrix was shown to increase the conductivity from 2.6×10^{-1} S/m to 6.6 S/m with the percolation threshold occurring at 0.2 wt % of CNTs loading.

3.5. Conclusions and outlook

This review covers one of the main strategies developed during the recent years for incorporation of CNTs and graphene into a polymer matrix based on the use of surfactants for improving the nanofillers dispersion. Over the last decade enormous progress in understanding the stabilization mechanisms has been achieved and efficient methods to disperse both CNTs and graphene utilizing various surfactants have been developed. The composite preparation methods using this strategy are mainly based on latex technology. This route to incorporate nanofillers into a polymer matrix appears to be very promising since it is simple and environmentally friendly. Furthermore, production at a large industrial scale can be expected to be relatively easy to achieve. The technique is very successful to produce conductive nanocomposites with low percolation thresholds for both CNTs and graphene, as well as good ultimate conductivity levels. Furthermore, it is very flexible with respect to the choice of the polymer matrix: it can be applied to any polymer synthesized by emulsion

polymerization, or brought into a polymer latex form in an artificial way and can utilize polymers of both high and low molecular weight.

The large area of transparent conductive films utilizes surfactant-stabilized solutions of CNTs and graphene, where commonly used anionic surfactants as well as conductive polymeric surfactants are applied for stabilizing the carbon nanofillers dispersion.

The surfactants mainly used for dispersion CNTs and graphene in water for subsequent composite preparation are low-molecular weight ionic surfactants. Although investigators aim for as much exfoliated material as possible it's not obvious that a dispersion of perfectly individualized carbon nanofillers in a polymer matrix results in a low percolation threshold and in a high conductivity above the percolation threshold, since some results indicate the opposite, namely that some limited agglomeration favors the formation of a network structure and results in high conductivity values.

The use of non-ionic surfactants, which were proven to disperse both CNTs and graphene, will probably have some disadvantages in terms of both percolation threshold and conductivity values due to their long hydrophilic tail and bulky character. The long tails will result in a relatively big distance between the tubes/graphene platelets which in turn will result in lack of contact. Nevertheless, the advantage of using such surfactants is apparent: when using a polymer latex for nanocomposite production, the CNTs/graphene dispersion stabilized with non-ionic surfactant can be mixed with any latex, irrespective of the charge of the polymer particles.

In addition to the mainly used water-based systems, some work has been done on the use of the systems where surfactants were applied for dispersion of CNTs in organic solvents. The polymer composites based on these dispersions also showed some promising results in terms of conductivity. However, the necessity to use surfactants for dispersing carbon nanofillers in organic solvents has decreased since it was recently discovered that CNTs and especially graphene can be dispersed not just in high boiling point solvents but also in low boiling point solvents, which widens the range of solvents to choose from, for composites preparation considerably. However, from environmental point of view the water/surfactant-based latex approach to make conductive polymer/carbon nanofillers composites seems to be the preferred route.

3.6. References

- [1] M. M. J. Treacy, T. W. Ebbesen, J. M. Gibson, *Nature* **1996**, *381*, 678.
- [2] J. W. G. Wildoer, L. C. Venema, A. G. Rinzler, R. E. Smalley, C. Dekker, *Nature* **1998**, *391*, 59.

- [3] K. S. Novoselov, A. K. Geim, S. V. Morozov, D. Jiang, M. I. Katsnelson, I. V. Grigorieva, S. V. Dubonos, A. A. Firsov, *Nature* **2005**, *438*, 197.
- [4] J. G. Smith, D. M. Delozier, J. W. Connell, K. A. Watson, *Polymer* **2004**, *45*, 6133.
- [5] J. H. Chen, M. Ishigami, C. Jang, D. R. Hines, M. S. Fuhrer, E. D. Williams, *Advanced Materials* **2007**, *19*, 3623.
- [6] H. X. Chang, G. F. Wang, A. Yang, X. M. Tao, X. Q. Liu, Y. D. Shen, Z. J. Zheng, *Advanced Functional Materials* **2011**, *20*, 2893.
- [7] M. Lotya, Y. Hernandez, P. J. King, R. J. Smith, V. Nicolosi, L. S. Karlsson, F. M. Blighe, S. De, Z. M. Wang, I. T. McGovern, G. S. Duesberg, J. N. Coleman, *Journal of the American Chemical Society* **2009**, *131*, 3611.
- [8] H. Wang, E. K. Hobbie, *Langmuir* **2003**, *19*, 3091.
- [9] N. H. Tai, M. K. Yeh, H. H. Liu, *Carbon* **2004**, *42*, 2774.
- [10] J. O. Aguilar, J. R. Bautista-Quijano, F. Aviles, *Express Polymer Letters* **2010**, *4*, 292.
- [11] J. Li, P. C. Ma, W. S. Chow, C. K. To, B. Z. Tang, J.-K. Kim, *Advanced Functional Materials* **2007**, *17*, 3207.
- [12] C. A. Martin, J. K. W. Sandler, M. S. P. Shaffer, M. K. Schwarz, W. Bauhofer, K. Schulte, A. H. Windle, *Composites Science and Technology* **2004**, *64*, 2309.
- [13] J. J. Hernandez, M. C. Garcia-Gutierrez, A. Nogales, D. R. Rueda, M. Kwiatkowska, A. Szymczyk, Z. Roslaniec, A. Concheso, I. Guinea, T. A. Ezquerro, *Composites Science and Technology* **2009**, *69*, 1867.
- [14] O. Regev, P. N. B. ElKati, J. Loos, C. E. Koning, *Advanced Materials* **2004**, *16*, 248.
- [15] H. J. Barraza, F. Pompeo, E. A. O'Rear, D. E. Resasco, *Nano Letters* **2002**, *2*, 797.
- [16] Q. H. Zhang, D. R. Lippits, S. Rastogi, *Macromolecules* **2006**, *39*, 658.
- [17] M. S. Strano, V. C. Moore, M. K. Miller, M. J. Allen, E. H. Haroz, C. Kittrell, R. H. Hauge, R. E. Smalley, *Journal of Nanoscience and Nanotechnology* **2003**, *3*, 81.
- [18] S. S. Vojutskiy, *Course of Colloid Chemistry*, Chemistry, Moscow, **1975**.
- [19] R. J. Hunter, *Introduction to Modern Colloid Science*, Oxford Science Publications, Oxford, **1994**.
- [20] J. N. Coleman, *Advanced Functional Materials* **2009**, *19*, 3680.
- [21] R. J. Smith, M. Lotya, J. N. Coleman, *New Journal of Physics* **2010**, *12*, 125008.
- [22] Z. Sun, V. Nicolosi, D. Rickard, S. D. Bergin, D. Aherne, J. N. Coleman, *Journal of Physical Chemistry C* **2008**, *112*, 10692.
- [23] N. Grossiord, P. J. J. Kivit, J. Loos, J. Meuldijk, A. V. Kyrylyuk, P. van der Schoot, C. E. Koning, *Polymer* **2008**, *49*, 2866.
- [24] S. D. Bergin, V. Nicolosi, H. Cathcart, M. Lotya, D. Rickard, Z. Sun, W. J. Blau, J. N. Coleman, *Journal of Physical Chemistry C* **2008**, *112*, 972.
- [25] B. Vigolo, A. Penicaud, C. Coulon, C. Sauder, R. Pailler, C. Journet, P. Bernier, P. Poulin, *Science* **2000**, *290*, 1331.

- [26] N. Grossiord, O. Regev, J. Loos, J. Meuldijk, C. E. Koning, *Analytical Chemistry* **2005**, *77*, 5135.
- [27] J. Yu, N. Grossiord, C. E. Koning, J. Loos, *Carbon* **2007**, *45*, 618.
- [28] M. Lotya, P. J. King, U. Khan, S. De, J. N. Coleman, *Acs Nano* **2010**, *4*, 3155.
- [29] M. J. O'Connell, S. M. Bachilo, C. B. Huffman, V. C. Moore, M. S. Strano, E. H. Haroz, K. L. Rialon, P. J. Boul, W. H. Noon, C. Kittrell, J. P. Ma, R. H. Hauge, R. B. Weisman, R. E. Smalley, *Science* **2002**, *297*, 593.
- [30] H. N. Patrick, G. G. Warr, *Colloids and Surfaces a-Physicochemical and Engineering Aspects* **2000**, *162*, 149.
- [31] I. A. Aksay, M. Trau, S. Manne, I. Honma, N. Yao, L. Zhou, P. Fenter, P. M. Eisenberger, S. M. Gruner, *Science* **1996**, *273*, 892.
- [32] C. Richard, F. Balavoine, P. Schultz, T. W. Ebbesen, C. Mioskowski, *Science* **2003**, *300*, 775.
- [33] W. Wenseleers, Vlasov, II, E. Goovaerts, E. D. Obraztsova, A. S. Lobach, A. Bouwen, *Advanced Functional Materials* **2004**, *14*, 1105.
- [34] V. C. Moore, M. S. Strano, E. H. Haroz, R. H. Hauge, R. E. Smalley, J. Schmidt, Y. Talmon, *Nano Letters* **2003**, *3*, 1379.
- [35] L. Vaisman, G. Marom, H. D. Wagner, *Advanced Functional Materials* **2006**, *16*, 357.
- [36] S. Stankovich, R. D. Piner, X. Q. Chen, N. Q. Wu, S. T. Nguyen, R. S. Ruoff, *Journal of Materials Chemistry* **2006**, *16*, 155.
- [37] E. Tkalya, M. Ghislandi, A. Alekseev, C. Koning, J. Loos, *Journal of Materials Chemistry* **2010**, *20*, 3035.
- [38] M. C. Hermant, B. Klumperman, A. V. Kyrlyuk, P. van der Schoot, C. E. Koning, *Soft Matter* **2009**, *5*, 878.
- [39] A. Dufresne, M. Paillet, J. L. Putaux, R. Canet, F. Carmona, P. Delhaes, S. Cui, *Journal of Materials Science* **2002**, *37*, 3915.
- [40] J. C. Grunlan, A. R. Mehrabi, M. V. Bannon, J. L. Bahr, *Advanced Materials* **2004**, *16*, 150.
- [41] N. Grossiord, J. Loos, C. E. Koning, *Journal of Materials Chemistry* **2005**, *15*, 2349.
- [42] J. Loos, A. Alexeev, N. Grossiord, C. E. Koning, O. Regev, *Ultramicroscopy* **2005**, *104*, 160.
- [43] J. Yu, K. Lu, E. Sourty, N. Grossiord, C. E. Koning, J. Loos, *Carbon* **2007**, *45*, 2897.
- [44] N. Grossiord, J. Loos, L. van Laake, M. Maugey, C. Zakri, C. E. Koning, A. J. Hart, *Advanced Functional Materials* **2008**, *18*, 3226.
- [45] M. C. Hermant, N. M. B. Smeets, R. C. F. van Hal, J. Meuldijk, H. P. A. Heuts, B. Klumperman, A. M. van Herk, C. E. Koning, *E-Polymers* **2009**, *022*, 1.
- [46] A. V. Kyrlyuk, M. C. Hermant, T. Schilling, B. Klumperman, C. E. Koning, P. van der Schoot, *Nature Nanotechnology* **2011**, *6*, 364.

- [47] Q. F. Liu, T. Fujigaya, H. M. Cheng, N. Nakashima, *Journal of the American Chemical Society* **2010**, *132*, 16581.
- [48] S. De, P. J. King, M. Lotya, A. O'Neill, E. M. Doherty, Y. Hernandez, G. S. Duesberg, J. N. Coleman, *Small* **2010**, *6*, 458.
- [49] S. Paul, Y. S. Kang, J. H. Yim, K. Y. Cho, D. W. Kim, *Current Applied Physics* **2010**, *10*, E101.
- [50] E. Kymakis, G. Klapsis, E. Koudoumas, E. Stratakis, N. Kornilios, N. Vidakis, Y. Franghiadakis, *European Physical Journal-Applied Physics* **2006**, *36*, 257.
- [51] J. Li, L. Hu, L. Wang, Y. Zhou, G. Gruner, T. J. Marks, *Nano Letters* **2006**, *6*, 2472.
- [52] S. D. Bergin, Z. Sun, D. Rickard, P. V. Streich, J. P. Hamilton, J. N. Coleman, *Acs Nano* **2009**, *3*, 2340.
- [53] H. T. Ham, Y. S. Choi, I. J. Chung, *Journal of Colloid and Interface Science* **2005**, *286*, 216.
- [54] A. O'Neill, U. Khan, P. N. Nirmalraj, J. Boland, J. N. Coleman, *Journal of Physical Chemistry C* **2011**, *115*, 5422.
- [55] Y. J. Kang, T. A. Taton, *Journal of the American Chemical Society* **2003**, *125*, 5650.
- [56] M. J. O'Connell, P. Boul, L. M. Ericson, C. Huffman, Y. H. Wang, E. Haroz, C. Kuper, J. Tour, K. D. Ausman, R. E. Smalley, *Chemical Physics Letters* **2001**, *342*, 265.
- [57] R. Shvartzman-Cohen, E. Nativ-Roth, E. Baskaran, Y. Levi-Kalisman, I. Szleifer, R. Yerushalmi-Rozen, *Journal of the American Chemical Society* **2004**, *126*, 14850.
- [58] G. Sun, G. Chen, J. Liu, J. Yang, J. Xie, Z. Liu, R. Li, X. Li, *Polymer* **2009**, *50*, 5787.
- [59] J. G. Deng, X. B. Ding, W. C. Zhang, Y. X. Peng, J. H. Wang, X. P. Long, P. Li, A. S. C. Chan, *European Polymer Journal* **2002**, *38*, 2497.

Chapter 4

Experimental and theoretical study of the influence of the state of dispersion of graphene on the percolation threshold of conductive graphene/polystyrene nanocomposites

ABSTRACT. The effect of the dispersed state of graphene is studied as a factor influencing the electrical percolation threshold of graphene/polystyrene (PS) nanocomposites. We find the percolation threshold of our nanocomposites, prepared with graphene dispersions of different thermodynamic stability, degree of exfoliation and size polydispersity, to range from 2 to 4.5 wt %. Connectedness percolation theory is applied to calculate percolation thresholds of the corresponding nanocomposites, based on the premise that size polydispersity of graphene platelets in the corresponding solutions must have a large influence on it. Theory and experimental results agree qualitatively.

4.1. Introduction

At the present time, a great deal of attention is being paid to the electrical properties of graphene-based polymer nanocomposites. The large variation in the reported percolation threshold values, which ranges from 0.1 to greater than 2 wt%, indicates that the dispersion states and other properties of graphene, affected by different processing conditions, must be important in determining the electrical properties of graphene/polymer nanocomposites.^[1-6] For carbon nanotubes/polymer nanocomposites the dispersed state of CNTs has been recognized as one of the critical factors governing the conductivity of composites as well as their physical properties. It is generally accepted that well-dispersed CNTs within the polymer matrix enhance the physical properties of the composite. However, a few studies suggest that CNT agglomeration could favor the formation of a percolating network.^[7-10] In this work the dispersed state of graphene in a polystyrene (PS) matrix is discussed as a parameter influencing the percolation threshold of the corresponding composites prepared with the well-known latex technology. In this work the dispersed state of graphene in a polystyrene (PS) matrix is discussed as a parameter influencing the percolation threshold of the corresponding composites prepared with latex technology.^[2, 11-14]

4.2. Results and discussion

4.2.1. Characterization of the nanofiller and its dispersions

Graphene used in this study was obtained by two different methods: thermal treatment of graphite oxide; and liquid-phase exfoliation of graphite.^[15, 16] Four aqueous graphene dispersions exhibiting different degrees of exfoliation and stability were prepared with the aid of sonication. Dispersions A, A-LC (LC standing for "low concentration") and A-HE (HE standing for high energy) were prepared from graphene, produced by thermal reduction of graphite oxide.^[15] Dispersions A and A-HE were prepared under similar conditions, meaning that the same energy was provided to both systems during the sonication process (**Table 1**).

The difference between those two are the graphene and surfactant concentrations; 1 mg/ml, 1:1 weight ratio graphene/sodium cholate (SC) and 0.1 mg/ml, 1:1 graphene/SC weight ratio for dispersion A and for dispersion A-HE respectively, meaning that dispersion A-HE was exposed to a ten times larger amount of energy per graphene unit than dispersion A. Dispersion A-LC with a graphene concentration of 0.1 mg/ml and a ratio graphene/SC 1:1 was exposed to a ten times lower amount of energy than dispersions A and A-HE.

Dispersion state vs. percolation threshold

Sample	Concentration, mg/ml	Energy provided during sonication, J	Added amount of energy per mg of graphene, J
A	1	2 200 000	22000
A-LC	0.1	220 000	22000
A-HE	0.1	2 200 000	220000
B	0.1	-	-

Table 1. Graphene dispersion used for composites preparation.

This implies that the absorbed amount of energy per graphene unit was the same as in the case of sample A and ten times less than for sample A-HE. Dispersion B was prepared from graphene produced by the liquid-phase exfoliation of graphite. Graphene for dispersion B did not have to be sonicated additionally, since it had been obtained in the form of a stable aqueous solution after 100 hours sonication of graphite of concentration 5 mg/ml in 0.1 mg/ml solution of SC, followed by centrifugation, resulting in a final concentration of graphene of 0.1 mg/ml.^[16]

The two different kinds of graphene used in this study were characterized by Raman spectroscopy. The 633 nm Raman spectra of graphene and bulk graphite are compared in **Figure 1**. The two most intense features for graphite are the *G* peak at $\sim 1575 \text{ cm}^{-1}$ and the *2D* peak at $\sim 2681 \text{ cm}^{-1}$. The *G* band represents a tangential shear mode of carbon atoms that corresponds to the stretching mode in the graphite plane. The *G* peak is due to the doubly degenerate zone center mode.^[17] The *2D* band has nothing to do with the *G* peak, but represents a second-order process from two-zone boundary longitudinal optical phonons. It is an intrinsic property of graphite, and present even in defect-free structures. Since zone-boundary phonons do not satisfy the fundamental Raman selection rule, they are not seen in first order Raman spectra of defect-free graphite. Such phonons give rise to a peak at $\sim 1350 \text{ cm}^{-1}$ in defect-containing graphite, called the *D* peak.^[18]

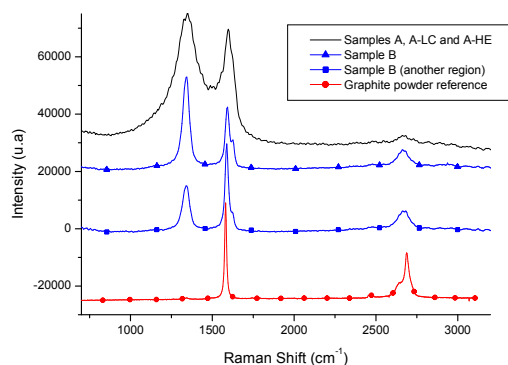


Figure 1. Raman spectra of graphene used for preparation of the aqueous dispersions.

The conventional Raman spectrum of graphite and graphene layers has been studied in great detail by Ferrari et al.^[18] Graphene shows a Raman spectrum very similar to that of graphite, and the differences observed mirror the missing interaction between the layers. The *2D* peak (second-order) changes in shape, width, and position with an increasing number of layers, reflecting the change in the electron bands via a double resonant Raman process. The *G* peak should exhibit slight shifts in position and a great decrease in the peak intensity of the ratio *G/2D*.

The spectra in Figure 1 show a significant change in shape and intensity of the *2D* peak of graphene compared to bulk graphite. The *2D* peak in bulk graphite presents a shoulder with roughly one fourth of the height of the *G* peak followed by a main peak with roughly half of the height of the *G* peak. For graphene sample B a single *2D* peak can be observed that is slightly shifted to lower wavenumbers. The intensity of the peak is never higher than the one obtained for the *G* peak, as expected for single layer graphene. We note that all graphene spectra have *D* bands significantly more intense than that of the graphite powder, indicating that processing, more specifically sonication, induces defects. We can divide such defects into two main types: body defects, such as point defects on the basal plane, and edge defects. The introduction of edge defects is unavoidable during processing as sonication cuts the initially large crystallites up into smaller flakes. These smaller flakes have more edges per unit mass resulting in an increase in the edge defect population.^[16] For the graphene samples A, A-LC and A-HE no clear *2D* peak can be identified. Chemical modifications like oxidation/reduction can lead to even more severe structural damage to the surface of these materials, introducing defects that may disrupt the band structure. The

broadness and high intensity of the defect D peak for samples A, A-LC and A-HE confirm this assumption.

During the sonication process the increasing number of exfoliated graphene platelets results in an increase of the UV-Vis absorbance due to an increase of the surface area of graphene.^[19-22]

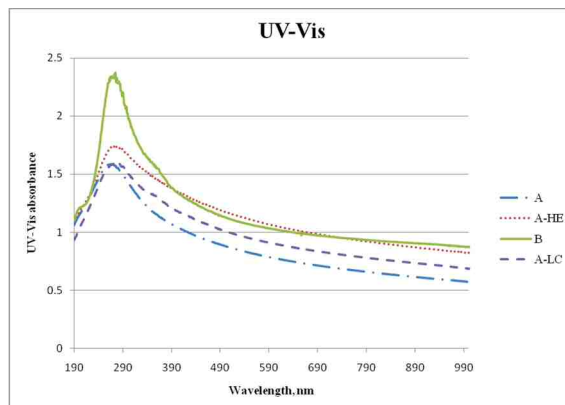


Figure 2. UV-Vis spectra of the aqueous dispersions A (2 200 000 J), A-LC(220 000 J), A-HE (2 200 000 J) and B.

As one can see in **Figure 2** the final aqueous dispersions exhibit different UV-Vis absorbances and hence different degrees of graphene exfoliation. The highest absorbance spectrum corresponds to dispersion B, whereas dispersions A, A-LC and A-HE exhibit lower absorbance spectra, which means that dispersion B contains the largest number of thin graphene layers in comparison with dispersions A, A-LC and A-HE, which in turn contain a higher number of agglomerates. When comparing samples A, A-LC and A-HE, one can conclude that apparently samples A and A-LC have more agglomerates than sample A-HE, which is in line with the lower amount of energy supplied to A and A-LC compared to A-HE. Sample A in turn looks just slightly more agglomerated than sample A-LC, but the difference is very small, which makes sense in view of the similar amount of energy supplied per mg of graphene in both systems A and A-LC. Visually both dispersions A-HE and B seem to be stable for a few weeks and months time respectively, whereas in dispersions A and A-LC slight sedimentation occurs within 24 hours after preparation.

The corresponding transmission electron microscopy (TEM) images (**Figure 3**) of the graphene platelets obtained by using the above processing conditions (samples A, A-HE and B) displayed some difference in size between the samples.

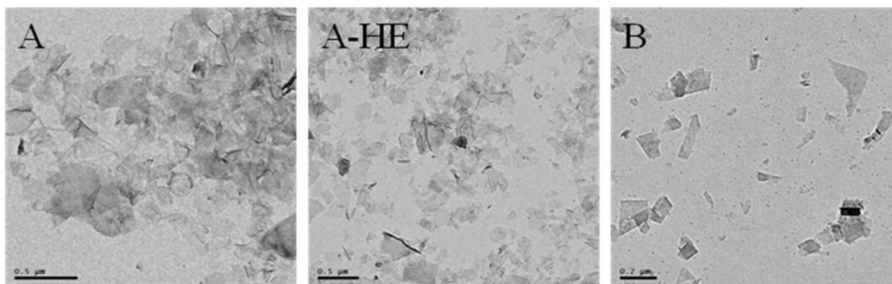


Figure 3. TEM pictures of the aqueous graphene dispersions A, A-HE and B.

Platelets obtained for dispersion A are slightly larger than those obtained for dispersions A-HE and B. This must be due to the different amounts of energy provided per mg of graphene during the sonication process.

The stability of the prepared graphene/SC dispersions was studied by recording UV-Vis absorbance spectra over time (**Figure 4**).

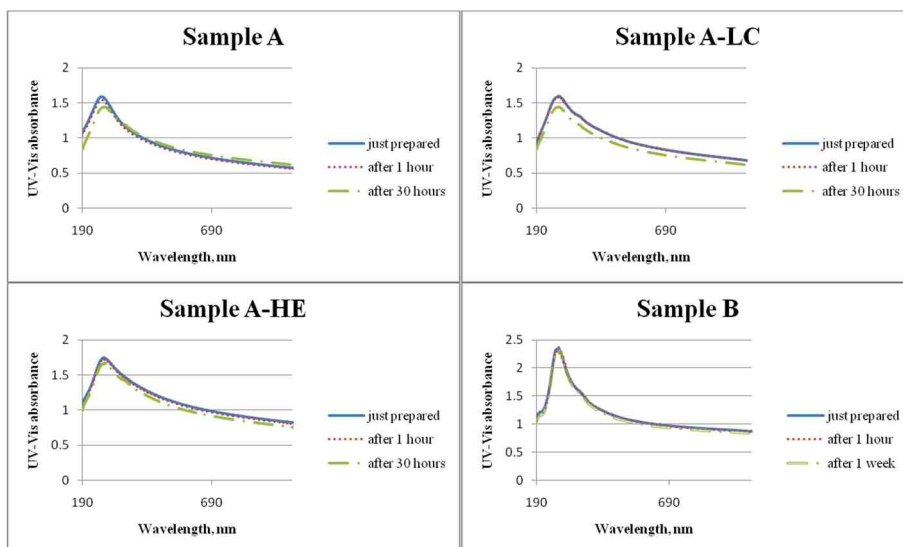


Figure 4. Stability of the systems A, A-LC, A-HE and B recorded over time by UV-Vis spectroscopy.

As one can see from the Figure 4, the maximum absorbance around 270 nm of both dispersions A and A-LC, which had an almost similar degree of exfoliation just after the sonication process,

decreases markedly over time, which in all likelihood is due to relatively fast aggregation occurring in both dispersions. During the same period of time there is a very slight decrease in the absorbance of sample A-HE, suggesting that dispersion A-HE exhibits a higher stability than dispersions A and A-LC. Sample B shows hardly any decrease in its UV-Vis absorbance maximum around 275 nm over long periods of time, indicating an extremely high stability of the dispersion and no aggregation processes occurring.

4.2.2. Nanocomposites characteristics

All four graphene/SC dispersions, A, A-LC, A-HE and B, were utilized for the preparation of conductive polymer nanocomposites via the so-called latex technology. For that the aqueous dispersions of graphene/SC were mixed with polystyrene latex, followed by freeze-drying and compression molding, resulting in a composite film.^[2] From now on the composites prepared from graphene dispersions A, A-LC, A-HE and B and PS latex are respectively indicated as nanocomposites A, A-LC, A-HE and B.

The electrical conductivity of the nanocomposites as a function of the nanofiller content is shown in **Figure 5**. At low graphene concentrations, as long as no conductive network of nanoplatelets is formed in the PS matrix, the conductivity of the nanocomposites remains very close to the conductivity value of the pure insulating PS matrix. The figure clearly shows that the percolation thresholds vary quite strongly with dispersion conditions. The percolation threshold of the composites prepared from dispersion B is high, about 4.5 wt%, which is related to the fact that graphene platelets stay separated one from another in the final composite films just as they were in the aqueous mixture of the PS latex and the graphene dispersion due to the very high degree of exfoliation and high stability, which brings about a lack of contacts between them. The nanocomposites obtained from dispersion A-HE show moderate percolation threshold in comparison with composites based on graphene dispersions B, presumably due to the lesser degree of exfoliation of the platelets, reduced thermodynamic stability of the dispersion and hence the presence of small agglomerates. The attractive interactions leading to the agglomerates plausibly induce additional contacts between sheets in the aqueous graphene/PS particle mixtures and hence subsequently also in the composite films.

The nanocomposites based on graphene dispersions A and A-LC exhibit the lowest percolation thresholds, viz. 2 wt % for A and 2.3 wt % for A-LC, because of their relatively low degrees of exfoliation and significantly reduced stability of the aqueous dispersions compared to the cases

discussed above. This results in some agglomeration and hence cluster formation in the aqueous graphene/polymer particle mixtures and, following that, in the solid composite too. We would like to emphasize that we are not dealing here with the worst possible scenario concerning the dispersed state of graphene, which would be the case for completely non-exfoliated graphite in the polymer matrix for which the percolation threshold experimentally proved to occur at very high filler loading, 10 wt %. When the composites are made from non-exfoliated graphite, then due to macroscopic phase separation there might be isolated graphite-rich regions along with a vast majority of composite volume that would be largely un-reinforced and polymer-rich.

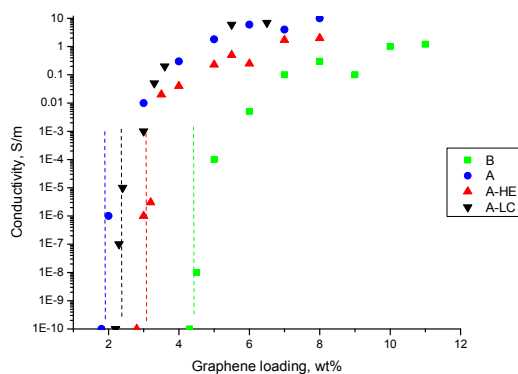


Figure 5. Electrical conductivity of graphene/PS composites A, A-LC, A-HE and B, prepared with aqueous dispersions A, A-LC, A-HE and B respectively, as a function of the graphene weight fraction in the final nanocomposite.

The organization of graphene sheets in the nanocomposites and their conductivity distribution was analyzed with nanometer resolution by means of conductive atomic force microscopy (C-AFM). Using a conductive AFM probe, in this case a gold-coated silicon tip, the local electrical conductivity was measured at exactly the same area of the specimen subsequent to the topography and phase contrast imaging. The C-AFM tip measures the current throughout the volume of the nanocomposite specimen at a given voltage, which is running via the graphene network to the ground contacts. Only platelets that are connected with the ground contacts can be monitored, and the observed differences in current are determined by the intra-network graphene junctions with highest resistivity. Graphene contributing to sub-networks without connection to the ground contacts show no current. In this way,

a current distribution image is obtained and the conductive platelets can be distinguished from the insulating polymer matrix.

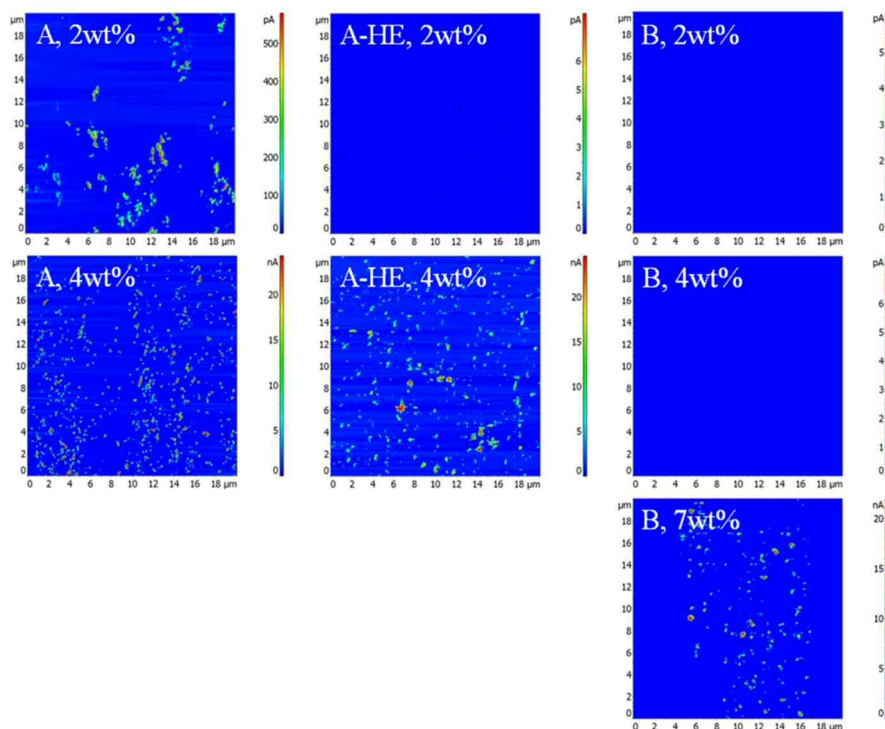


Figure 6. Conductive-AFM images of the graphene/PS nanocomposites with different graphene loadings (indicated in the pictures) obtained as electrical current distribution images showing the graphene platelets that are connected with the ground electrode.

As one can see in **Figure 6** at 2 wt% graphene loading, only nanocomposite A that shows some small conductive clusters, exhibits some degree of conductivity, whereas both samples A-HE and B do not. At a higher loading, 4 wt%, both samples prepared from graphene dispersions A and A-HE show conductivity, but samples B still do not exhibit any network formation. Finally at 7 wt% loading a conductive network is easily visible in nanocomposite sample B as well.

4.2.3. Theoretical predictions

We also employed dynamic light scattering (DLS) to obtain a rough indication of the size distributions in the exfoliated aqueous dispersions of graphene/SC (**Figure 7**).

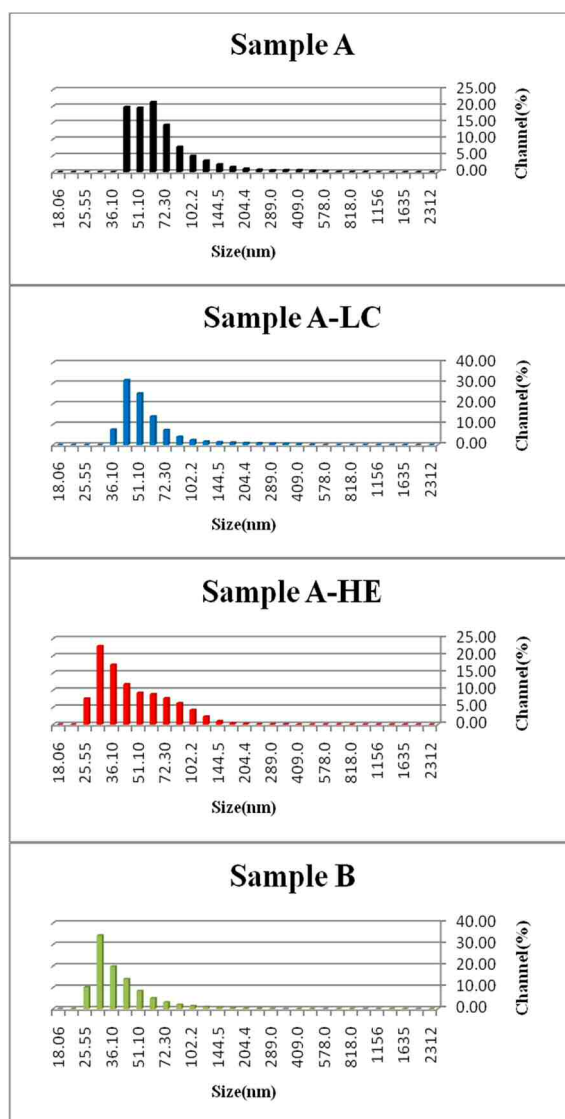


Figure 7. Dynamic light scattering data of the size distributions of the aqueous graphene dispersions A, A-LC, A-HE and B.

Since DLS analysis assumes that the measured objects are of a spherical shape, whereas graphene platelets can be more accurately described as two-dimensional objects, the data obtained from DLS measurements are not the real dimensions of the platelets but rather the effective hydrodynamic diameter of an equivalent sphere described by tumbling platelets.^[23]

From the DLS measurements the dispersions turned out to have quite some variation in their size distributions with a difference in the average values as well as a difference in the thickness of the tail of the distribution for large sheets. In order to rationalize these experimental observations we attempt to assess whether the difference in the percolation thresholds could be explained by the variations in the size distributions. For this we make use of a recently formulated connectivity percolation theory that predicts the effect on the percolation threshold of a size polydispersity of impenetrable and rigid plate-like particles.^[24]

The theory presumes charge transport to take place via electron hopping if two neighbouring particles are sufficiently close to each other, and predicts a very sensitive dependence of the percolation threshold on the shape of the size distribution of the plate-like particles.

We compute the critical volume fraction φ_p of graphene required to obtain a system-spanning network as given by Eq. (24) of the referred paper that reads

$$\varphi_p = 4\langle L_k D_Y^2 \rangle_{kY} \frac{B - \sqrt{B^2 - C}}{\lambda C},$$

with

$$B = 4(\pi + 5)\langle L_k D_Y \rangle_{kY} + (5\pi + 6)\langle D_Y^2 \rangle_Y + (7\pi + 16)\lambda \langle D_Y \rangle_Y$$

and

$$C = (\pi + 6)\{-16\pi \langle D_Y \rangle_Y \langle D_Y^3 \rangle_Y - (\pi + 6)\langle D_Y^4 \rangle_Y + (17\pi + 6)\langle D_Y^2 \rangle_Y^2\},$$

where the angle brackets denote an average over the distribution of thicknesses L_k and diameters D_Y . This volume fraction φ_p is then converted into a weight fraction using a conversion factor of 2, because the density of graphene is twice that of the polymer. To determine the required moments of the distribution, we presume the thickness of the graphene sheets to be a constant and, hence, the diameter and thickness distribution to be independent. This may be a tenuous approximation because one might expect that because of the sonication process the probability of a thinner sheet to break up into smaller ones is larger than that of a thicker one. However, due to a lack of information on this coupling of the distributions, we use this approximation that should allow us to assess whether the discrepancies in the observed percolation thresholds are caused by a polydispersity in the diameters.

Given the distributions of diameters there are two tuneable parameters in the model: the sheet thickness L and the hopping distance λ , which is the largest separation between two particles that still

allows a charge carrier to hop from one graphene sheet to the other. We take $L = 0.3$ nm as a typical value and given the sensitive dependence of the model on λ and the fact that its exact value is not known accurately, we take three sensible values for λ to fit the data: $\lambda = 0.9$, 1.2 and 1.5 nm.^[25] The results are shown in **Table 2**.

dispersion	A (wt %)	A-HE (wt %)	A-LC (wt %)	B (wt %)
experiment	2.0	3.0	2.3	4.5
theory ($\lambda = 0.9$ nm)	3.4	4.9	4.3	4.6
theory ($\lambda = 1.2$ nm)	2.6	3.7	3.2	3.4
theory ($\lambda = 1.5$ nm)	2.0	2.9	2.5	2.7

Table 2. Experimentally determined percolation thresholds for PS/graphene nanocomposites based on the four aqueous graphene dispersions A, A-LC, A-HE and B and the corresponding theoretical predictions for different values of the hopping distance λ .

The agreement between theory and experiment is remarkably good, considering the crudeness of the model. Indeed, for all three values of the hopping distance λ , the trends fully agree. For $\lambda = 1.5$ nm the numerical agreement between theory and experiment is almost perfect for composites A, A-HE, and A-LC, but this value underestimates the experimental value of composite B. For $\lambda = 0.9$ nm nanocomposite B exhibits the best numerical agreement, but the other three theoretical values are significantly larger than the corresponding experimental ones. Hence, $\lambda = 0.9$ nm and $\lambda = 1.5$ nm give a lower and upper bound on the hopping distance, whereas the value $\lambda = 1.2$ nm provides a compromise that fits all four systems reasonably well.

As already alluded to, we use three values of the hopping distance because its value is not known accurately, and the thickness is kept at a constant value $L = 0.3$ nm. However, nanocomposite B shows the highest UV absorbance and therefore has the highest degree of exfoliation. This means that the sheets in dispersion B are presumably thinner than those in the other three dispersions and that $L = 0.3$ nm is quite accurate for dispersion B but it may be too low a value for the other three systems, i.e., the sheets of the other three may consist of a few layers of graphene and are not actually graphene but graphite platelets. However, a larger value of the thickness L as a fit parameter would only raise the theoretically predicted values and make the discrepancy larger for any value of the hopping distance λ . An interesting point to note here is that the graphene sheets are modelled as

flat disks in the model, which obviously is not the case in practice. Indeed, if the sheets in aqueous graphene dispersion B are thinner than those in the other three dispersions because of the higher degree of exfoliation, their effective diameter as observed in the DLS measurements should be smaller, which in fact is the case. The diameter in the model then represents this effective sheet diameter, which leads to a good agreement between experiment and theory for the PS/graphene nanocomposite based on this dispersion.

Again, one could argue that even though the theoretical values of the percolation thresholds for the nanocomposites based on dispersions A, A-HE and A-LC are too high for $\lambda = 1.2$ and $\lambda = 1.5$ nm and would be even higher with a larger thickness as indicated above, the trend in them agrees with that in the experimental values. This means that there could be a systematic deviation in the theoretical predictions, which could e.g. be due to attractive van der Waals interactions that are not accounted for in the model and that have been shown to lower the percolation threshold of carbon nanotubes in a PS matrix considerably.^[27] Here, it must be noted that the attraction should not be too large because that would lead to stacking of sheets (or bundling of nanotubes), which would raise the percolation threshold of the PS/graphene nanocomposite. So, if the effect of such a systematic deviation in nanocomposites A, A-LC and B is the same, then we could argue that the differences between their percolation thresholds are indeed related to the polydispersities of their sheet diameters.

4.3. Conclusions

Both experimental and theoretical studies were applied to determine an effect of dispersion state on percolation threshold of graphene-based polystyrene nanocomposites prepared with the aid of latex technology. Graphene/polystyrene composites were prepared using four graphene dispersions with different degrees of exfoliation and stability, and their electrical properties were characterized. The degree of exfoliation of graphene and the stability of the dispersions were characterized with UV-Vis spectroscopy. It was shown that PS/graphene nanocomposites prepared from PS latex and aqueous graphene dispersions with relatively low stability and relatively low degrees of exfoliation exhibit a lower percolation threshold than the composites based on dispersions with larger degree of graphene exfoliation and higher dispersion stability.

Theoretical predictions were employed to calculate percolation thresholds of the nanocomposites, inserting the degree of polydispersity of the graphene platelets as obtained from our DLS measurements. Theory and experiments show the same trends for the series of samples, suggesting

that size polydispersity is indeed an important factor determining the electrical percolation threshold. The comparison provides a lower and upper bound for the hopping distance of $\lambda = 0.9$ nm and $\lambda = 1.5$ nm. We note here, however, that this was based on the assumption of a constant value of the graphene thickness $L = 0.3$ nm, whereas nanocomposite B shows a higher degree of exfoliation, both in the aqueous state as well as in the final nanocomposite, and a higher stability than in the other composites that exhibit cluster formation. This means that the particles in composite B are presumably somewhat thinner than those in the other composites.

Despite the higher quality of the nanofiller loading of composite B, confirmed by Raman spectroscopy, nanocomposites based on aqueous dispersions of graphene of lower quality, but in which the nanofiller particles do form clusters in solution, and accordingly in view of our mild and almost shear-free compression molding step furnishing the nanocomposite films, also in the final PS/graphene nanocomposite, exhibit lower percolation thresholds. This important finding, as far as we know demonstrated for the first time for graphene-based polymer nanocomposites, is in excellent agreement with the works described by Li, Martin, Aguilar and Hernandez on polymer/carbon nanotube composites.^[7-10]

4.4. Experimental

Chemicals

Sodium dodecyl sulfate (SDS) (90%, Merck), sodium carbonate (99%, Aldrich), sodium peroxydisulfate (SPS) (90%, Merck) and sodium cholate (SC) (99%, Aldrich) were used as received. Styrene (99%, Merck) was passed over an inhibitor remover column. The inhibitor-free monomers were kept under refrigeration for later use. Water used in all reactions was double de-ionized water obtained from a purification system. SP-2 graphite from Bay Carbon and natural flake graphite from Branwell Graphite Ltd. (Grade RFL 99.5) were used as provided. Graphene was obtained via graphite (SP-2 Bay Carbon) oxidation and thermo-expansion process and via graphite (Branwell Graphite Ltd) exfoliation in sodium cholate/water solution.^[15, 16]

Preparation and characterization of PS latex

PS latex was synthesized via conventional free radical emulsion polymerization. The reaction was performed at 70° C with an impeller speed of 400 rpm. The reactor was charged with the following: styrene (252 g), SDS (26 g, 0.09 mol), sodium carbonate (0.7 g, 6.6 mmol) and H₂O (712.2 g). The reaction mixture was degassed by purging with argon for 30 min. A solution of SPS (0.45 g,

1.9 mmol) in H₂O (10 g) was also degassed. The reaction was started upon the introduction of the initiator solution and the reaction time was roughly 1 hour. The average particle size determined by dynamic light scattering was 90 nm. Size exclusion chromatography analysis showed M_n, M_w and PDI values of 495 kg/mol, 944 kg/mol and 1.9, respectively.

Preparation of graphene dispersions

Exfoliated graphene dispersions from thermally reduced graphite oxide were prepared with the use of surfactant and energy supplied by ultrasound. The ultrasound was provided by a Sonics Vibracell VC750 horn sonicator with a 10 mm diameter tip. The sonication power was maintained at 100 W during the exfoliation, and the solution was cooled in an ice-bath. Volumes were kept under 100 ml to achieve the best sonication for the complete solution. Graphene dispersion made from graphite exfoliated via liquid-phase exfoliation route was prepared as described elsewhere.^[16]

Composites processing

The graphene dispersion was mixed with PS latex, the mixture was frozen in liquid nitrogen for several minutes and the frozen water was removed with a Christ Alpha 2–4 freeze dryer operated at 0.2 mbar and 20 °C overnight. The resulting composite powder was compression molded into films for 20 min at 180 °C between Teflon sheets with a Collin Press 300G.

UV–Vis spectroscopic measurements

UV–Vis absorption spectra were recorded with a Hewlett– Packard 8453 spectrometer operating between 200 and 1100 nm. Small sample volumes were taken after the sonication process and diluted, resulting in a graphene concentration of 0.0125 mg ml⁻¹. The blank used was the original SC solution, diluted and analyzed under the same conditions as the samples themselves.

Electrical conductivity measurements: The electrical conductivity was measured using a standard four-point method. Parallel contact lines 0.5 cm in length and with a 0.5 cm interval were drawn with conductive-silver paint (Fluka) on the composite film, and all conductivity measurements were performed at room temperature with a Keithley 6512 programmable electrometer. For each sample, conductivity data represent the average value of 10 consecutive measurements.

Atomic force microscopy investigations

The conductive AFM measurements on composites cross sections were performed by an NTEGRA Tomo (NTMDT Co.). The device is a combination of a microtome EM UC6-NT (Leica) and

an SPM measuring head. Such design allows for alternate microtome cutting and SPM measurements of the sample block-face. The local current measurements were performed in C-AFM mode with a gold-coated silicon cantilever NSC36/Cr-Au (Micromash). The sample was electrically connected to a grounded holder; a bias of 2 V was applied.

Transmission electron microscopy

TEM images were taken using a Sphera type Technai 20 (Fei Co.). This was operated with a 200 kV LaB6 filament and a bottom mounted 1024 x 1024 Gatan CCD camera. A carbon coated gold grid was used.

Raman spectroscopy

A LABRAM confocal Raman spectroscope equipped with an optical microscope was utilized. Samples were irradiated with red high polarized laser (632 nm) supplied by Melles Griot.

Dinamic Light Scattering

DLS measurements were performed on Nanotracc Particle Size Analyzer (Microtrac Inc).

4.5. References

- [1] S. Stankovich, D. A. Dikin, G. H. B. Dommett, K. M. Kohlhaas, E. J. Zimney, E. A. Stach, R. D. Piner, S. T. Nguyen, R. S. Ruoff, *Nature* **2006**, *442*, 282.
- [2] E. Tkalya, M. Ghislandi, A. Alekseev, C. Koning, J. Loos, *Journal of Materials Chemistry* **2010**, *20*, 3035.
- [3] H. Kim, Y. Miura, C. W. Macosko, *Chemistry of Materials* **2010**, *22*, 3441.
- [4] H. J. Salavagione, M. A. Gomez, G. Martinez, *Macromolecules* **2009**, *42*, 6331.
- [5] H. Kim, C. W. Macosko, *Polymer* **2009**, *50*, 3797.
- [6] H. Kim, C. W. Macosko, *Macromolecules* **2008**, *41*, 3317.
- [7] J. Li, P. C. Ma, W. S. Chow, C. K. To, B. Z. Tang, J. K. Kim, *Advanced Functional Materials* **2007**, *17*, 3207.
- [8] C. A. Martin, J. K. W. Sandler, M. S. P. Shaffer, M. K. Schwarz, W. Bauhofer, K. Schulte, A. H. Windle, *Composites Science and Technology* **2004**, *64*, 2309.
- [9] J. O. Aguilar, J. R. Bautista-Quijano, F. Aviles, *Express Polymer Letters* **2010**, *4*, 292.
- [10] J. J. Hernandez, M. C. Garcia-Gutierrez, A. Nogales, D. R. Rueda, M. Kwiatkowska, A. Szymczyk, Z. Roslaniec, A. Concheso, I. Guinea, T. A. Ezquerra, *Composites Science and Technology* **2009**, *69*, 1867.
- [11] O. Regev, P. N. B. ElKati, J. Loos, C. E. Koning, *Advanced Materials* **2004**, *16*, 248.

-
- [12] N. Grossiord, J. Loos, C. E. Koning, *Journal of Materials Chemistry* **2005**, *15*, 2349.
- [13] N. Grossiord, J. Loos, O. Regev, C. E. Koning, *Chemistry of Materials* **2006**, *18*, 1089.
- [14] J. Yu, K. Lu, E. Sourty, N. Grossiord, C. E. Koning, J. Loos, *Carbon* **2007**, *45*, 2897.
- [15] M. J. McAllister, J.-L. Li, D. H. Adamson, H. C. Schniepp, A. A. Abdala, J. Liu, M. Herrera-Alonso, D. L. Milius, R. Car, R. K. Prud'homme, I. A. Aksay, *Chemistry of Materials* **2007**, *19*, 4396.
- [16] M. Lotya, P. J. King, U. Khan, S. De, J. N. Coleman, *Acs Nano* **2010**, *4*, 3155.
- [17] F. Tuinstra, J. L. Koenig, *Journal of Chemical Physics* **1970**, *53*, 1126.
- [18] A. C. Ferrari, J. C. Meyer, V. Scardaci, C. Casiraghi, M. Lazzeri, F. Mauri, S. Piscanec, D. Jiang, K. S. Novoselov, S. Roth, A. K. Geim, *Physical Review Letters* **2006**, *97*, 187401.
- [19] S. Stankovich, R. D. Piner, X. Q. Chen, N. Q. Wu, S. T. Nguyen, R. S. Ruoff, *Journal of Materials Chemistry* **2006**, *16*, 155.
- [20] L. Q. Jiang, L. Gao, J. Sun, *Journal of Colloid and Interface Science* **2003**, *260*, 89.
- [21] A. G. Ryabenko, T. V. Dorofeeva, G. I. Zvereva, *Carbon* **2004**, *42*, 1523.
- [22] O. N. Torrents, D. E. Milkie, M. Zheng, J. M. Kikkawa, *Nano Letters* **2006**, *6*, 2864.
- [23] S. Stankovich, R. D. Piner, S. T. Nguyen, R. S. Ruoff, *Carbon* **2006**, *44*, 3342.
- [24] R. H. J. Otten, P. van der Schoot, *Journal of Chemical Physics* **2011**, *134*, 094902.
- [25] A. V. Kyrlyuk, P. van der Schoot, *Proceedings of the National Academy of Sciences of the United States of America* **2008**, *105*, 8221.

Chapter 5

Dependence of percolation threshold of graphene/polymer nanocomposites on surfactant used for graphene dispersion in the aqueous state of the latex concept.

ABSTRACT: The composite applications of graphene produced by thermal reduction of graphite oxide require its exfoliation and dispersion in a polymer matrix. One of the main approaches to disperse and exfoliate graphene in a polymer matrix is based on the use of surfactants in the aqueous state of a latex-based concept. Here we compare the ability of some conventional surfactants such as sodium dodecylbenzene sulfonate (SDBS), sodium cholate (SC), sodium poly (sodium 4-styrene sulfonate) (PSS) and Tween-80 to disperse graphene in water. We determine optimum conditions for all the surfactants to disperse graphene at concentration of 1 mg/ml. For the ionic surfactants used in this work the same percolation thresholds as well as ultimate conductivity values were obtained. The use of Tween-80 for graphene dispersion results in a higher percolation threshold and in a lower conductivity compared with ionic surfactants-based systems. A conductive polymeric surfactant, namely poly(3,4-ethylenedioxythiophene):poly(styrene sulfonate) (PEDOT:PSS) was also used to disperse graphene in water for preparation of the polystyrene (PS)-based composites. The use of PEDOT:PSS greatly reduces the percolation threshold in comparison with the systems utilizing conventional surfactants. The morphology of the graphene/PEDOT:PSS system was investigated and an explanation why it lowers the percolation threshold is given.

5.1. Introduction

One of the most promising approaches to incorporate graphene produced via thermal reduction of graphite oxide into a polymer matrix is based on the use of a third component, i.e. a surfactant. Surfactant-assisted dispersion of graphene in water is perhaps the most environmentally friendly concept because the use of toxic solvents is avoided. Of course the water needs to be eliminated in one of the subsequent steps following the water-based step. A drawback is that the mechanical properties of the nanocomposite deteriorate because of the high amount of surfactant necessary for the particles stabilization, realizing that the surfactant remains present in the final polymer nanocomposite. The tensile strength and modulus after processing can be below the values for the neat polymers, but this seems to be not a major problem if one focuses on electrical properties. It was demonstrated that via liquid phase exfoliation of graphite in water graphene can be dispersed with the following surfactants: sodium dodecyl sulfate (SDS), SDBS, lithium dodecyl sulfate (LDS), cetyltrimethyl ammoniumbromide (CTAB), tetradecyl trimethyl ammonium bromide (TTAB), SC, sodium deoxycholate (DOC), sodium taurodeoxycholate (TDOC), IGEPAL CO-890 (polyoxyethylene(40) nonylphenyl ether), Triton X-100 (polyethylene glycol p-(1,1,3,3-tetramethylbutyl)-phenyl ether), Tween-20 (Polyoxyethylene (20) sorbitan monolaurate) and Tween-80 (Polyoxyethylene (20) sorbitan monooleate), although for most of the surfactants optimized conditions were not found and final graphene concentrations obtained in water were quite low.^[1] In this work we disperse graphene obtained via thermal reduction of graphite oxide using some conventional surfactants, namely SDBS, PSS, SC and Tween-80, and compare the conductive properties of the prepared PS nanocomposites.

Conductivity as high as 600,000 S/m was reported for a single graphene platelet.^[2] However, when conductivities are measured for graphene/polymer composites, and even for graphene bucky-papers, these are always orders of magnitude lower than the conductivity measured for an individual platelet. This is because of imperfect contacts present between adjacent graphene platelets. For the case of polymer-based graphene composites, an additional resistance can arise from interfacial polymer layers present within the graphene junctions. A drawback of utilizing conventional surfactants for manufacturing polymer/graphene nanocomposites is that, if the surfactant is not displaced from the graphene surface after the final processing steps during composite preparation, an insulating shell remains around the platelets that could be detrimental for the inter-platelet charge transport in the final product as was demonstrated for CNTs in CNT/polymer nanocomposites.^[3] Contact resistance for both CNTs and graphene networks dominates the overall film/composite

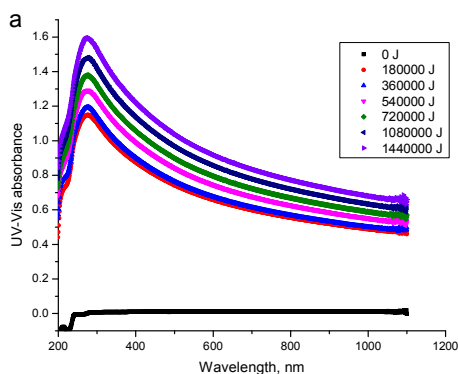
conductivity. It was shown that in the case of CNTs the presence of conductive polymeric surfactant at the intertube junctions can greatly reduce the contact resistance and alter both percolation threshold and ultimate conductivity of a single-walled carbon nanotubes network in a polymer matrix.^[4, 5] Applying these conductive polymers to a water-based system to prepare polymer nanocomposites requires the conductive polymer to have a surfactant-like nature. Conductive polymeric surfactant poly(3,4-ethylenedioxythiophene):poly(styrene sulfonate) (PEDOT:PSS) has been used to disperse SWCNTs in water for the preparation of PS nanocomposites.^[6] Here we apply PEDOT:PSS latex to reduce percolation thresholds of corresponding graphene/polymer composites for which conventional surfactants were used for graphene dispersion in the aqueous step of the latex concept (see chapter 2). The contact resistivity in the graphene network is decreased by replacing an insulating surfactant by a conductive one and by the formation of conductive bridges between adjacent graphene platelets in the graphene network.

5.2. Results and discussion.

5.2.1. Optimization of the graphene exfoliation conditions.

It was shown that when dispersing CNTs in water the surfactant concentration generally needs to be above the critical micelle concentration (CMC) and the surfactant concentration also needs to exceed the CNTs concentration.^[6-9] The latter condition is not always justified when dispersing graphene in water as sodium cholate for instance performs better at concentrations below the CMC and when not exceeding the graphene concentration during liquid phase graphite exfoliation.^[10] The dispersion quality of the CNTs improves as the filler concentration decreases.^[8] We also observed this for graphene using SC as surfactant, as was shown in chapter 4. For the production of nanocomposites with the latex-based concept, it is preferable to be able to work at relatively high concentrations of exfoliated graphene platelets for both reproducibility purposes and for commercial reasons. That's why we chose a standard work concentration of graphene 1 mg/ml. This concentration allows us to prepare a full series of nanocomposites with different graphene loadings by diluting one and the same graphene/surfactant dispersion. We disperse graphene using a sonication tip. It was observed for CNTs that, under the same experimental conditions, for the same total energy provided to the system, CNTs sonicated at high powers are shorter (so they are more damaged) than CNTs sonicated at lower powers.^[11] Exfoliation of graphite or a few stacked graphene layers obviously requires providing a higher amount of energy due to a bigger interaction surface and

subsequently stronger van der Waals forces compared to bundled CNTs. Bearing this in mind, we decided to check whether it would result in a different degree of exfoliation when the exfoliations of graphene platelets were carried out at different sonication powers, namely 100 W and 50 W. For that we prepared two dispersions containing 0.1 wt % of graphene and 0.1 wt % of PSS at different sonication powers. As was demonstrated in the previous chapters UV-Vis spectroscopy can be applied to monitor the degree of exfoliation of graphene sheets. During sonication, the increasing amount of exfoliated platelets results in an increasing area below the lines representing the absorbance. Since the power of sonication is kept constant throughout the experiments there is a direct relationship between a specific sonication time and the energy delivered to the sample during this time interval. Therefore, it is equivalent to plot the absorbance at a certain wavelength versus the time of sonication or versus the energy supplied to the solution. The mixtures were sonicated until the maximum exfoliation (or UV-Vis absorbance) was reached (**Figure 1a,b,c**). The figure shows that exfoliation of both graphene/PSS mixtures occurs approximately with the same speed, which can be deduced from the very similar absorbance values obtained at very similar amounts of energy provided to the systems. The comparison of the evolution of the UV-Vis absorbance at 276 nm versus the energy provided to the two graphene dispersions studied, shows that the power of sonication used to achieve the maximum exfoliation of the graphene sheets does not significantly influence the process (see Figure 1c). In other words, only the energy provided to the system needs to be taken into account to reach the maximum exfoliation, since this maximum is reached after the same addition of the same amount of energy which was provided to the samples, regardless of the value of the power of sonication employed.



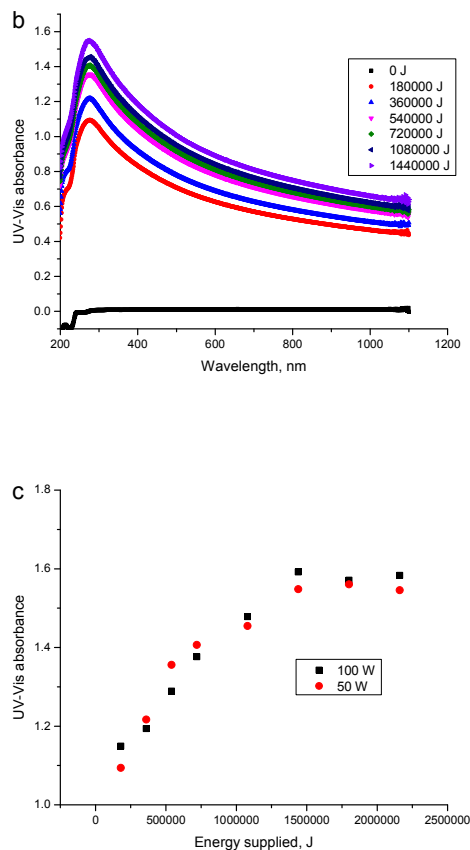
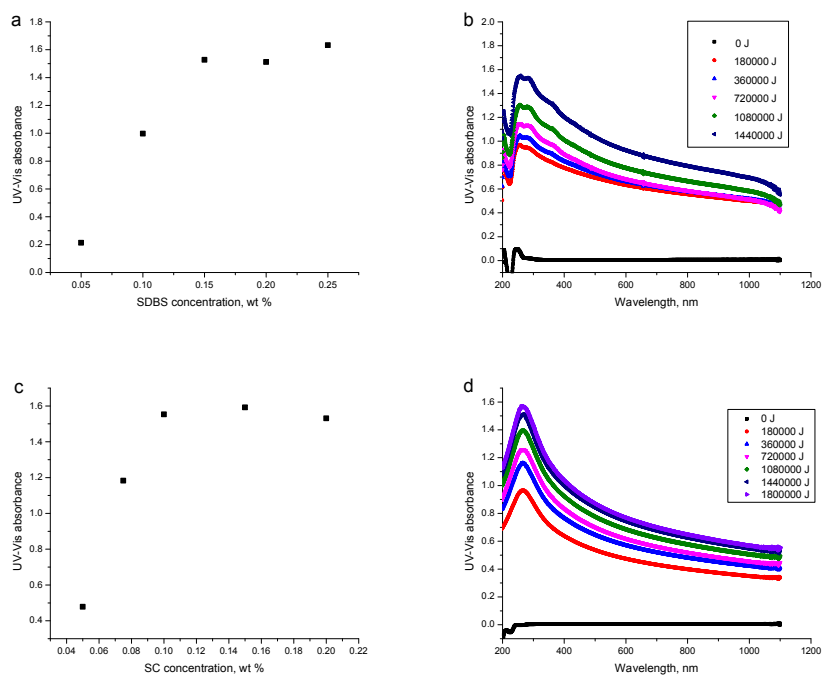


Figure 1. Evolution of UV–Vis spectra of an aqueous 0.1 wt% graphene/ 0.1 wt% PSS solution as a function of energy provided during sonication at a power of: (a) 100 W; (b) 50 W. (c) The comparison of the evolution of the UV-Vis absorbance at 276 nm versus the energy provided to the two graphene dispersions.

For the practical reasons we chose a sonication power of 100 W for further work since sonication at 50 W requires much longer time to complete the exfoliation and the dispersion of graphene in an aqueous surfactant solution. We determined the minimum concentration of surfactant, which is necessary to exfoliate graphene platelets to the maximum degree by using UV-Vis. If a too small number of surfactant molecules is present in solution during the sonication, only a part of the total number of graphene sheets, which can potentially be peeled off from the initial graphene aggregates or pieces of graphite, can be stabilized. As a result, the exfoliation of the graphene is far from complete, and the value of the absorbance at the end of the exfoliation is lower than when all the

platelets, which can in principle be exfoliated from the aggregates, are individualized. On the contrary, if a big amount of surfactant is present in the final composite it influences its mechanical properties. Based on this fact it's necessary to determine a minimum concentration of surfactant required for exfoliation and dispersion of graphene for preparing polymer nanocomposites. We determined a required surfactant concentration by comparing the maximum absorbance values of the absorbance at the end of the exfoliation as a function of surfactant concentration. We mixed 0.1 wt % of thermally reduced graphene oxide with a range of concentrations of SDBS, SC, PSS and Tween-80. When measuring the UV-Vis absorbance versus surfactant concentration one obviously should observe an increase of absorbance until a critical surfactant concentration is reached, which corresponds to the minimum amount of surfactant needed to stabilize graphene platelets (**Figure 2**).



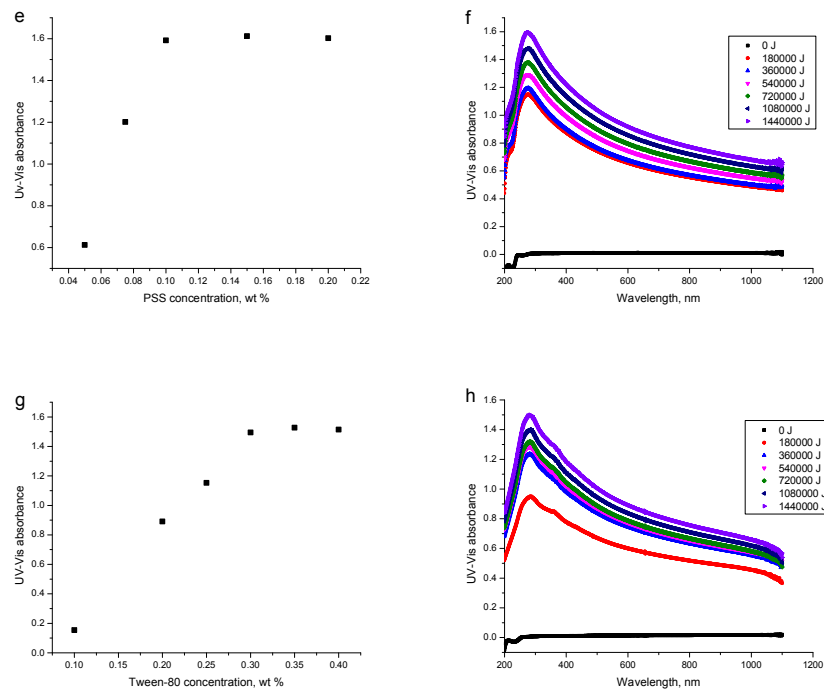


Figure 2. Absorbance at 276 nm of 0.1 wt % graphene dispersions, recorded at the end of the exfoliation process when the maximum absorbance was obtained, plotted as a function of the surfactant concentration: (a) SDBS; (c) SC; (e) PSS; (g) Tween-80 and evolution of UV–Vis spectra of aqueous 0.1 wt% graphene solutions dispersed at optimum concentrations of the corresponding surfactants as a function of sonication energy: (b) SDBS; (d) SC; (f) PSS; (h) Tween-80.

A further enhancement of the surfactant concentration does not result in a further increase of the absorbance, and a plateau value is reached. Figure 2 shows that for exfoliation and dispersion of graphene at a concentration of 0.1 wt % the following minimum surfactant concentrations are required: 0.15 wt %, 0.1 wt %, 0.1 wt % and 0.3 wt % for SDBS, SC, PSS and Tween-80, respectively. It was shown for ionic surfactants, which stabilize a nanofiller by electrostatic repulsions, that the dispersion quality and degree of the exfoliation/individualization of CNTs scale with the zeta potential ζ , which in turn scales with surfactant molecular weight, meaning that low molecular weight surfactants that pack tightly on the CNTs surface are ideal, since they provide higher absolute ζ values.^[6] Interestingly, this is not always the case for graphene. A graphene/SC dispersion was shown to possess a lower absolute value of the zeta potential than a graphene/SDBS dispersion but

SC disperses graphene more effectively, as was demonstrated for graphene obtained by liquid phase exfoliation of graphite.^[1] The same we observe here for graphene obtained by thermal reduction of graphite oxide. In Figure 2 one can see that Tween-80 which stabilizes graphene by steric effects, seems to be the least effective among the surfactants we used to disperse graphene in water.

To compare the platelets after exfoliation with different surfactants transmission electron microscopy (TEM) was performed on graphene dispersions prepared with PSS, SC and Tween-80. The exfoliated platelets exhibit the dimensions of about 0.5 μm in length and width. There is some difference in background between the micrographs of ionic surfactants- and Tween-80-stabilized graphene, probably due to the fact that Tween-80 is a liquid at room temperature and stays being a liquid on the TEM grid after water evaporation, contrary to the other surfactants.

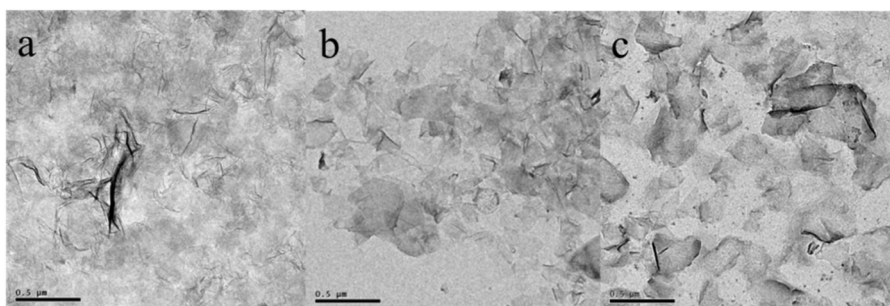


Figure 3. TEM pictures of the graphene platelets exfoliated with the aid of: (a) PSS; (b) SC; (c) Tween-80.

5.2.2. Composite conductivities

After the maximum obtainable exfoliation was achieved, the aqueous dispersions of graphene/SDBS, graphene/SC, graphene/PSS and graphene/Tween-80 were mixed with polystyrene latex, followed by freeze-drying and compression molding, resulting in a composite film. The advantage of a non-ionic surfactant like Tween-80 is the possibility to prepare nanocomposites using polymer latexes comprising either positively or negatively charged or even uncharged particles. For the systems stabilized with ionic surfactants we used PS latex stabilized with SDS, whereas for Tween-80-stabilized graphene we used both a latex containing PS particles stabilized with SDS (negatively charged) and a latex containing PS particles stabilized with CTAB (positively charged). Moreover, the average molecular weights M_w of the two PS latexes are different: 1,000,000 g/mol for the SDS-stabilized PS latex and 150,000 g/mol for CTAB-stabilized PS latex, respectively. This

difference was deliberately chosen in order to check whether the difference in molecular weight influences the percolation threshold of these graphene/PS nanocomposites. The results of the conductivity measurements for all the systems are presented in **Figure 4**.

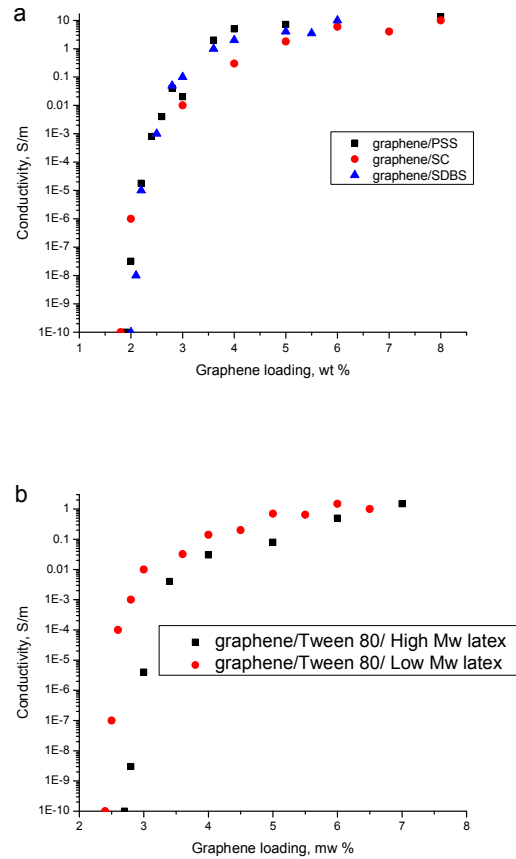


Figure 4. Conductivity curves of the following systems: (a) the anionically stabilized systems (all the composites prepared with the high molecular weight PS latex): graphene/PSS/PS, graphene/SC/PS and graphene/SDBS/PS; (b) graphene/Tween-80/PS nanocomposites containing high and low molecular weight PS.

As one can see in Figure 4a all the systems containing high molecular weight PS and graphene dispersed with ionic surfactants exhibit the same percolation threshold (at 2 wt %) and the same level of conductivity (around 10 S/m) above the percolation threshold, which can mean that all the

dispersions possess the same level of exfoliation of graphene. In contrast to that graphene/Tween-80/PS nanocomposites based on high molecular weight PS exhibit a percolation threshold at higher loading level and lower conductivity above the percolation threshold, namely 2.8 wt % and 1 S/m, respectively. This can be due to the presense of a big amount (ratio Tween-80:graphene is 3 to 1) of very bulky surfactant (which has very long hydrophilic tail) on the surface of the graphene platelets which stabilizes the graphene platelets in the aqueous phase by a steric effect and at the same time keeps platelets quite far apart from each other in the final nanocomposite.

It was shown that the viscosity of the polymer melt, which is a function of the molecular weight distribution, plays a role in the time it takes for the filler nanoparticles, more specifically CNTs, to attain their equilibrium structure in the melt.^[7, 12] This implies that the measured percolation threshold should be a function of the compression molding time (see experimental part) and of the temperature at which the compression molding takes place. If the initial structure does not represent an electrically percolating network but the final equilibrium structure does, then the time allowed to the system to equilibrate should determine whether or not electrical percolation is actually achieved in the final product.^[7] For the PS latex of molecular weight of 1,000,000 g/mol it was demonstrated that the percolation threshold for both SWCNTs and MWCNTs/PS composites prepared by means of latex technology is heavily influenced by the processing time. To be more specific enhancing of the processing time (from 2 minutes up to 30, 45 and 60 minutes) lowered the percolation threshold and raised the conductivity of the corresponding nanocomposites by pushing the system towards its equilibrium state.^[7] However, when we raised the time for the final (compression molding) step of nanocomposites preparation, from 2 minutes up to 1 hour we didn't observe any change in the percolation threshold, which can be due to the difference in shape between CNTs and graphene. We propose that for a system based on large graphene platelets it should take much longer time to reorganize itself in a highly viscous polymer matrix in a direction perpendicular to its plane, which implies that the earlier mentioned "equilibrium" structure in the melt is much more difficult to achieve than for the thin CNTs.

When replacing the high molecular weight PS latex by the low molecular weight PS latex for preparation of the nanocomposites we observe a shift in percolation threshold for the graphene/Tween-80 system from 2.8 wt % of graphene loading to 2.5 wt %. It was shown for CNTs that an addition of a low molecular weight polymer to a high molecular weight polymer which forms the composite matrix can strongly affect the percolation threshold of CNTs within both poly (methyl methacrylate) (PMMA) and PS matrixes. A significant decrease in the percolation threshold was

observed upon the introduction of low molecular weight polymer, the shift being most pronounced for higher amounts of low molar mass polymer.^[12] It was speculated that low molecular weight polymer can displace the surfactant from the surface of a nanofiller which can induce changes in both percolation threshold and ultimate conductivity due to a difference in dielectric constant values of surfactant and polymer matrix. The evidence for such a displacement was claimed to be the changes in the matrix glass transition temperatures that were observed in CNTs/polymer composites.^[13] However, such a decrease in percolation threshold was also observed for the CNTs-based composites for which no changes in glass transition temperatures occurred. In addition to that for the latex systems there was no change in the ultimate conductivity of the referred system.^[12] Also in the present work no differences in the maximum conductivity values were observed for the graphene/Tween-80/PS composites based on the low molecular weight polymer matrix in comparison to the composites prepared with high molecular weight matrix. Therefore we doubt that the surfactant displacement is really important for the percolation threshold and the ultimate conductivity and we think that the reason for the decrease in percolation threshold upon addition of low molecular weight matrix material is a rheological change of the melt, i.e. a decrease in its viscosity, which in turn can influence the extent to which the graphene platelets are able to reach an equilibrium organization during the compression molding stage of the composite preparation. Whether this equilibrium distribution is more or less aggregated than the initial dispersion state after freeze-drying is not clear. The fact that a higher compression molding temperature, implying also a reduced melt viscosity, also reduces the percolation threshold supports the importance of a rheological change.^[7]

5.2.3. Lowering percolation threshold using PEDOT:PSS as surfactant

5.2.3.1. Graphene exfoliation

The efficiency of PEDOT:PSS to stabilize graphene sheets was evaluated using UV-Vis spectroscopy. We tried different ratios of graphene to PEDOT:PSS, namely 1 to 0.5, 1 to 1, 1 to 1.4 which corresponds to the ratio graphene:PSS of 1 to 1, 1:2 and 1:3. The exfoliation profile for the 1 to 1.4 weight ratio is shown in **Figure 5**. For the ratios of graphene to surfactant of 1:0.5 and 1:1 the maximum absorbance level was lower than for the 1 to 1.4 system, whereas the ratios 1:2 and 1:3 showed almost no further improvement over the 1:1.4 system.

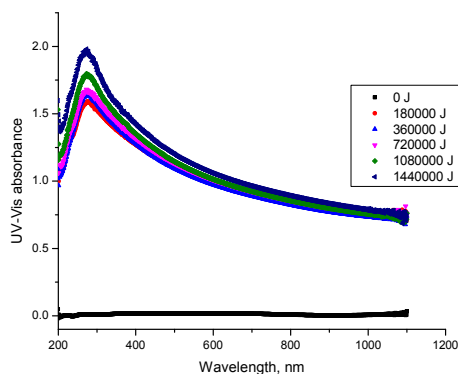


Figure 5. Evolution of UV–Vis spectra of an aqueous 0.1 wt% graphene/ 0.14 wt% PEDOT:PSS dispersion as a function of sonication time.

Comparing the exfoliation profiles of the graphene/PSS (see Figure 2f) and graphene/PEDOT:PSS systems one can notice a difference in the final absorbance value between PEDOT:PSS and PSS systems, namely the dispersion containing PEDOT:PSS exhibits a higher degree of exfoliation. This we can attribute to the fact that PEDOT:PSS can stabilize graphene not just by a electrostatic repulsion but also by a steric effect. If PEDOT particles which are covered by PSS adsorbed onto the graphene surface due to π - π interaction, they can prevent graphene platelets to come close one to another. If graphene particles are stabilized just by PSS whereas PEDOT:PSS particles do not adsorb onto graphene surface and stay in solution it still can prevent graphene platelets from aggregation because they are separated by PEDOT particles which are also stabilized by PSS.

5.2.3.2. Blends of PS and PEDOT:PSS

A control series of films was prepared by mixing of PEDOT:PSS and high molecular weight PS latex to investigate at what loading of conductive polymer the system becomes conductive. Polymer blends do not show true percolation thresholds as defined for fillers, but for a combination of two polymers at distinct volume fractions the morphology of the blend will be such that at least one phase is continuous. If this phase is conductive, an insulator–conductor transition could be observed as soon as continuity is achieved.^[5, 14] A percolation threshold at a loading of around 20 wt % of PEDOT:PSS was reported for a drop-casted blend prepared via solution mixing with poly(vinylpyrrolidone).^[15] For blends containing polyaniline as a conductive component, based on polymer latexes as organic templates, a percolation threshold of 5 wt % was reported.^[16] Low

percolations values of around 2 wt % of conductive polymer have been reported for polythiophene/PS composites in which morphology of polythiophene is whisker-like.^[17]

The results of our control experiments are shown in **Figure 6**. As one can see PEDOT:PSS percolates in a PS matrix at around 2.2 wt %, which is in agreement with earlier reports.^[5, 18] The maximum conductivity achieved for the blend is 600 S/m.

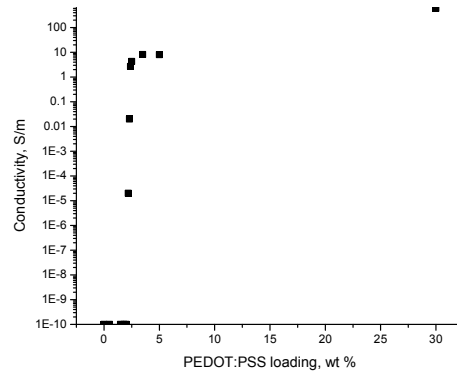


Figure 6. Conductivity curve of PEDOT:PSS/PS blends.

PEDOT:PSS is known to film-form on a substrate it is deposited on. Scanning Electron Microscopy (SEM) images of a PEDOT:PSS drop-casted film on a silicon wafer, as shown in **Figure 7**, exhibit a smooth structured surface with some big PEDOT:PSS particles on top.

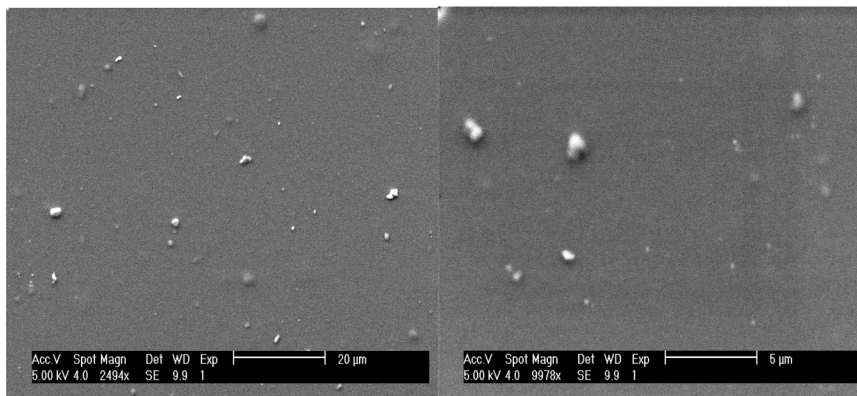


Figure 7. SEM image of PEDOT:PSS on silicon wafer at different magnification.

Such a morphology is probably due to the high thickness of the film comprising few layers of PEDOT:PSS particles.^[19] The PEDOT:PSS film consists of horizontal layers of flattened PEDOT-rich particles that are separated by quasi continuous PSS lamellas.^[20, 21] Such a pancake shape of PEDOT particles, implying an increase of the aspect ratio ($L/D > 1$), can explain a quite low percolation threshold of PEDOT:PSS in a blend of PS and PEDOT:PSS. Another factor which induces the quite low percolation threshold of PEDOT:PSS in PS composites can be that PEDOT:PSS is pushed into interstitial space between PS particles, and stays more or less there even after flow of PS latex. The preparation of the PEDOT:PSS/PS blends is performed by mixing PEDOT:PSS latex in the desired ratios with PS latex followed by freeze-drying to remove water and compression molding at 180 °C to make the final composite films. To check how the heating up to 180 °C affects PEDOT:PSS the polymer was spin-coated on glass substrate and placed into an oven for half an hour to mimic the processing conditions. Atomic Force Microscopy (AFM) analysis of the film before and after annealing was carried out (**Figure 8**). AFM shows that annealing hardly affects the morphology of the PEDOT:PSS particles which is also in agreement with an earlier report.^[19]

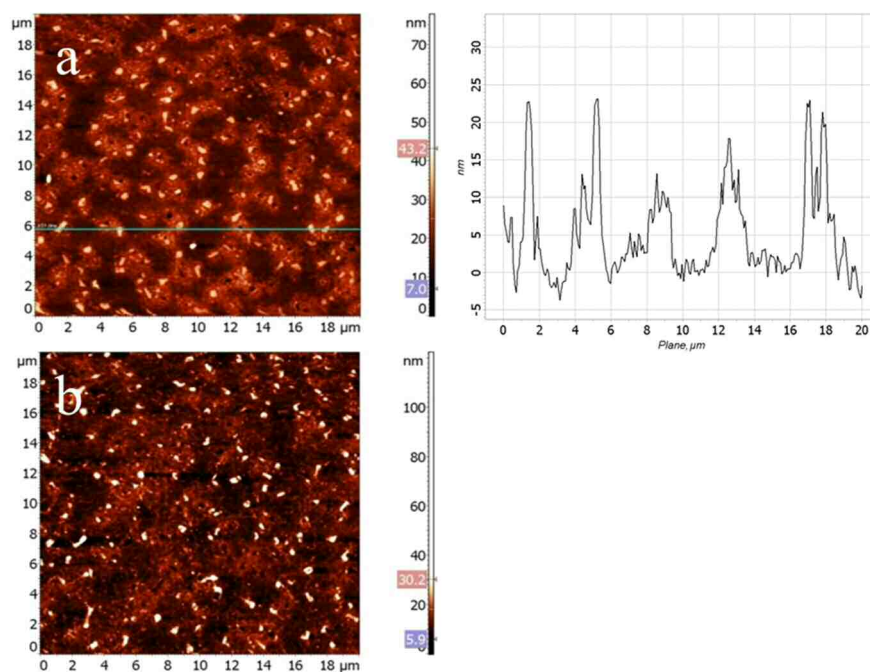


Figure 8. AFM image of PEDOT:PSS on glass before (a) and after annealing (b) at 180 °C.

We also analyzed the morphology of PEDOT:PSS in the PEDOT:PSS/PS powder obtained after freeze-drying and deposited on a silicon wafer (**Figure 9**). For this PEDOT:PSS and PS latexes were mixed in such a way that the weight ratio of PEDOT:PSS to PS in the final film would be 1 to 1 in order to maximize the visibility of both polymers. As one can see in the major part of the dark PS matrix the lighter colored PEDOT:PSS particles have a slightly elongated (oval) shape (Figure 9a), which also confirms the earlier assumption that the aspect ratio of the PEDOT:PSS particles increases when this soft material is placed on a hard substrate. The film in Figure 9b looks smooth, and not any single particle can be distinguished, which can imply that the PEDOT:PSS film on the PS particles is quite thick.

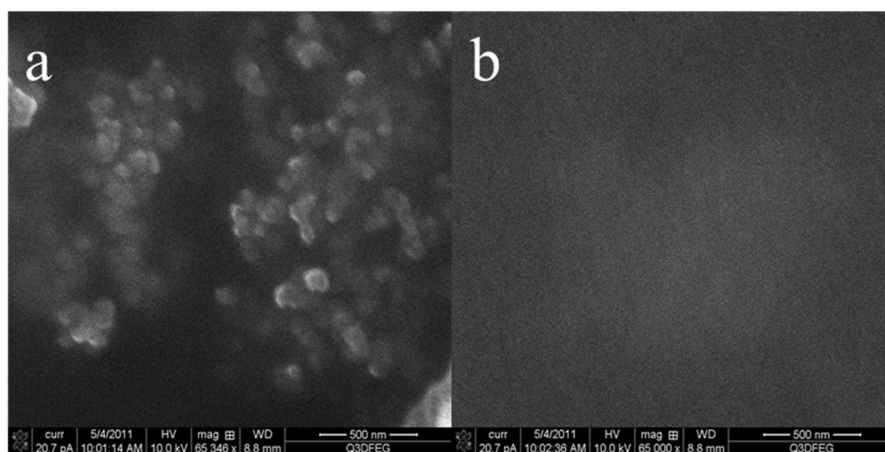


Figure 9. SEM image of the different parts of a freeze-dried PEDOT:PSS/PS powder. In the majority of the PS matrix PEDOT:PSS particles have slightly elongated shape (a); PS particles are covered with a thick layer of PEDOT:PSS. The film has a smooth surface (b).

5.2.3.3. Conductivity of graphene/PEDOT:PSS/PS

The percolation thresholds observed for PEDOT:PSS- and PSS-stabilized graphene are shown in **Figure 10**. Composites prepared with PSS-stabilized graphene have a graphene percolation threshold value of 2 wt %. The ultimate conductivity above the percolation threshold is 20 S/m. Composites prepared with PEDOT:PSS-stabilized graphene show a clear decrease in percolation threshold to 0.5 wt % and an ultimate conductivity level of 550 S/m. This level is comparable with that achieved for a PEDOT:PSS/PS blend which exhibits a conductivity of 600 S/m. Thus it can be speculated that, based on the fact that the final conductivities achieved for both the PEDOT:PSS/PS

blends and the graphene/PEDOT:PSS system are very similar, the origin of the increase from 20 S/m for the graphene/PSS to 550 S/m for the graphene/PEDOT:PSS systems, is due to the presence of the PEDOT:PSS.

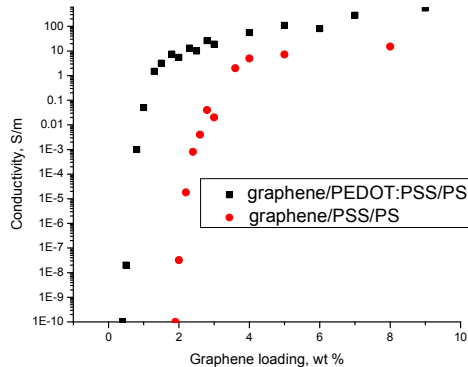


Figure 10. Percolation thresholds for composites prepared with PSS-stabilized graphene and PEDOT:PSS-stabilized graphene (the weight ratio graphene to PEDOT:PSS is 1 to 1.4).

The morphology of the graphene/PEDOT:PSS system can be threefold. In the first scenario graphene can be stabilized by PSS molecules which are present in excess in the PEDOT:PSS system (weight ratio PSS to PEDOT is 2.5:1). The result of this can be a system consisting of a mixture of conductive rods and spheres. The reduction in percolation is then induced simply by the addition of different conductive filler particles to graphene platelets which are present in the system. In this case PEDOT:PSS particles most probably build conductive bridges between the neighboring platelets as well as between the platelets which are further apart from each other. In the second possible scenario the sheets are completely covered with PEDOT:PSS pancakes due to π - π interactions. By covering the graphene sheets PEDOT:PSS “increases the thickness” of the platelets which in turn makes the distance between neighboring platelets smaller and thus decreases the percolation threshold with respect to graphene. Free PEDOT:PSS particles can be still present in the composite organizing conductive bridges between graphene platelets covered with PEDOT pancakes. In the third possible scenario graphene platelets can be just partially covered by PEDOT:PSS particles. In this case PEDOT:PSS particles can also organize conductive bridges between partially covered graphene platelets. From ultimate conductivity values it is not absolutely

clear which scenario is true due to the fact that the intrinsic conductivities of both graphene and PEDOT:PSS, are very similar. The conductivity of this type of PEDOT:PSS according to the supplier is 1000 S/m, whereas conductivity of bucky papers produced from the graphene/PSS dispersion exhibit values up to 5500 S/m.

We applied TEM to see the level of individualization of graphene platelets in a dispersion prepared with PEDOT:PSS (**Figure 11a**). There is no marked difference between the graphene platelets dispersed with the aid of ionic surfactants used described in this chapter and platelets dispersed with the aid of PEDOT:PSS. It is impossible to see the extent to which the PEDOT:PSS covers the graphene sheets, if this is really the case. We also applied Scanning Electron Microscopy (SEM) to check the morphology of the graphene/PEDOT:PSS system prepared by the freeze-drying process (**Figure 11b**).

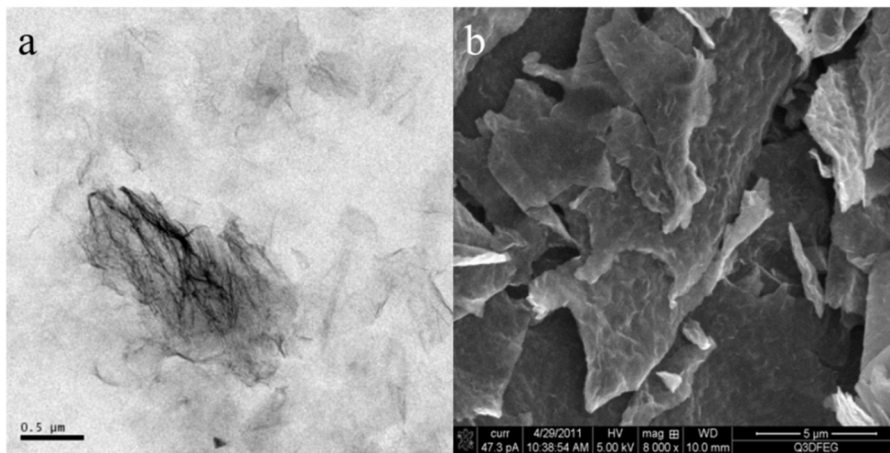


Figure 11. (a) TEM micrograph of graphene exfoliated in the presence of PEDOT:PSS; (b) SEM image of graphene covered with PEDOT:PSS.

When looking at the picture shown in Figure 11b one can notice that there is no indication of the presence of spherical objects, which could be PEDOT:PSS particles. On contrary we can observe graphene platelets having a rough and very bumpy surface, which can be the indication of its covering by PEDOT:PSS pancakes.

5.2.3.4. Utilizing low conductive PEDOT:PSS

To find out more about the morphology of the graphene/PEDOT:PSS/PS composites we also utilized a different PEDOT:PSS latex exhibiting low conductivity, namely 0.2 S/m according to the supplier. From now on we will call this latex LCPEDOT:PSS, which stands for low conductive PEDOT:PSS. The weight ratio of PSS to PEDOT in this system is 6 to 1. The exfoliation profile of a graphene/LCPEDOT:PSS dispersion with the same weight ratio of graphene to PEDOT:PSS as we used in the case of utilizing highly conductive PEDOT:PSS, namely 1:1.4, is shown in **Figure 12**.

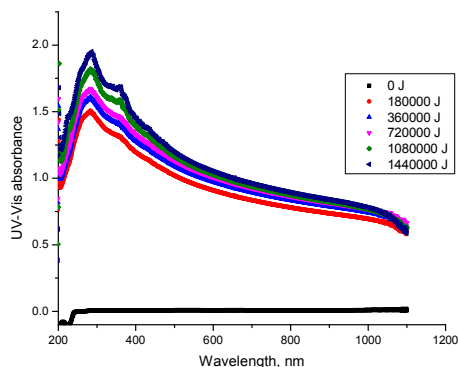


Figure 12. Evolution of UV–Vis spectra of an aqueous 0.1 wt% graphene/ 0.14 wt% LCPEDOT/PSS dispersion as a function of sonication energy.

The graphene/LCPEDOT:PSS system exhibits an absorbance level very similar to the system containing highly conductive PEDOT:PSS, which can mean that roughly the same degree of graphene exfoliation was achieved for both systems.

The results of the control blend of LCPEDOT:PSS and PS are shown in **Figure 13**. As one can see LCPEDOT:PSS in the PS matrix percolates at around 3.5 wt %, which is much higher than the value of the percolation threshold for highly conductive PEDOT:PSS in the same PS matrix. The final conductivity above the percolation threshold of this system is only 0.14 S/m. After the maximum obtainable exfoliation was achieved, the graphene/LCPEDOT:PSS dispersion was mixed with polystyrene latex, followed by freeze-drying and compression molding, resulting in a composite film. The conductivity curve is shown in Figure 13b. We compared these data with the data obtained for the graphene/PSS system and surprisingly found that whereas the percolation threshold of the

system containing LCPEDOT:PSS decreased to the value of 1.6 wt %, which is logical since we added a second conductive filler, the conductivity above the percolation threshold also dropped in comparison to the values of the graphene/PSS system.

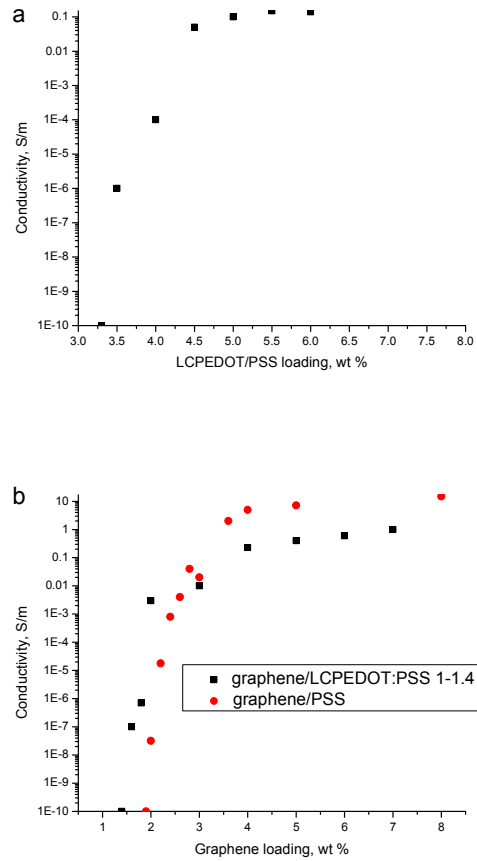


Figure 13. Conductivity curves: (a) LCPEDOT:PSS/PS nanocomposites; (b) graphene/PSS/PS and graphene/LCPEDOT:PSS/PS nanocomposites.

We also prepared aqueous dispersions of graphene with two other graphene/LCPEDOT:PSS ratios, namely 1 to 1 and 1 to 2.8. The conductivity curves of these systems are presented in **Figure 14**. One can notice that the percolation threshold of the system containing a weight ratio of graphene to LCPEDOT:PSS of 1:2.8 went down in comparison to the composites utilizing a graphene/LCPEDOT:PSS ratio of 1:1.4 (1.4 wt % vs. 1.6 wt %), but the conductivity values above the

percolation threshold also went slightly down (0.3 S/m vs. 1 S/m). The opposite happens if we disperse graphene with a ratio to LCPEDOT:PSS of 1 to 1. The decrease in the amount of LCPEDOT:PSS raises the percolation threshold to 1.9 wt % but also increases the conductivity of the nanocomposites above the percolation threshold up to 7 S/m. To summarize what we observe in the systems utilizing low conductive PEDOT:PSS we can state that with increasing amount of LCPEDOT:PSS with respect to graphene when making the aqueous graphene dispersion the percolation threshold of the final nanocomposites goes to the lower values, but the final conductivity also drops.

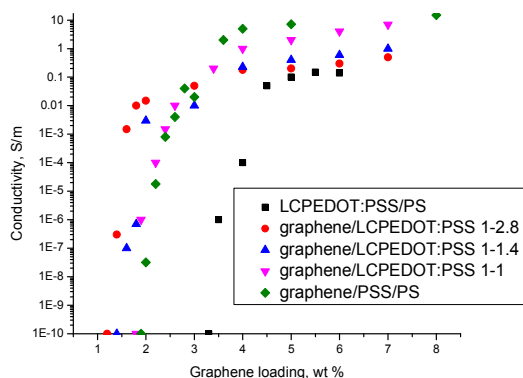


Figure 14. Conductivity curve of the graphene/LCPEDOT:PSS/PS nanocomposites with different weight ratios between the graphene and LCPEDOT:PSS.

The decrease in percolation threshold upon the addition of more and more of the second conductive nanofiller to the graphene/PS system is logical, since more conductive material is present for building a conductive network in the PS matrix. The fact that by adding more and more LCPEDOT:PSS we also lower the conductivity values can be attributed to the fact that if the low conductive PEDOT:PSS fully covers the graphene surface, then we predominantly measure the conductivity of this low conductive polymer. When graphene is not completely covered with PEDOT:PSS it also contributes to the conductivity of the nanocomposites. Thus the higher coverage of graphene surface results in a lower contribution of graphene to the conductivity of the corresponding nanocomposites. On the other hand one can say that graphene is not necessarily fully covered by PEDOT:PSS particles. It can be just partially covered by PEDOT:PSS (which makes dispersion of graphene stable) and PEDOT:PSS particles which are still available in the system can

“connect” the platelets by forming the bridges and contributing to the formation of a conductive network. This can also limit conductivity values in the case of utilizing LCPEDOT:PSS, since partial coverage still separates the platelets one from another, preventing them from contacting each other and in addition to that the presence of low conductive LCPEDOT:PSS bridges between graphene sheets lowers the conductivity due to junction resistivity. We think we can exclude the scenario where graphene platelets are covered just by PSS which is present in excess in the PEDOT:PSS system, since if it was the case graphene platelets would directly contact each other (having just PSS in between) and the conductivity values at high loading of graphene in graphene/LCPEDOT:PSS/PS systems with a ratio graphene/PEDOT:PSS 1 to 1.4 and 1 to 2.8 respectively would not differ that much from the conductivity of graphene/PSS/PS composites.

5.3. Conclusions

In order to make well performing conductive nanocomposites it is crucial to optimize each step of the latex-based process. In particular this is applicable for the first step, which is exfoliation and dispersion of a nanofiller in water. In this work we have found optimum conditions for the exfoliation and dispersion of graphene obtained by thermal reduction of graphite oxide at a concentration of 1 mg/ml using conventional surfactants such as SDBS, SC, PSS and Tween-80. We used these obtained dispersions for the preparation of nanocomposites. The composites prepared out of dispersions stabilized with ionic surfactants exhibit the same percolation threshold and the same values of the final conductivity, which means that graphene possesses the same degree of exfoliation in all the systems and the dispersion conditions had been optimized for the used surfactants. When preparing nanocomposites using Tween-80-stabilized graphene dispersions we observed higher percolation thresholds and lower conductivities in comparison with the systems utilizing SDBS, SC and PSS. This is due to a big amount of the bulky surfactant present on the graphene surface which stabilizes the dispersion by a steric effect. Such a steric effect can increase the distance between neighboring graphene platelets. We also demonstrated that applying a polymer of a low molecular weight for preparation of the nanocomposites lowers the percolation threshold in comparison with high molecular weight matrix but does not increase the conductivity above a percolation threshold. This can be attributed to the decrease in melt viscosity during compression molding step of the composites preparation, which in turn can influence the extent to which the graphene platelets reach an equilibrium organization. But it is not clear if this equilibrium organization is more or less aggregated than the initial state of graphene after freeze-drying just before the compression molding

step. For composites prepared by the latex concept and based on aqueous graphene/Tween-80 dispersions we successfully used both negatively charged and positively charged PS latex, which proves the advantage of utilizing this non-ionic surfactant for graphene dispersion, in water, since the charge of the latex is not an issue.

We demonstrated that the introduction of a highly conductive polymeric surfactant in the water dispersion step and finally into graphene/PS nanocomposites can significantly lower the percolation threshold and increase the ultimate conductivity. By applying SEM and replacing a highly conductive PEDOT:PSS by a low conductive one we obtained an idea about the morphology of the graphene/PEDOT:PSS system. It looks as if graphene is covered with this conductive polymer. The higher the coverage is, lower the contribution of graphene to the conductivity of the composite becomes. The use of a low conductive PEDOT:PSS can decrease the percolation threshold but by breaking the contacts between the highest conductive particles in this system, namely the graphene platelets, can also decrease the conductivity values above the percolation threshold due to the “shielding” of the graphene.

5.4. Experimental

Chemicals

Sodium dodecyl sulfate (SDS) (90%, Merck), sodium carbonate (99%, Aldrich), sodium peroxydisulfate (SPS) (90%, Merck), sodium cholate (SC) (99%, Aldrich), poly(sodium 4-styrene sulfonate) (PSS) (Aldrich, Mw 70000 g/mol) Tween-80 (Acros Organics), N-cetyl-N,N,N-trimethyl ammoniumbromide (CTAB) (99%, VWR) and 4,4'-azobis(4-cyanovaleric acid) (ACVA) (98%, Fluka) were used as received. PEDOT:PSS dispersions, grade name Clevios P (weight ratio PEDOT to PSS is 1 to 2.5) and Clevios P VP Al 4083 (weight ratio PEDOT to PSS is 1 to 6), were purchased from H. C. Starck and used as received. Styrene (99%, Merck) was passed over an inhibitor remover column. The inhibitor-free monomer was kept under refrigeration for later use. Water used in all reactions was double de-ionized water obtained from a purification system. SP-2 graphite from Bay Carbon was used as provided. Graphene was obtained via graphite (*SP-2 Bay Carbon*) oxidation and subsequent reduction via thermo-expansion process.^[22]

Preparation and characterization of PS latex

PS latex of high molecular weight was synthesized via conventional free radical emulsion polymerization. The reaction was performed at 70° C with an impeller speed of 400 rpm. The reactor

was charged with the following: styrene (252 g), SDS (26 g, 0.09 mol), sodium carbonate (0.7 g, 6.6 mmol) and H₂O (712.2 g). The reaction mixture was degassed by purging with argon for 30 min. A solution of SPS (0.45 g, 1.9 mmol) in H₂O (10 g) was also degassed. The reaction was started upon the introduction of the initiator solution and the reaction time was roughly 1 hour. The average particle size determined by dynamic light scattering was 90 nm. Size exclusion chromatography analysis showed M_w and PDI values of 944 kg/mol and 1.9, respectively.

Positively charged latex was prepared by means of a batch emulsion polymerizations performed in a 250 ml thermostated glass reactor, equipped with a reflux condenser, an argon purge inlet, four baffles and a 4-bladed stainless steel pitched blade impeller. The reactor was charged with styrene (140.1 g, 1.35 mol), CTAB (5.4 g, 0.83 mol) and H₂O (150 g). The temperature was gradually raised to the reaction temperature of 75°C and the reactor content was simultaneously purged with argon for an hour prior to initiator addition. The injection of an aqueous solution of 4,4'-azobis(4-cyanovaleric acid) (1.4 g, 5 mmol, in 5 ml of water) started the polymerization. The polymerization reached 100% conversion after ten hours. DLS measurements were performed on the final latex to determine its particle size distribution (PSD). The recorded average particle size was 380 nm. SEC was performed on the final polymer to determine the MWD. An M_w value of 150 kg/mol was recorded along with a PDI of 4.

Preparation of graphene dispersions

Exfoliated graphene dispersions from thermally reduced graphite oxide were prepared with the use of surfactant and energy supplied by ultrasound. The ultrasound was provided by a Sonics Vibracell VC750 horn sonicator with a 10 mm diameter tip. The sonication power was maintained at 100 W during the exfoliation, and the solution was cooled in an ice-bath. Volumes were kept under 100 ml to achieve the best sonication for the complete solution.

Composites processing

The graphene dispersion was mixed with PS latex, the mixture was frozen in liquid nitrogen for several minutes and the frozen water was removed with a Christ Alpha 2–4 freeze dryer operated at 0.2 mbar and 20 °C overnight. The resulting composite powder was compression molded into films for 2 min at 180 °C between Teflon sheets with a Collin Press 300G (we raise temperature from 160 °C to 180 °C for 18 minutes and then press the sample for 2 minutes).

UV–Vis spectroscopic measurements

UV–Vis absorption spectra were recorded with a Hewlett– Packard 8453 spectrometer operating between 200 and 1100 nm. Small sample volumes were taken after the sonication process and diluted, resulting in a graphene concentration of 0.0125 mg/ml. The blank used was the original surfactant solution, diluted and analyzed under the same conditions as the samples themselves.

Electrical conductivity measurements

The electrical conductivity was measured using a standard four-point method. Parallel contact lines 0.5 cm in length and with a 0.5 cm interval were drawn with conductive-silver paint (Fluka) on the composite film, and all conductivity measurements were performed at room temperature with a Keithley 6512 programmable electrometer. For each sample, conductivity data represent the average value of 10 consecutive measurements.

Transmission electron microscopy

TEM images were taken using a Sphera type Technai 20 (Fei Co.). This was operated with a 200 kV LaB6 filament and a bottom mounted 1024 x 1024 Gatan CCD camera. A carbon coated gold grid was used.

Scanning electron microscopy

SEM images were obtained with a Quanta 3D FEG (Fei Co.) equipped with a field emission electron source. High vacuum conditions were applied and a secondary electron detector was used for image acquisition. Additional sample treatment, such as coating with a conductive layer, was not applied. Standard acquisition conditions for charge contrast imaging were used.

5.5. References

- [1] R. J. Smith, M. Lotya, J. N. Coleman, *New Journal of Physics* **2010**, *12*, 125008.
- [2] X. Du, I. Skachko, A. Barker, E. Y. Andrei, *Nature Nanotechnology* **2008**, *3*, 491.
- [3] E. K. Hobbie, J. Obrzut, S. B. Kharchenko, E. A. Grulke, *Journal of Chemical Physics* **2006**, *125*, 044712.
- [4] Y. Ma, W. Cheung, D. Wei, A. Bogozzi, P. L. Chiu, L. Wang, F. Pontoriero, R. Mendelsohn, H. He, *Acs Nano* **2008**, *2*, 1197.
- [5] M. C. Hermant, B. Klumperman, A. V. Kyrlyuk, P. van der Schoot, C. E. Koning, *Soft Matter* **2009**, *5*, 878.
- [6] Z. Sun, V. Nicolosi, D. Rickard, S. D. Bergin, D. Aherne, J. N. Coleman, *Journal of Physical Chemistry C* **2008**, *112*, 10692.

- [7] N. Grossiord, P. J. J. Kivit, J. Loos, J. Meuldijk, A. V. Kyrlyuk, P. van der Schoot, C. E. Koning, *Polymer* **2008**, *49*, 2866.
- [8] S. D. Bergin, V. Nicolosi, H. Cathcart, M. Lotya, D. Rickard, Z. Sun, W. J. Blau, J. N. Coleman, *Journal of Physical Chemistry C* **2008**, *112*, 972.
- [9] N. Grossiord, O. Regev, J. Loos, J. Meuldijk, C. E. Koning, *Analytical Chemistry* **2005**, *77*, 5135.
- [10] M. Lotya, P. J. King, U. Khan, S. De, J. N. Coleman, *Acs Nano* **2010**, *4*, 3155.
- [11] S. Badaire, P. Poulin, M. Maugey, C. Zakri, *Langmuir* **2004**, *20*, 10367.
- [12] M. C. Hermant, N. M. B. Smeets, R. C. F. van Hal, J. Meuldijk, H. P. A. Heuts, B. Klumperman, A. M. van Herk, C. E. Koning, *E-Polymers* **2009**, *022*, 1.
- [13] N. Grossiord, H. E. Miltner, J. Loos, J. Meuldijk, B. Van Mele, C. E. Koning, *Chemistry of Materials* **2007**, *19*, 3787.
- [14] S. Hotta, S. Rughooputh, A. J. Heeger, *Synthetic Metals* **1987**, *22*, 79.
- [15] S. Ghosh, J. Rasmusson, O. Inganas, *Advanced Materials* **1998**, *10*, 1097.
- [16] P. Beadle, S. P. Armes, S. Gottesfeld, C. Mombourquette, R. Houlton, W. D. Andrews, S. F. Agnew, *Macromolecules* **1992**, *25*, 2526.
- [17] G. Lu, H. Tang, Y. Qu, L. Li, X. Yang, *Macromolecules* **2007**, *40*, 6579.
- [18] M. C. Hermant, P. van der Schoot, B. Klumperman, C. E. Koning, *Acs Nano* **2010**, *4*, 2242.
- [19] B. Friedel, P. E. Keivanidis, T. J. K. Brenner, A. Abrusci, C. R. McNeill, R. H. Friend, N. C. Greenham, *Macromolecules* **2009**, *42*, 6741.
- [20] A. M. Nardes, M. Kemerink, R. A. J. Janssen, J. A. M. Bastiaansen, N. M. M. Kiggen, B. M. W. Langeveld, A. J. J. M. van Breemen, M. M. de Kok, *Advanced Materials* **2007**, *19*, 1196.
- [21] A. M. Nardes, M. Kemerink, R. A. J. Janssen, *Physical Review B* **2007**, *76*, 085208.
- [22] M. J. McAllister, J.-L. Li, D. H. Adamson, H. C. Schniepp, A. A. Abdala, J. Liu, M. Herrera-Alonso, D. L. Milius, R. Car, R. K. Prud'homme, I. A. Aksay, *Chemistry of Materials* **2007**, *19*, 4396.

Chapter 6

Conductive cellulose-based polymer nanocomposites

ABSTRACT: The conductive polymer poly(3,4-ethylenedioxythiophene):poly(styrene sulfonate) (PEDOT:PSS) was used as surfactant for dispersing multi-walled carbon nanotubes (MWCNTs) in water. This stable dispersion was mixed with a polystyrene (PS) latex. After freeze-drying and compression molding conductive PS composites were obtained. The use of conductive polymer decreased the percolation threshold of the composites in comparison to the use of the conventional surfactant sodium dodecyl sulphate (SDS). To evaluate the contribution of the two conductive components to the overall conductivity of the composites one of them, *i.e.* the MWCNTs, was replaced with a non-conductive analogue with a similar aspect ratio, *i.e.* cellulose whiskers. PS composites based on aqueous dispersions of MWCNTs and cellulose whiskers in the presence of PEDOT:PSS were prepared using the same weight ratio of the nanofiller to the conductive polymer and both percolation thresholds and conductivity values were compared. The results revealed that the role of the MWCNTs and the cellulose is structural, and seems to be that of a scaffold or template for the organization of the conductive polymer and the contribution of the MWCNTs to the overall conductivity of the system is minimal, even at low loadings of the PEDOT:PSS. Conductive cellulose/PEDOT:PSS-based PS composites were developed. The addition of the cellulose whiskers allowed to lower the percolation threshold of PEDOT:PSS in the PS matrix drastically.

6.1. Introduction

Carbon nanotubes (CNTs) are quasi-one-dimensional carbon structures with large aspect ratio and low density which possess a unique combination of properties such as excellent mechanical, thermal and electrical properties.^[1] On account of their superior electrical properties CNTs is a natural choice for the production of conductive polymeric composites with potentially low percolation thresholds.^[2] Electrical percolation at very low filler concentration in CNTs/polymer composites leads to production of cost-effective composites.^[3] The difficulty of utilizing CNTs as a filler for nanocomposites is that CNTs as produced are held together in bundles due to van der Waals interactions. The challenge is to incorporate individualized CNTs inside a polymer matrix to lower the percolation threshold, since CNTs tend to remain bundled. CNTs-based composites prepared via the so-called latex technology demonstrated improved percolation behavior, *i.e.*, very low percolation thresholds.^[2, 4-6] However processes based on aqueous dispersions have a disadvantage because a third component, a surfactant is needed for dispersing and stabilizing the individual or small bundles of CNTs in water. If the surfactant is not displaced from the CNT walls during the processing steps of the composites preparation, an insulating shell remains around every CNT that could be detrimental for the intertube charge transport in the final composite.^[2, 7, 8] Also in polymer composites an additional resistance can arise from interfacial polymer layers present within the CNTs junctions.^[7] It was demonstrated theoretically that the presence of a conductive polymer within the intertube junctions can decrease the contact-potential barrier significantly which in turn can increase the ultimate electrical conductivity of the CNTs/polymer composite.^[9] Utilizing of poly(3,4-ethylenedioxythiophene):poly(styrene sulfonate) (PEDOT:PSS) as a conductive polymeric surfactant to disperse CNTs in water for the preparation of polymer composites through a latex-based route was shown to both increase the ultimate conductivity of the corresponding composites and alter the observed percolation threshold.^[2, 7] However, it was argued that the contribution of the CNTs to the ultimate conductivity of such a composite should not be overestimated, since the difference in the final conductivity of the composites observed for the systems based on CNTs of largely different quality, and respectively exhibiting different levels of intrinsic conductivity, was much lower than the difference in the intrinsic conductivities of both types of CNTs themselves.^[7] The way to investigate the contribution of the CNTs to the overall conductivity of CNTs/polymer composites containing an additional conductive polymeric component is to replace the CNTs with a non-conductive filler of a similar aspect ratio, e.g. cellulose nanowhiskers.

Cellulose is the most abundant macromolecule on earth, produced at the rate of 10^{11} - 10^{12} tons per year by nature.^[10] The cellulose nanowhiskers used in this work were obtained from sisal, resulting in nanowhiskers with an average cross section of 4 nm and an average length of 250 nm.^[11] Nanocomposite materials based on cellulose nanowhiskers have attracted much attention recently due to their mechanical properties.^[11-13] The main advantages of cellulose nanowhiskers are their renewable nature, the wide variety of fillers available throughout the world, their nonfood agricultural based economy, their low energy consumption, cost and low density, their high specific strength and modulus, the high sound attenuation of cellulose-based composites, the comparatively easy processability due to their nonabrasive nature, which allows high filling levels resulting in significant cost savings and their relatively reactive surface.^[12, 14-16]

In recent years, composite materials consisting of cellulose and conductive polymers have received significant attention.^[17-23] A drawback of many of such composites is that composites prepared with conductive polymers as the bulk matrix material often suffer from poor mechanical properties and processability. For composite films for which the bulk material properties of conductive polymers are not sufficiently good, it is necessary to “dilute” the matrix material with a second polymer that has the required mechanical and processing properties.^[2] Another drawback of such systems is that often very high loadings of conductive polymer, e.g. polyaniline and polypyrrole, are required for of the composites to conduct in a satisfactory way. A recent study templated polypyrrole onto cellulose nanowhiskers using electropolymerization resulting in a porous network which homogeneously grew from the electrode surface.^[24] The thin polypyrrole layer (~5nm) on the nanowhiskers was found to conduct, it displayed a high capacitance with near-ideal capacitive behavior, and the negative surface charge on the oxidized nanowhiskers stabilized the polypyrrole more effectively during charge-discharge cycles than the quivalent polypyrrole/carbon nanotube composite.^[24]

In this study we evaluate the role of multi-walled carbon nanotubes (MWCNTs) and conductive polymeric surfactant PEDOT:PSS in polystyrene (PS) composites, prepared via “latex technology” by replacing MWCNTs by a non-conductive filler with a similar aspect ratio, namely cellulose nanowhiskers, and by comparing electrical percolation thresholds and ultimate conductivities of the corresponding PS composites.

6.2. Results and discussion

Blends of PS and PEDOT:PSS were discussed in chapter 5 in the section 5.2.3.2.

6.2.1. MWCNTs- and cellulose whiskers-based polymer composites

MWCNTs tend to agglomerate in bundles due to van der Waals interactions and hence exfoliation of the nanotube bundles and the incorporation of CNTs as individual entities or as very thin bundles into a polymer matrix is an important issue. The sonication-driven exfoliation of aggregates and bundles of CNTs in an aqueous surfactant solution can be easily monitored by UV–Vis spectroscopy.^[25, 26] MWCNTs were dispersed in an aqueous sodium dodecyl sulphate (SDS) solution at a weight ratio CNTs/surfactant 1:2, which was determined to be optimal for the dispersion of these particular MWCNTs.^[27] The UV–Vis spectra recorded for aqueous MWCNTs dispersions, obtained after different energy-inputs (sonication times), are given in **Figure 1**. During sonication, the increasing amount of exfoliated MWCNTs results in an increasing area below the lines representing the absorbance. Since the power of sonication is kept constant throughout the experiments, there is a direct relationship between a specific sonication time and the energy delivered to the sample during this time interval. Therefore, it is equivalent to plot the absorbance at a certain wavelength versus the time of sonication or versus the energy supplied to the solution.

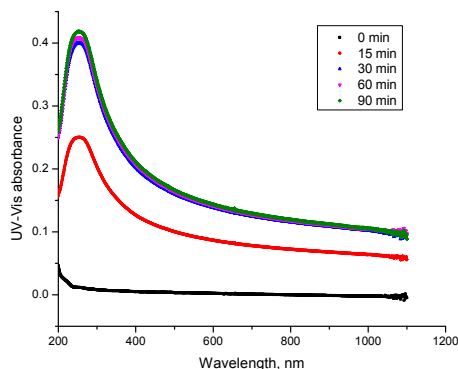


Figure 1. Evolution of UV–vis spectra of an aqueous 0.1 wt% MWCNT/ 0.2 wt% SDS (diluted 150 times) solution as a function of sonication time at continuous power of 20 W.

Figure 2 shows the absorbance around 250 nm as a function of the energy supplied to the aqueous MWCNTs/SDS solution. After an increase at the beginning of the sonication process, the value of the absorbance reaches a plateau value, namely after an energy input of ca. 40,000 J. The

leveling off and the ultimate limit of the absorbance, which follows the initial increase, correspond to the maximum achievable degree of exfoliation of the MWCNTs.^[28]

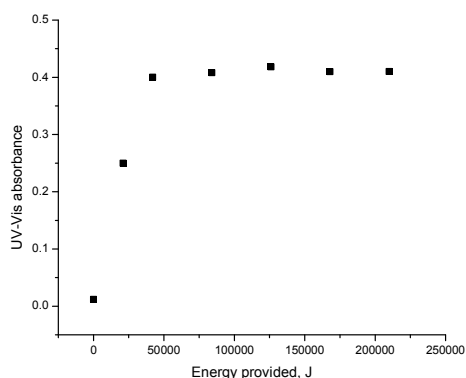


Figure 2. Evolution of the value of the absorbance at wavelength 252 nm for an aqueous 0.1 wt% MWCNT/0.2 wt% SDS solution as a function of energy provided to the system.

The efficiency of PEDOT:PSS to stabilize individual or thin bundles of MWCNTs in water was evaluated using UV-Vis spectroscopy. It was shown that for the efficient dispersion of the MWCNTs a four-fold weight excess of PEDOT:PSS is required, which is similar to what was reported for different kinds of single-walled nanotubes.^[2, 7] For the MWCNTs dispersion and exfoliation, weight ratios of 1 : 2 and 1 : 6 of MWCNTs to PEDOT:PSS were attempted. For the 1 to 2 ratio the maximum absorbance level reached was lower than that for the 1 : 4 system, whereas for the 1 to 6 ratio there was no further improvement observed. The exfoliation profile for the dispersion of MWCNTs in water using PEDOT:PSS as surfactant versus time is given in **Figure 3**. The evolution of the UV-Vis spectra of MWCNTs/PEDOT:PSS at wavelength of 252 nm as function of energy provided is shown in **Figure 4**. The profiles show that the dispersion of MWCNTs as a function of the ultrasonication energy input proceeds at somewhat lower rate when using PEDOT:PSS than when applying SDS. The final absorbance level reached, after correcting for the absorbance of the PEDOT:PSS surfactant at 252 nm, is comparable for both systems.

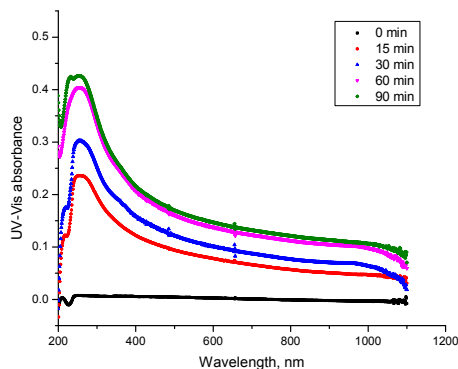


Figure 3. Following the exfoliation process of 0.1 wt % MWCNTs/ 0.4 wt % PEDOT:PSS (diluted 150 times) by UV-Vis.

The similarity between the two systems (the final absorbance values in Figures 2 and 4 are similar) could indicate that the maximum level of individualization for MWCNTs in water when using PEDOT:PSS is the same as when using SDS as surfactant.

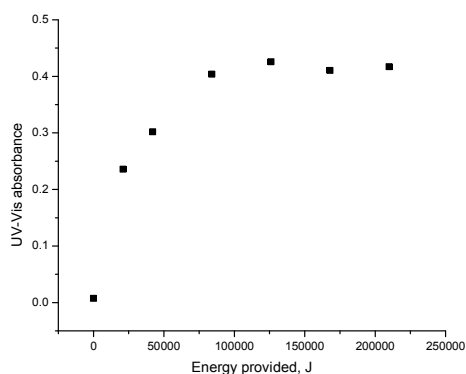


Figure 4. Evolution of the value of the absorbance at wavelength 252 nm for an aqueous 0.1 wt% MWCNT– 0.4 wt% PEDOT:PSS solution as a function of energy provided to the system.

The percolation thresholds observed for PS nanocomposites based on SDS- and PEDOT:PSS-stabilized MWCNTs are shown in **Figure 5**. Composites prepared with SDS-stabilized MWCNTs

have a percolation threshold value of 1.1 wt %. The ultimate conductivity achieved above percolation is 40 S/m. Composites prepared with PEDOT:PSS stabilized MWCNTs show a clear decrease in percolation threshold to 0.3 wt % (almost by factor 4) and an ultimate conductivity level of 500 S/m. This level is also comparable to that achieved for the PEDOT:PSS/PS blend (600 S/m, see Figure 6 in chapter 5). Considering the error in the conductivity measurements, a change in 100 S/m is not considered to be significant. This implies that, due to the fact that the final conductivity achieved for both the PEDOT:PSS/PS blends and the PEDOT:PSS/MWCNT system is similar, the origin of the increase from 40 S/m for the SDS/MWCNT system to 500 S/m for the PEDOT:PSS/MWCNT systems, is due to the presence of the PEDOT:PSS.

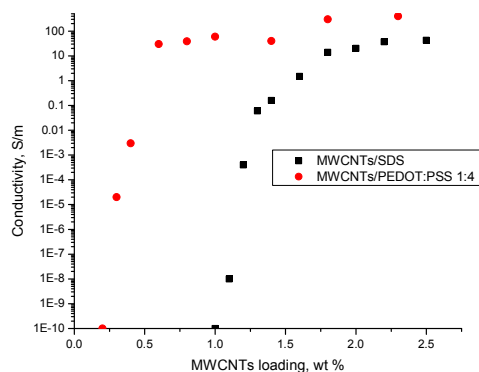


Figure 5. Conductivity curve of MWCNT/SDS/PS and MWCNT/PEDOT:PSS(1:4)/PS.

The morphology of the MWCNTs/PEDOT:PSS/PS composite can be twofold (**Figure 6**). In the first scenario CNTs can be stabilized by PSS which is present in excess in the PEDOT:PSS system (weight ratio PEDOT:PSS is 1 to 2.5). In this case CNTs can be partially covered 1) by both PEDOT:PSS particles which can be absorbed on the CNTs surface due to π - π interactions and partially by PSS or 2) just by PSS. The result of the first scenario can be a mixture of conductive rods and spheres (Figure 6a). The reduction in percolation is then induced simply by the addition of a different type of conductive filler particles to the CNTs present in the system, in this case PEDOT:PSS particles, which build conductive bridges between the neighboring tubes as well as between the tubes which are far apart. This scenario can also be considered as the so-called “excluded volume” scenario, since the CNTs, occupying a certain volume in a composite, push the

conductive polymer particles into “free” space and by doing this create a network of conductive polymer in addition to the network formed by the CNTs.

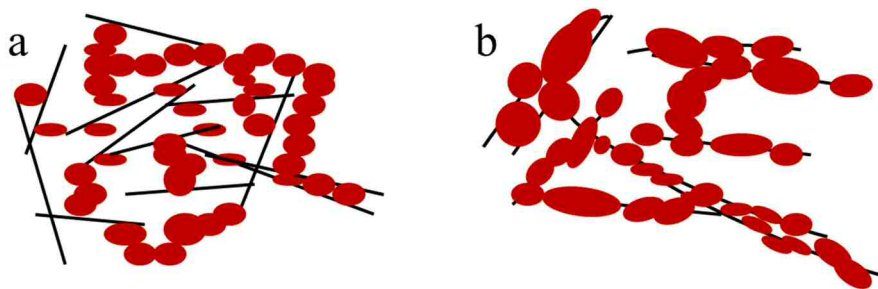


Figure 6. Possible morphologies of the MWCNTs/PEDOT:PSS system in a polymer matrix: (a) mixture of the CNTs and PEDOT particles stabilized by PSS; (b) the CNTs are covered with PEDOT pancakes.

In the second possible scenario (Figure 6b) the MWCNTs are nearly completely covered with PEDOT:PSS pancakes due to π - π interactions which “increase the diameter” of the tubes and their bundles which in turn decreases the distance between the tubes thereby obviously decreasing the percolation threshold with respect to the CNTs. Free PEDOT:PSS particles can be still present in the composite building conductive bridges between neighboring rods and bundles covered with PEDOT:PSS. From ultimate conductivity values it is not apparent which scenario is true due to the fact that the intrinsic conductivity of both nanofillers, MWCNTs and PEDOT:PSS, is comparable. Conductivity of PEDOT:PSS according to the supplier is 1000 S/m, whereas the conductivity of the bucky papers produced from the MWCNTs/SDS dispersions exhibit values up to 6000 S/m.

In order to understand the role of both conductive nanofillers one of the nanofillers should be replaced by a non-conductive one. We decided to replace the MWCNTs by cellulose nanowhiskers. A transmission electron microscopy (TEM) micrograph and a Scanning Electron Microscopy (SEM) image of dispersion of the cellulose nanowhiskers in water are given in **Figure 7**. The average nanowhisker length and diameter are 250 nm and 4 nm, respectively, resulting in an aspect ratio about 60.^[11] This close to the aspect ratio of the MWCNTs with an average length of ca. 1500 nm and an average diameter of ca. 20 nm.^[27]

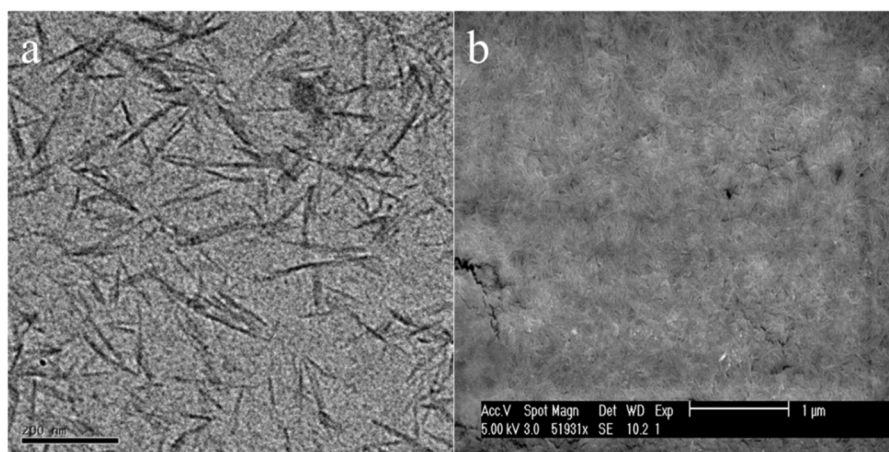


Figure 7. (a) TEM micrograph of exfoliated cellulose whiskers; (b) SEM image of exfoliated cellulose whiskers covered with gold.

For the preparation of the cellulose-based nanocomposites the nanowhiskers were mixed with PEDOT:PSS latex at 1 to 4 weight ratio. The percolation threshold of the cellulose/PEDOT:PSS/PS composites occurs at 0.35 wt % of the cellulose loading, meaning 1.4 wt % of PEDOT:PSS (**Figure 8**). The composites exhibit an ultimate conductivity of 500 S/m. The difference between the percolation thresholds of the MWCNTs- and cellulose-based systems is very small, 0.30 wt % for the CNTs versus 0.35 wt % for the cellulose. Now, one should take into account that cellulose whiskers do not conduct and subsequently cellulose-based PS composites do not exhibit any conductive percolation threshold. On the other hand MWCNTs/SDS-based PS composites percolate at 1.1 wt %. Then, if the conductivity of the conductive network would be composed of a summation of the contributions from the PEDOT:PSS and the conductive filler or cellulose whiskers, one might expect that the percolation threshold of the MWCNTs/PEDOT:PSS system would differ greatly from the cellulose/PEDOT:PSS system and would be significantly lower. However, the observed difference in the percolation thresholds is just 14 %! The great similarity in percolation thresholds of both systems implies that the electronic contribution of the MWCNTs is negligible in the system involving PEDOT:PSS-stabilized MWCNTs, meaning that the major role of both the MWCNTs and the cellulose is a structural one. In addition to that the ultimate conductivities of the PEDOT:PSS/PS, MWCNTs/PEDOT:PSS/PS and cellulose/PEDOT:PSS/PS composites are very similar, namely 600 S/m, 500 S/m and 500 S/m respectively. This is another factor which indicates that the conductivity of all the systems is predominantly determined by PEDOT:PSS, whereas the contribution of the

percolating MWCNTs is similar to the contribution of the percolating cellulose nanowhiskers, i.e. structural, where the rods play the role of a scaffold or template.

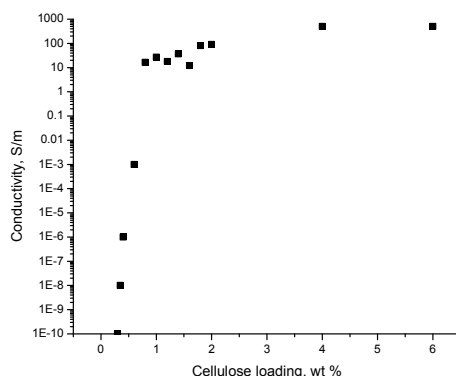


Figure 8. Conductivity curve of cellulose/PEDOT:PSS(1:4 weight ratio)/PS composites.

To increase the role of the CNTs and the cellulose whiskers the amount of the conductive polymer was decreased to a 1 to 1 weight ratio with respect to the nanofillers. Since for dispersion and exfoliation of the MWCNTs a minimum ratio MWCNTs/PEDOT:PSS of 1 to 4 is required (see earlier), the CNTs were dispersed with the aid of SDS and then mixed with PEDOT:PSS latex at the required ratio.

As one can see in **Figure 9** both the percolation thresholds of the two systems and their ultimate conductivities differ more significantly than for the systems where the weight ratio of the nanofillers to the conductive polymer was 1 to 4. The MWCNTs-based system exhibits a percolation threshold at 0.5 wt % and a conductivity of 100 S/m at 2.3 wt % of MWCNTs loading. Percolation of the cellulose nanowhiskers-based composites occurs at 0.7 wt % and the maximum conductivity measured is 3 S/m at 2.3 wt % cellulose loading. The differences in percolation thresholds between these two systems as well as in the conductivity values are clearly more pronounced than it was when the weight ratio the nanofiller/surfactant was 1 to 4, but still rather small if one takes into account the intrinsic properties of the MWCNTs and cellulose. This can indicate that the contribution of the conductive filler to the overall conductivity becomes slightly more important but still not very significant. Indeed, if the nanofiller is not completely covered with conducting polymer, MWCNTs can still provide a charge transfer bridge between discrete conducting polymer sections due to its own

conductivity, whereas this cannot occur for the non-conducting cellulose nanowhiskers. This is more likely to occur as the conducting polymer content is reduced.

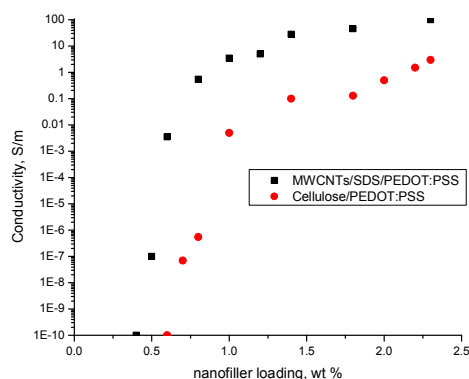


Figure 9. Conductivity curves of the MWCNTs- and cellulose-based PS composites prepared with a nanofiller/PEDOT:PSS weight ratio of 1 to 1.

Normally “latex-technology” for preparing electrically conductive nanocomposites consists of the following steps: 1) dispersion of the filler in the presence of surfactant (in the case of cellulose it’s mixing the cellulose whiskers with PEDOT:PSS); 2) mixing the nanofiller dispersion with polymer latex; 3) freeze-drying followed by compression molding. To check how the processing conditions influence conductive properties of the composites we performed experiments where we replaced the freeze-drying step by a water evaporation step by means of heating the mixture of the dispersed nanofiller and the polymer latex at 70 ° C. We did these experiments for the PS composites based on merely PEDOT:PSS and for the nanocomposites based on the cellulose/PEDOT:PSS mixture with the weight ratio of the cellulose whiskers and conductive polymer being 1 to 1. The results of the experiments are present in **Figure 10**.

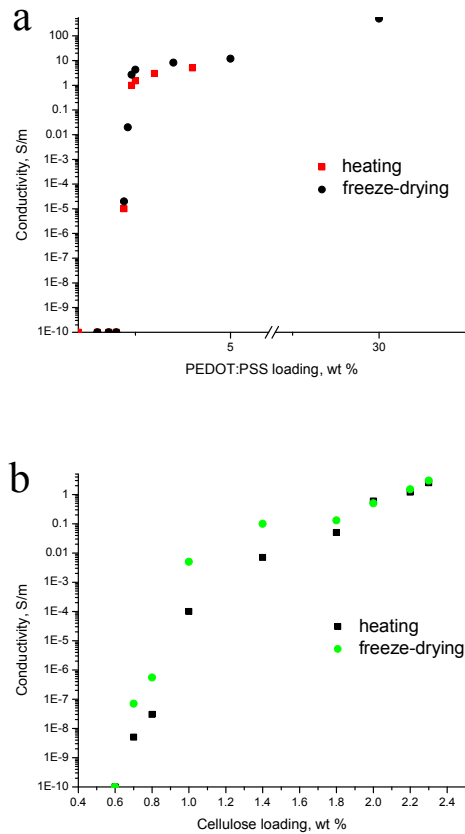


Figure 10. Conductivity curves of PEDOT:PSS/PS (a) and cellulose/PEDOT:PSS/PS (b) after applying different processing conditions for water removal: freeze-drying and drying by heating at 70 °C. The curves show that there is no influence of the method of water removal from the nanofiller/PEDOT:PSS/PS mixtures.

During the freeze-drying process the removal of water occurs under vacuum at negative temperature values since before placing the system under vacuum we freeze it by means of liquid nitrogen. One could suspect that at such conditions all the components of the system, namely the PEDOT:PSS and PS particles in one case and the cellulose, PEDOT:PSS and PS particles in the other case, are fixed at certain positions in the frozen water and that the PEDOT:PSS particles can not film-form and significantly adapt their aspect ratio during the drying process because no plasticizing water is present in this case. When drying the systems via water evaporation at elevated temperatures water can act as a plasticizer for PEDOT:PSS and thus facilitate the film formation.

Having said that one could expect that either freeze-drying or evaporation of water by means of heating could result in a different PEDOT:PSS morphology in the corresponding composites which in turn would result in different percolation thresholds for the PEDOT:PSS/PS and cellulose/PEDOT:PSS/PS composites prepared by the two different processing conditions. However there was not any difference observed in percolation thresholds when measuring the conductivity of the composites, as shown in Figure 10. Some difference in conductivity values just above the percolation thresholds can be seen when comparing the conductivity curves of both PEDOT:PSS/PS and cellulose/PEDOT:PSS/PS prepared by the two different methods. This difference is explained by some inhomogeneities observed in the systems when evaporating the water at 70 °C. Thus it's possible to conclude that replacing freeze-drying by heating for water removal from the PEDOT:PSS/PS or cellulose/PEDOT:PSS/PS mixtures doesn't affect the morphology of the conductive polymer in the corresponding systems. The reason for that can be that when transferring the composites from the freeze-dryer to the pressing machine for production of the composite films the hygroscopic PEDOT:PSS can attract some plasticizing water from the air.

The morphology of the MWCNTs/SDS/PEDOT:PSS and the cellulose/PEDOT:PSS drop-casted films and the cellulose/PEDOT:PSS freeze-dried powder was studied by SEM (**Figure 11**). The films and the powder were prepared with CNTs and cellulose concentrations of 1 mg/ml as was used for the composites preparation and with the nanofiller weight ratio with respect to PEDOT:PSS being 1 to 1. When looking at the film the CNTs are invisible, which can mean that they are covered with the PEDOT:PSS particles (Figure 11a). PEDOT:PSS is unstable under the laser beam which results in its burning when not covered with gold. When focusing a laser beam for a certain time at one spot the CNTs become visible due to the disappearing of the PEDOT:PSS layer (Figure 11b). To make the cellulose visible for SEM it has to be covered with gold. As one can see in Figure 11c,d there is no any clear indication of the cellulose whiskers being present on the surface or sticking out from the surface. Only PEDOT:PSS particles of different shape and size, which can be indication of the change of the aspect ratio of the original spherical PEDOT:PSS particles and some agglomeration, are visible. The freeze-dried powder of the cellulose/PEDOT:PSS (Figure 11e,f) exhibits a somewhat different morphology of the PEDOT:PSS particles in comparison with the drop-casted cellulose/PEDOT:PSS film. Individual PEDOT:PSS particles are not distinguishable. Instead one can see a smooth film of the conductive polymer. In the freeze-dried powder, both for the gold-covered and for the non-covered samples, some parts of the material seem to have some kind of rod-like shape, which could be the cellulose whiskers covered with PEDOT:PSS.

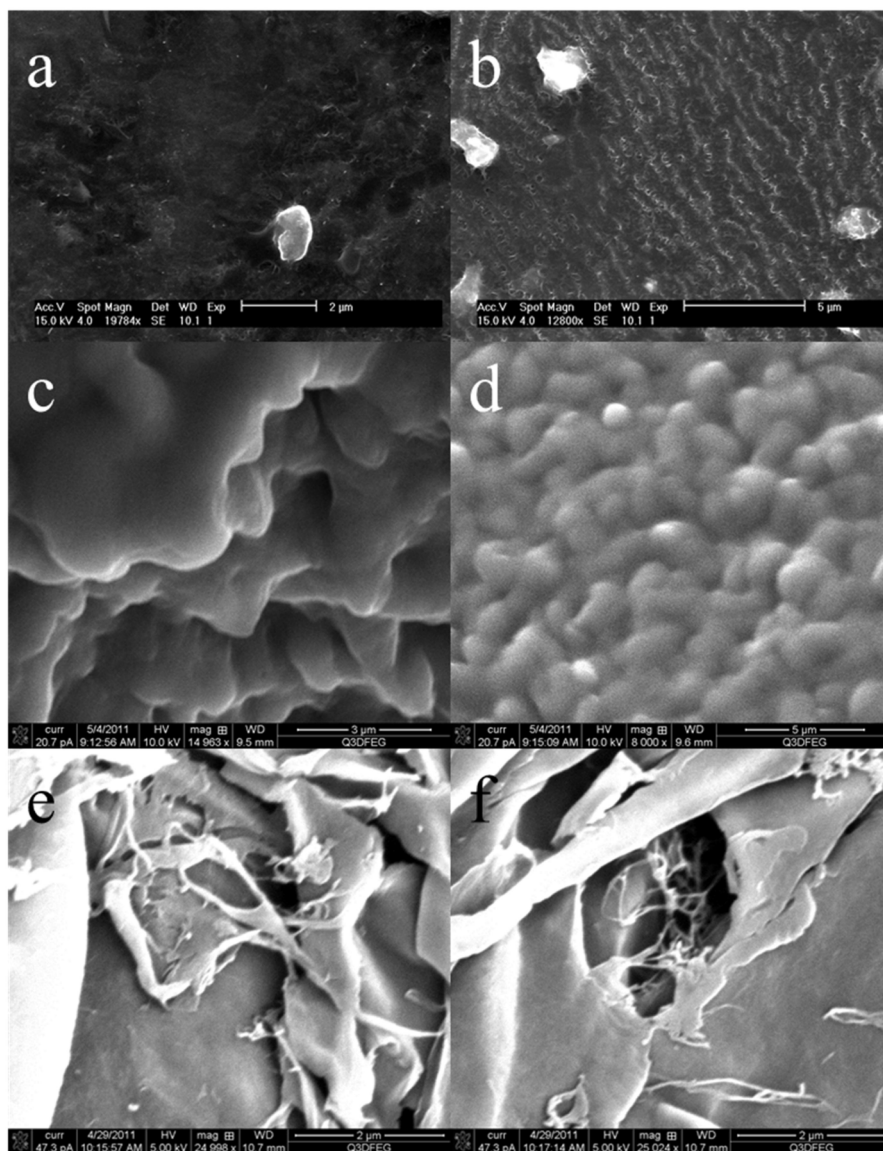


Figure 11. SEM of drop-casted MWCNT/SDS/PEDOT:PSS film (a and b), drop-casted cellulose/PEDOT:PSS film (c and d) and freeze-dried cellulose/PEDOT:PSS powder (e and f) on carbon tape: (a) the CNTs are almost invisible due to covering by PEDOT:PSS; (b) under affect of the laser beam the PEDOT:PSS layer locally disappears from the CNTs, which makes them visible; (c,d) different regions of the cellulose/PEDOT:PSS film covered with gold; (e) freeze-dried cellulose/PEDOT:PSS powder covered with gold; (f) freeze-dried cellulose/PEDOT:PSS powder not covered with gold. Weight ratio MWCNT/PEDOT:PSS and cellulose/PEDOT:PSS is 1:1.

On the other hand the conductivity data indicate that the MWCNT and cellulose nanofillers can not be fully covered with PEDOT:PSS, since if this was the case there wouldn't be any difference observed in percolation thresholds and conductivity values of the two systems. Apparently the MWCNTs contribute to the overall conductivity by contacting each other as well as the PEDOT:PSS particles, whereas the cellulose contacts can not at all contribute to the conductivity of the corresponding system. Nevertheless, the main role of MWCNTs seems to be the organization of the PEDOT:PSS.

To see if it's possible to further decrease the percolation threshold of the cellulose nanowhiskers-based PS composites with respect to the PEDOT:PSS content we prepared composites in which the weight ratio cellulose/PEDOT:PSS was 2 to 1. The conductivity curves with respect to both the cellulose content and the conductive polymer present in one and the same nanocomposite, are shown in **Figure 12**. As the figure shows the system percolates at 0.8 wt % cellulose loading and 0.4 wt % of the PEDOT:PSS loading, which is extremely low compared with PEDOT:PSS/PS composites without added cellulose whiskers. The conductivity reaches 5 S/m at 2.8 wt % of the conductive polymer.

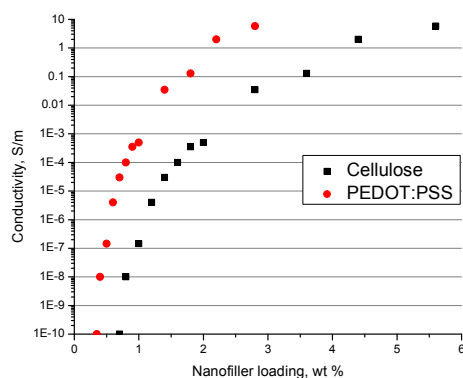


Figure 12. Conductivity curves of the cellulose/PEDOT:PSS/PS nanocomposites with the weight ratio between the cellulose and PEDOT:PSS of 2 to 1. Data points indicate cellulose or PEDOT:PSS content in one and the same nanocomposite.

We took SEM pictures of the drop-casted cellulose/PEDOT:PSS films with the weight ratio cellulose/PEDOT:PSS being 2 to 1. For the sample preparation we diluted the initial mixture from the working concentration of the cellulose (1 mg/ml) to 0.05 mg/ml to avoid crowding. The samples were

not covered with gold. As **Figure 13** shows PEDOT:PSS exhibits a certain network organization, which can be due to the fact that it covers cellulose whiskers and thus follows the network formation of the cellulose. This is somewhat similar to electrodeposited polypyrrole on cellulose nanowhiskers.^[24]

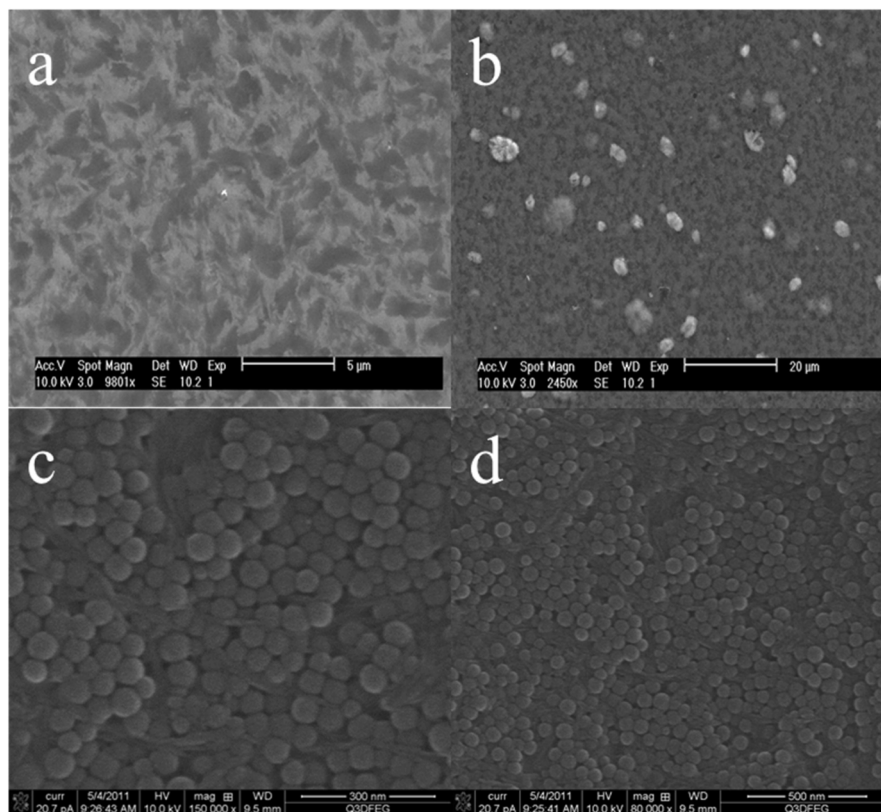


Figure 13. SEM of drop-casted cellulose/PEDOT:PSS film at different magnification (a and b), and freeze-dried cellulose/PS powder containing 5 wt % of cellulose at different magnification (c and d).

We also looked with the aid of SEM at the network formed when mixing the cellulose whiskers and PS latex (Figure 13c,d). Mixing a nanofiller with a polymer latex, which is one of the steps of the latex technology, is the most important step of the process, since it determines the effective incorporation of the filler into the polymer matrix. Then, the mixture of the two types of colloidal particles, i.e. the cellulose nanowhiskers and latex particles, is freeze-dried. In principle, the

sublimation of the water induced by freeze-drying is not expected to significantly modify the aggregated state of the cellulose nor the quality of mixing of the cellulose and the polymer latex particles.^[27] Of course, drying induces a compaction of the nanofiller network that becomes denser because of the water removal. After compaction of the powder consisting of submicron polymer particles and cellulose whiskers, cellulose whiskers are forced into the interstitial space between the polymer latex particles and organize themselves in a network which can be built up from individual cellulose whiskers as well as some bundles. If PEDOT:PSS indeed covers the cellulose nanowhiskers when mixed with them and follows the cellulose network formation between the PS latex particles before these are deformed and fused together in the compression molding step it can explain the very low percolation threshold of this conductive polymer in the cellulose/PS composites.

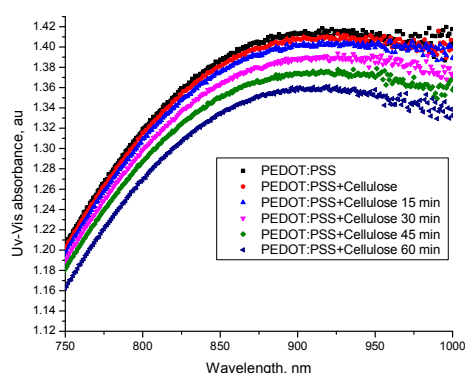


Figure 14. Following the interaction process between PEDOT:PSS and cellulose by UV-Vis. The absorbance is decreasing in time.

An interaction between cellulose whiskers and PEDOT:PSS can be monitored with UV-Vis absorbance measurements.^[29] For that we used a dispersion of the cellulose whiskers at a concentration of 1 mg/ml with the weight ratio 2 to 1 with respect to the PEDOT:PSS (**Figure 14**). We measured the UV-Vis absorbance in time. As a reference a diluted PEDOT:PSS water dispersion of the same concentration as in the cellulose dispersion was taken. When comparing the absorbance curves one can see that immediately after mixing the conductive polymer with cellulose the UV-Vis absorbance slightly decreases. The decrease continues over time, which indicates that interaction of the conductive polymer and cellulose occurs. We didn't measure the absorbance after more than 1

hour since this is the time we used for mixing the cellulose whiskers with PEDOT:PSS before subsequent mixing with the PS latex and freeze-drying of the final mixture. The decrease in the absorbance can be attributed to the adsorbance of PEDOT:PSS on the cellulose surface and the inherent decrease in the surface area of the PEDOT:PSS particles due to agglomeration around individual cellulose whiskers or their bundles. One might expect that this interaction of the cellulose whiskers and conductive polymer can be due to the formation of hydrogen bonds between hydroxyl groups of the cellulose and sulfonate groups of the conductive polymer. Infrared spectroscopy didn't show any chemical interaction between these two fillers, meaning that PEDOT:PSS physically adsorbs on the cellulose surface. The results of the UV-Vis experiments support our hypothesis that the cellulose nanowhiskers form a template on which the PEDOT:PSS adsorbs.

6.3. Conclusions

We investigated the cooperative nature of the two conductive fillers in MWCNTs/PEDOT:PSS/PS composites with the focus on the contribution of the CNTs to the overall composite conductivity. For that we replaced the CNTs by non-conductive fillers with an almost similar aspect ratio, namely cellulose whiskers and the two systems MWCNTs/PEDOT:PSS/PS and cellulose/PEDOT:PSS/PS were compared. Cellulose whiskers do not exhibit any conductivity, whereas the bucky papers prepared with the MWCNTs exhibit a conductivity up to 6000 S/m. The PS composites based on SDS-stabilized MWCNTs percolate at 1.1 wt % and show an ultimate conductivity of 40 S/m. As was seen in both systems, when adding a large excess of the conductive PEDOT:PSS to the PS-based nanocomposites containing either CNTs or the cellulose, percolation thresholds with respect to the MWCNTs and cellulose as well as conductivity values didn't differ and were not depending on the intrinsic conductive properties of the nanofillers, *i.e.* either MWCNTs or cellulose nanowhiskers. This means that MWCNTs didn't significantly contribute to the ultimate conductivity of the MWCNTs/PEDOT:PSS/PS system but played a role of scaffold for the conductive polymer. When decreasing the amount of PEDOT:PSS with respect to the MWCNTs and cellulose to the weight ratio of 1 to 1 a slight difference in percolation thresholds of the two systems occurs. The difference in the conductivity values is two orders of magnitude, which is still much lower than the difference in the intrinsic conductivities of the nanofillers. These results imply that even at quite low loadings of the conductive polymer it plays the main role in the determining the overall conductivity of the corresponding composites whereas the role of the CNTs is that of forming a template, meaning that the CNTs can be replaced in this case by the cheap and most abundant natural material, *i.e.*

cellulose. By replacing the CNTs in the composites by cellulose nanowhiskers using the four-step latex technology utilizing conductive surfactant, PEDOT:PSS, we developed cellulose-based PS composites with an extremely low percolation threshold of the conductive polymer. The percolation threshold of 2.2 wt % of PEDOT:PSS for PEDOT:PSS/PS composites was lowered to 0.4 wt % by adding 0.8 wt % of the cheap cellulose whiskers. Such a low percolation threshold of PEDOT:PSS is attributed to the fact that PEDOT:PSS adsorbs on a cellulose surface and by doing that follows the network formed by the cellulose whiskers in the PS matrix. UV-Vis experiments indeed point to an interaction between PEDOT:PSS and the cellulose whiskers.

6.4. Experimental

Chemicals

Sodium dodecyl sulfate (SDS) (90%, Merck), sodium carbonate (99%, Aldrich), sodium peroxydisulfate (SPS) (90%, Merck) and sodium cholate (SC) (99%, Aldrich) were used as received. Styrene (99%, Merck) was passed over an inhibitor remover column. The inhibitor-free monomers were kept under refrigeration for later use. Water used in all reactions was double de-ionized water obtained from a purification system. MWCNTs were produced by Nanocyl Co (Belgium). They were made using a CVD-based process (thin MWCNTs Nanocyl-3100, batch 060213) and purified by the manufacturer by a mild non-oxidative acidic treatment. These CNTs were used as-received.

Cellulose nanowhiskers preparation

Cellulose nanowhiskers derived from sisal were prepared using an earlier published procedure.^[11] After preparation and purification, they were sonicated with a Branson sonifier at 40W for 5 min to obtain a stable dispersion in water.

Preparation and characterization of PS latex

PS latex was synthesized via conventional free radical emulsion polymerization. The reaction was performed at 70° C with an impeller speed of 400 rpm. The reactor was charged with the following: styrene (252 g), SDS (26 g, 0.09 mol), sodium carbonate (0.7 g, 6.6 mmol) and H₂O (712.2 g). The reaction mixture was degassed by purging with argon for 30 min. A solution of SPS (0.45 g, 1.9 mmol) in H₂O (10 g) was also degassed. The reaction was started upon the introduction of the initiator solution and the reaction time was roughly 1 hour. The average particle size determined by

dynamic light scattering was 90 nm. Size exclusion chromatography analysis showed M_n , M_w and PDI values of 495 kg/mol, 944 kg/mol and 1.9, respectively.

Composites processing

The aqueous MWCNTs/cellulose dispersions were mixed with PS latex, the mixture was frozen in liquid nitrogen for several minutes and the frozen water was removed with a Christ Alpha 2–4 freeze dryer operated at 0.2 mbar and 20 °C overnight. The resulting composite powder was compression molded into films for 20 min at 180 °C between Teflon sheets with a Collin Press 300G.

UV–Vis spectroscopic measurements

UV–Vis absorption spectra were recorded with a Hewlett–Packard 8453 spectrometer operating between 200 and 1100 nm. Small sample volumes of MWCNTs were taken after the sonication process and diluted 150 times. The blanks used were the original SDS or PEDOT:PSS solution, diluted and analyzed under the same conditions as the samples themselves.

Electrical conductivity measurement

The electrical conductivity was measured using a standard four-point method. Parallel contact lines 0.5 cm in length and with a 0.5 cm interval were drawn with conductive-silver paint (Fluka) on the composite film, and all conductivity measurements were performed at room temperature with a Keithley 6512 programmable electrometer. For each sample, conductivity data represent the average value of 10 consecutive measurements.

Transmission electron microscopy

TEM images were taken using a Sphera type Technai 20 (Fei Co.). This was operated with a 200 kV LaB6 filament and a bottom-mounted 1024 x 1024 Gatan CCD camera. A carbon coated gold grid was used.

Scanning electron microscopy

SEM images were obtained with a Quanta 3D FEG (Fei Co.) equipped with a field emission electron source. High vacuum conditions were applied and a secondary electron detector was used for image acquisition. Additional sample treatment, such as coating with a conductive layer, has been applied when necessary before surface scanning. Standard acquisition conditions for charge contrast imaging were used.

6.5. References

- [1] A. V. Kyrlyuk, M. C. Hermant, T. Schilling, B. Klumperman, C. E. Koning, P. van der Schoot, *Nature Nanotechnology* **2011**, *6*, 364.
- [2] M. C. Hermant, B. Klumperman, A. V. Kyrlyuk, P. van der Schoot, C. E. Koning, *Soft Matter* **2009**, *5*, 878.
- [3] M. Arjmand, M. Mahmoodi, G. A. Gelves, S. Park, U. Sundararaj, *Carbon* **2011**, *49*, 3430.
- [4] M. C. Hermant, M. Verhulst, A. V. Kyrlyuk, B. Klumperman, C. E. Koning, *Composites Science and Technology* **2009**, *69*, 656.
- [5] O. Regev, P. N. B. ElKati, J. Loos, C. E. Koning, *Advanced Materials* **2004**, *16*, 248.
- [6] A. Dufresne, M. Paillet, J. L. Putaux, R. Canet, F. Carmona, P. Delhaes, S. Cui, *Journal of Materials Science* **2002**, *37*, 3915.
- [7] M. C. Hermant, P. van der Schoot, B. Klumperman, C. E. Koning, *Acs Nano* **2010**, *4*, 2242.
- [8] E. K. Hobbie, J. Obrzut, S. B. Kharchenko, E. A. Grulke, *Journal of Chemical Physics* **2006**, *125*.
- [9] D. L. Carroll, R. Czerw, S. Webster, *Synthetic Metals* **2005**, *155*, 694.
- [10] W. Thielemans, C. R. Warbey, D. A. Walsh, *Green Chemistry* **2009**, *11*, 531.
- [11] N. L. G. de Rodriguez, W. Thielemans, A. Dufresne, *Cellulose* **2006**, *13*, 261.
- [12] S. J. Eichhorn, A. Dufresne, M. Aranguren, N. E. Marcovich, J. R. Capadona, S. J. Rowan, C. Weder, W. Thielemans, M. Roman, S. Renneckar, W. Gindl, S. Veigel, J. Keckes, H. Yano, K. Abe, M. Nogi, A. N. Nakagaito, A. Mangalam, J. Simonsen, A. S. Benight, A. Bismarck, L. A. Berglund, T. Peijs, *Journal of Materials Science* **2010**, *45*, 1.
- [13] R. J. Moon, A. Martini, J. Nairn, J. Simonsen, J. Youngblood, *Chemical Society Reviews* **2011**, *40*, 3941.
- [14] M. Samir, F. Alloin, A. Dufresne, *Biomacromolecules* **2005**, *6*, 612.
- [15] L. J. Nielsen, S. Eyley, W. Thielemans, J. W. Aylott, *Chemical Communications* **2010**, *46*, 8929.
- [16] S. Eyley, W. Thielemans, *Chemical Communications* **2011**, *47*, 4177.
- [17] G. Nystrom, A. Mihranyan, A. Razaq, T. Lindstrom, L. Nyholm, M. Stromme, *Journal of Physical Chemistry B* **2010**, *114*, 4178.
- [18] J. A. Li, X. R. Qian, J. H. Chen, C. Y. Ding, X. H. An, *Carbohydrate Polymers* **2010**, *82*, 504.
- [19] C. Y. Ding, X. R. Qian, G. Yu, X. H. An, *Cellulose* **2010**, *17*, 1067.
- [20] W. Hu, S. Chen, Z. Yang, L. Liu, H. Wang, *Journal of Physical Chemistry B* **2011**, *115*, 8453.
- [21] Z. L. Mo, Z. L. Zhao, H. Chen, G. P. Niu, H. F. Shi, *Carbohydrate Polymers* **2009**, *75*, 660.

- [22] M. Micusik, M. Omastova, J. Prokes, I. Krupa, *Journal of Applied Polymer Science* **2006**, *101*, 133.
- [23] I. Wistrand, R. Lingstrom, L. Wagberg, *European Polymer Journal* **2007**, *43*, 4075.
- [24] S. Y. Liew, W. Thielemans, D. A. Walsh, *Journal of Physical Chemistry C* **2010**, *114*, 17926.
- [25] N. Grossiord, J. Loos, J. Meuldijk, O. Regev, H. E. Miltner, B. Van Mele, C. E. Koning, *Composites Science and Technology* **2007**, *67*, 778.
- [26] J. Yu, N. Grossiord, C. E. Koning, J. Loos, *Carbon* **2007**, *45*, 618.
- [27] N. Grossiord, P. J. J. Kivit, J. Loos, J. Meuldijk, A. V. Kyrlyuk, P. van der Schoot, C. E. Koning, *Polymer* **2008**, *49*, 2866.
- [28] N. Grossiord, O. Regev, J. Loos, J. Meuldijk, C. E. Koning, *Analytical Chemistry* **2005**, *77*, 5135.
- [29] E. Montibon, L. Jarnstrom, M. Lestelius, *Cellulose* **2009**, *16*, 807.

Chapter 7

Technology assessment

ABSTRACT. In this chapter we highlight the main conclusions of the thesis. The advantages and disadvantages of using graphene of different types for the preparation of conductive polymer nanocomposites in terms of their possible industrial applications are discussed. An outlook for future research is presented.

7.1. Highlights and industrial application

Polymer nanocomposites based on carbon black and carbon nanotubes have been used for improved mechanical, thermal, electrical, and gas barrier properties of polymers.^[1, 2] The discovery of graphene with its combination of extraordinary physical properties and ability to be dispersed in various polymer matrices has created a new class of polymer nanocomposites.^[3] The work described in this thesis is a contribution to this research field. For the preparation of conductive polymer nanocomposites via latex technology we utilized graphene produced from graphite via three different methods, namely 1) via oxidation of graphite and subsequent chemical reduction of graphite oxide (GO) in the presence of surfactant (sodium poly(styrene sulfonate) (PSS)), 2) via oxidation of graphite and subsequent thermal reduction of GO and 3) via liquid phase exfoliation of graphite by bath sonication in the presence of surfactant (sodium cholate (SC)). In general, these methods are suitable for large scale graphene production required for industrial polymer nanocomposite applications. Starting from graphite or its derivatives offers significant economic advantages over the methods like mechanical exfoliation, chemical vapor deposition and epitaxial growth. Graphite is a commodity material with an annual global production of over 1.1 million tons at \$825/ton in 2008.^[3]

The three used methods for graphene preparation provide graphene of different quality, which can easily be proven by Raman spectroscopy (**Figure 1**).

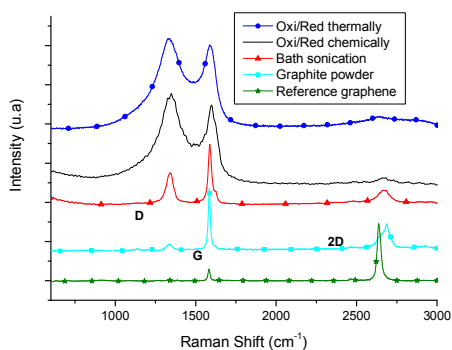


Figure 1. Raman spectra of graphene prepared via: oxidation and subsequent chemical reduction in the presence of surfactant (PSS); via oxidation and subsequent thermal reduction; and via liquid phase exfoliation by bath sonication in the presence of surfactant (SC). Spectra of raw graphite powder and mechanically cleaved graphene are used as references.

For graphene prepared via both oxidation/chemical reduction (oxi/red chem.) and oxidation/thermal reduction (oxi/red therm.), the prominent D peak (absent in mechanically cleaved graphene and graphite powder) is attributed to the presence of sp^3 carbons in the carbon basal plane and different residual functionalities such as carboxylic acid groups, epoxides, or ketones. These and other forms of defects can increase the D band intensity. The intensity of the 2D peak with respect to the D and G peaks is really small, probably due to the structural disorder. Since it is difficult to conclude much from the 2D peak for these samples due to its low intensity and broadness, we only note a small Raman shift to a lower wavenumber and absence of any prominent shoulder, indicating the proximity of the formation of a single layer of graphene.

The introduction of edge defects during processing into graphene, prepared via liquid phase exfoliation, is unavoidable, since long-term sonication cuts the initially large sheets into smaller flakes. However, the majority of the D bands observed for graphene flakes of this type is both narrower and less intense in comparison to the graphene produced via oxidation/reduction methods, strongly suggesting that the aqueous dispersions produced have flakes with very low defect contents and are of a higher quality.^[4] This is confirmed by the conductivity measurements of the bucky papers produced from the three different types of graphene. The bucky papers produced from the graphene made via both oxidation/reduction methods exhibit conductivities up to 6,000 S/m, whereas the conductivities of the bucky papers prepared from the graphene produced via liquid phase exfoliation reach values up to 17,000 S/m.^[5]

Atomic force microscopy (AFM) was extensively applied to determine the sheet thicknesses, morphological features and lateral dimensions of the graphene samples (**Figure 2**). AFM analyses of graphene prepared by both oxidation/chemical reduction and oxidation/thermal reduction show that, on average, a visible wrinkling of the platelets is present. It was also observed that agglomeration and a reduction of the lateral size occurs in comparison to the GO just before the reduction processes. This size reduction is just indicative, as the folding/agglomeration of graphene makes it difficult to obtain reliable statistical data. It seems that the wrinkling is more severe for the oxi/ therm. red graphene. Nevertheless, the measurements on flat areas indicated that the majority of the material consists of graphene flakes with a thickness of 1-5 nm for both oxidized/reduced systems. Still, the rugosity of both graphene flat surface areas is higher as compared to similar measurements done by our group on mechanically cleaved graphene, probably due to defects or unremoved side groups on the surface. Differently from results reported elsewhere and controversial to Raman analysis, the AFM analysis on the graphene produced via bath sonication of graphite in water in the

presence of sodium cholate (SC) shows in addition to thin graphene platelets the presence of some thicker platelets, namely sheets with thicknesses between 5 and 25 nm.^[4, 5]

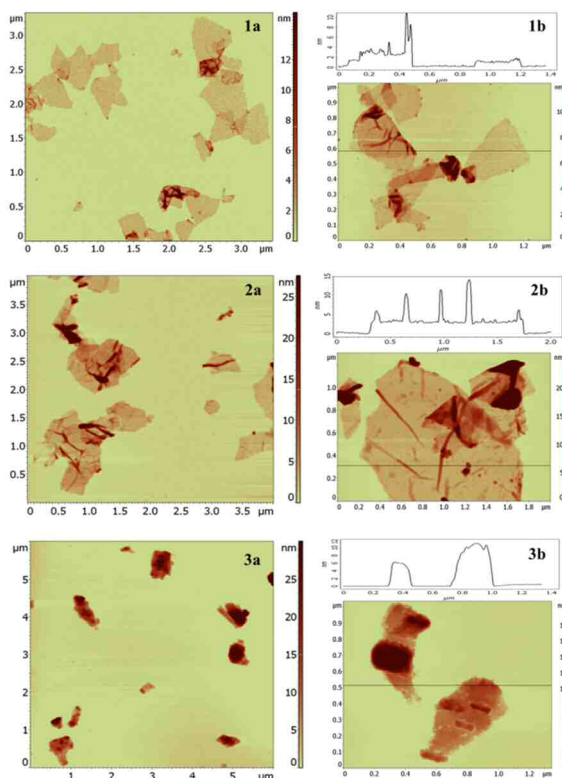


Figure 2. AFM tapping mode topography of graphene prepared via (1a,b): oxidation/chemical reduction; (2a,b): oxidation/thermal reduction; (3a,b): liquid phase exfoliation.

Also it has to be said that dispersions of graphene produced via liquid phase exfoliation of graphite in the presence of surfactant exhibit a higher stability in comparison to graphene produced via oxidation/reduction methods.

With a view on industrial application one can say that production of graphene via oxidation of graphite with subsequent thermal reduction of graphite oxide is more attractive than the other two methods due to the shorter time needed for the preparation of graphene. Oxidation of graphite to graphite oxide via the method described by Hummers requires about 3 hours, whereas the subsequent thermal reduction and exfoliation of the generated GO requires only a few minutes.^[6, 7]

To complete the exfoliation and to disperse this graphene in water by tip-sonication in the presence of surfactant another 3-4 hours are needed. In contrast, chemical reduction and exfoliation of GO can take up to 70 hours depending on the level of reduction needed.^[8, 9] Another disadvantage of the chemical reduction is that it requires a huge excess of a surfactant (namely a weight ratio surfactant:GO up to 10:1) which in turn requires filtration of the final product to remove the excess of the surfactant. The disadvantage of the graphite liquid phase exfoliation method for the preparation of graphene in comparison to the oxidation/thermal reduction method is that, depending on the concentration of graphene needed, it requires from 100 up to 400 hours of bath sonication of graphite in water followed by centrifugation.^[4, 5]

The electrical conductivity of the polystyrene (PS)-based nanocomposites prepared via latex technology, utilizing graphene produced via the three mentioned methods, as a function of the graphene content is shown in **Figure 3**.

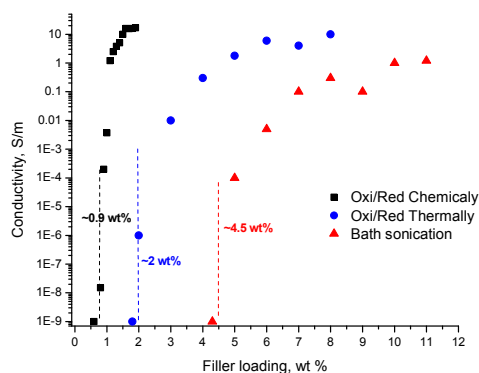


Figure 3. Electrical conductivity of graphene/PS nanocomposites as a function of graphene weight fraction.

As one can see the percolation thresholds differ a lot depending on the type of graphene used for the preparation of polymer nanocomposites. A percolation threshold depends mainly on the dispersion state, the electron transport mechanism (depending on the presence of surfactant/polymer at or around the nanofiller surface or on impurities present in between the platelets) and filler morphology/dimensions (in fact the length/thickness or 'aspect' ratio). In our work we demonstrated that despite the higher quality of graphene itself and the smaller number of defects introduced into

the graphene structure during processing, nanocomposites based on graphene produced via liquid phase exfoliation of graphite exhibit the highest percolation threshold and the lowest conductivity at loadings of graphene up to 12 wt % in comparison to the nanocomposites based on graphene obtained by the oxidation/reduction methods. Taking this into account we can assume that for production of polymer nanocomposites on an industrial scale graphene produced by thermal reduction of GO should be utilized, since it has an important advantage over the other two methods in terms of time needed for the preparation of graphene and it also exhibits a clear advantage over graphene prepared via liquid phase exfoliation method in terms of a lower percolation threshold and a higher conductivity level which can be reached at relatively low loadings of the thermally reduced graphene.

In this work we prepared PS nanocomposites based on graphene obtained by *in-situ* reduction of graphene oxide during the last step of the latex-technology process, namely during compression molding. This method for the preparation of conductive graphene/polymer nanocomposites exhibits a big advantage over the methods utilizing graphene preliminary produced via the three methods discussed above in terms of time consumption and the easiness of the process. GO produced via Hummers method can be easily exfoliated and dispersed in water by stirring or by mild sonication, giving graphene oxide which can be stored in this state at quite high concentrations, namely up to 1 mg/ml, for a long period of time without aggregation. Even if slightly aggregated graphene oxide is formed during storage this can be easily redispersed. Another big advantage of the *in-situ* preparation method is that it doesn't require sonication of the nanofiller at big sonication power, which prevents excessive degradation and accordingly results in larger graphene flakes with higher aspect ratios in the final product in comparison to the methods using preliminary produced graphene. Stirring when mixing with polymer latex homogeneously distributes graphene oxide in the water-based system, which results in its homogeneous distribution in a final nanocomposite film. The reduction of graphene oxide in this case is caused by a high temperature (180 °C) treatment during a processing step which is required anyway. In our case this method didn't result in composites exhibiting very high conductivity values, but the conductivity levels achieved (0.15 S/m) might be high enough for antistatic, and maybe even for electromagnetic interference (EMI) shielding applications.

In the present work we have also demonstrated that utilizing a conductive surfactant such as PEDOT:PSS in the aqueous graphene dispersion step of the latex concept can significantly decrease the percolation threshold of graphene/polymer nanocomposites with respect to using conventional surfactant for the dispersion of graphene in water. Moreover the addition of the conductive surfactant

raises the maximum conductivity up to a few hundreds of S/m at graphene loadings below 5 wt %. Graphene can be dispersed in water with the aid of PEDOT:PSS, and the presence of an additional surfactant is not needed. PEDOT:PSS is commercially available and extensively used in the electrical and electronics industry as well as in the production of solar cells, but it is a relatively expensive conductive polymer (200-400 Euros per liter). Nevertheless, since a quite low loading of this polymer is required for obtaining high conductivity values for the corresponding nanocomposites it can be used on industrial scale for the applications where highly conductive polymer composites with high added value are needed. We have also shown that for obtaining highly conductive graphene/PEDOT:PSS/PS nanocomposites only PEDOT:PSS exhibiting an intrinsic conductivity comparable to or higher than that of graphene should be used, since we have some preliminary indications that both in the aqueous graphene/PEDOT:PSS dispersions as well as in the final polymer nanocomposite the PEDOT:PSS at least partially covers the graphene sheets and hence largely determines the conductivity of the corresponding system. Thus, using a relatively low conductive PEDOT:PSS for dispersing graphene in water can limit the conductivity of the graphene sheets-based network in the corresponding nanocomposites.

We have demonstrated that when utilizing a conductive polymer as a surfactant, *i.e.* PEDOT:PSS latex, for dispersing a nanofiller (for example carbon nanotubes) in water for the subsequent preparation of the polymer nanocomposites, a conductive filler can be replaced by a non-conductive one. We replaced CNTs with an aspect ratio of around 60 by cellulose whiskers with a similar aspect ratio of ca. 60. It was shown that even at quite low loadings of the conductive polymer, even quite far below the percolation threshold of the conductive polymer itself, it plays the main role in determining the overall conductivity of the corresponding composites whereas the role of the CNTs seems to be that of forming a scaffold or template for the conductive surfactant adsorbing thereon, meaning that the CNTs could in principle be replaced by the cheap and most abundant natural material, *i.e.* cellulose. By replacing the CNTs in the composites by cellulose nanowhiskers and using the four-step latex technology utilizing conductive surfactant, PEDOT:PSS, we developed cellulose-based PS composites with an extremely low percolation threshold of the conductive polymer. The percolation threshold of 2.2 wt % of PEDOT:PSS for PEDOT:PSS/PS composites was lowered to 0.4 wt % by adding 0.8 wt % of the cheap cellulose whiskers. This exciting concept brings commercialization of this type of hybrid nanocomposites significantly closer to reality. It has been shown that cellulose nanofibres have great potential as reinforcements in nanocomposites.^[10] They also, due to their size and the ability to chemically modify their surface, have great potential for a wide variety of

applications: foams, adhesives, hierarchical materials and electronic display materials.^[10] The advantages of the cellulose nanowhiskers over CNTs are apparent: 1) cellulose is cheap and available throughout the world; 2) non-crystalline nanocomposites based on this material exhibit high transparency (Hiroyuki Yano and colleagues have demonstrated experimentally the advantage of nanoscale reinforcements using cellulose nanofibres).^[11] They obtained transparent composites by reinforcing various types of resins even at fiber contents as high as 70 wt%). By applying cellulose whiskers and conductive polymer, such as PEDOT:PSS for instance, commercially attractive conductive polymer composites with high transparency exhibiting conductivity at very low loadings of conductive polymer can be developed. If the system can be further optimized it cannot be excluded that these hybrid nanocomposites could play a future role as topcoats on bumpers, fenders and hoods in the automotive industry for on-line electrostatic painting.

For preparing commercially more attractive cellulose/PEDOT:PSS/PS nanocomposites we tried to replace the industrially expensive freeze-drying step for the removal of water by a heating process. Despite the fact that both processes resulted in quite similar percolation thresholds the composites prepared by the method utilizing the heating step exhibited lower conductivity values just above the percolation threshold in comparison to the freeze-dried samples. This might be due to some phase separation occurring during water removal by the heating process. However, the heating step for the water removal can probably be optimized by increasing the surface area for evaporation of water and the speed of the evaporation. On larger scale a flash step could be envisaged, which is already in use for the work-up of some engineering plastics like Nylon 4.6.

7.2. Summarizing and outlook

The work presented in this thesis describes a possible route for the preparation of graphene-based polymer nanocomposites utilizing graphene obtained via different methods on the one hand and cellulose-based polymer nanocomposites on the other hand. The advantages and disadvantages for using each type of graphene are shown.

For composites based on graphene prepared from graphite via the oxidation/chemical reduction process it would be worth to investigate the use of different surfactants which can be applied for graphene stabilization during the reduction of graphene oxide in order to lower the ratio surfactant/graphene oxide (we found that for PSS the weight ratio surfactant/graphene can be lowered from 10:1 to 4:1, which is still high). The lowering of the surfactant/graphene oxide ratio

could possibly avoid a filtration step for the removal of the excess of surfactant, which has to be used when applying PSS as a surfactant.

For the composites based on graphene produced by thermal reduction of graphite oxide and subsequent tip-sonication in water in the presence of surfactants, bath sonication for dispersing the graphene can be tried. It can result in a bigger size of graphene flakes and accordingly in higher length/thickness ratios, which is favorable for lowering the percolation threshold. In comparison to the graphite liquid phase exfoliation method for graphene preparation in this case bath sonication should not take that long, since the starting point (flakes consisting of merely a few layers of graphene) is much closer to a single graphene sheet, than in the mentioned method. Such a change in processing step can significantly affect the percolation threshold.

In this work we prepared all the nanocomposites using polystyrene as a matrix material. When preparing nanocomposites based on *in-situ* reduced graphene oxide changing the matrix material for one which can stand higher temperatures can significantly improve the ultimate conductivity, since processing at higher temperatures can result in a higher degree of reduction of graphene oxide and hence in higher conductivity values of the corresponding nanocomposites.

Cellulose nanowhiskers-based polymer nanocomposites utilizing PEDOT:PSS as a conductive filler were described in this thesis and were produced by the latex technology, the two final steps of which are the freeze-drying and the compression molding steps. It can be interesting to prepare these nanocomposites by replacing these two steps by a spin-coating process. Such a replacement can result in thin transparent conductive films with thicknesses in the order of magnitude of 30-50 nm, whereas the compression molding step gives films with a thickness of several hundreds of microns. Finally it can be worthwhile to try to replace our 'standard' freeze-drying step of the latex technology for water removal, which is quite expensive for an industrial application in terms of operating costs and energy consumption, by a simple water evaporation at elevated temperature.

7.3. References

- [1] J. C. Huang, *Advances in Polymer Technology* **2002**, *21*, 299.
- [2] M. Moniruzzaman, K. I. Winey, *Macromolecules* **2006**, *39*, 5194.
- [3] H. Kim, A. A. Abdala, C. W. Macosko, *Macromolecules* **2010**, *43*, 6515.
- [4] M. Lotya, Y. Hernandez, P. J. King, R. J. Smith, V. Nicolosi, L. S. Karlsson, F. M. Blighe, S. De, Z. M. Wang, I. T. McGovern, G. S. Duesberg, J. N. Coleman, *Journal of the American Chemical Society* **2009**, *131*, 3611.
- [5] M. Lotya, P. J. King, U. Khan, S. De, J. N. Coleman, *Acs Nano* **2010**, *4*, 3155.

- [6] W. S. Hummers, R. E. Offeman, *Journal of the American Chemical Society* **1958**, *80*, 1339.
- [7] M. J. McAllister, J. L. Li, D. H. Adamson, H. C. Schniepp, A. A. Abdala, J. Liu, M. Herrera-Alonso, D. L. Milius, R. Car, R. K. Prud'homme, I. A. Aksay, *Chemistry of Materials* **2007**, *19*, 4396.
- [8] S. Stankovich, R. D. Piner, X. Q. Chen, N. Q. Wu, S. T. Nguyen, R. S. Ruoff, *Journal of Materials Chemistry* **2006**, *16*, 155.
- [9] E. Tkalya, M. Ghislandi, A. Alekseev, C. Koning, J. Loos, *Journal of Materials Chemistry* **2010**, *20*, 3035.
- [10] S. J. Eichhorn, A. Dufresne, M. Aranguren, N. E. Marcovich, J. R. Capadona, S. J. Rowan, C. Weder, W. Thielemans, M. Roman, S. Renneckar, W. Gindl, S. Veigel, J. Keckes, H. Yano, K. Abe, M. Nogi, A. N. Nakagaito, A. Mangalam, J. Simonsen, A. S. Benight, A. Bismarck, L. A. Berglund, T. Peijs, *Journal of Materials Science* **2010**, *45*, 1.
- [11] H. Yano, J. Sugiyama, A. N. Nakagaito, M. Nogi, T. Matsuura, M. Hikita, K. Handa, *Advanced Materials* **2005**, *17*, 153.

Summary

Graphene-based polymer nanocomposites

The latex-based concept to introduce graphene platelets into polymers has been shown to be highly versatile and to produce conductive nanocomposites with different loadings of graphene depending on the method of graphene preparation. For the preparation of conductive polymer nanocomposites via latex technology we utilized graphene produced from graphite via three different methods, namely 1) via oxidation of graphite and subsequent chemical reduction of graphite oxide (GO) in the presence of a surfactant (poly(sodium styrene sulfonate) (PSS)), 2) via oxidation of graphite and subsequent thermal reduction of GO and 3) via liquid phase exfoliation of graphite by bath sonication in the presence of a surfactant (sodium cholate (SC)). The three used methods for graphene preparation provide graphene of different quality, which was proven by Raman spectroscopy. A Raman study of graphene prepared by both chemical and thermal reduction of GO reveals big structural defects which are attributed to the presence of sp^3 carbons in the carbon basal plane and different residual functionalities such as carboxylic acid groups, epoxides, or ketones.

Preparation of polystyrene (PS) nanocomposites based on graphene prepared via oxidation of graphite with subsequent exfoliation and chemical reduction of graphite oxide is described in Chapter 2. Aqueous dispersions of graphene were obtained via oxidation and exfoliation of graphite and subsequent reduction with the aid of hydrazine in the presence of PSS which acted as a surfactant. Different amounts of aqueous graphene dispersions were then mixed with the PS latex and composites were prepared by freeze-drying and subsequent compression molding. The percolation threshold for conduction was found to be about 0.9 wt % of graphene in the composites, and a maximum conductivity of about 15 S/m could be achieved for 1.6-2 wt% nanofiller.

Nanocomposites via in-situ reduction of graphene oxide were also prepared. The reduction of graphene oxide occurred during the compression molding step. This way of preparation allows us to eliminate the time consuming chemical reduction step and gives a homogeneous distribution of graphene platelets in the composite film due to the ability of graphene oxide to be readily exfoliated and dispersed in water because of its hydrophilic nature. Due to incomplete reduction the ultimate conductivity of the composites is 0.1 S/m although the percolation threshold is low, namely 0.6 wt%.

The main strategies developed during the recent years for incorporation of carbon nanotubes (CNTs) and graphene into a polymer matrix based on the use of surfactants for improving the nanofillers dispersion are covered in Chapter 3. The main focus is given to water-based systems.

Chapter 4 studies the effect of the dispersion state of graphene as a factor influencing the electrical percolation threshold of graphene/polystyrene nanocomposites. Graphene used in this study was obtained by two different methods: thermal treatment of graphite oxide and liquid-phase exfoliation of graphite. It was shown that graphene/PS nanocomposites prepared from a PS latex and aqueous graphene dispersions with relatively low stability and relatively low degrees of exfoliation, exhibit a lower percolation threshold than the composites based on dispersions with a larger degree of graphene exfoliation and a higher dispersion stability. This trend is observed despite the fact that the dispersion exhibiting the highest stability and degree of graphene exfoliation is based on graphene produced by the liquid phase exfoliation method, which gives graphene of higher quality than the material produced by thermal reduction of graphite oxide since it contains a lot of defects due to the presence of different functional groups on its surface.

In order to make well performing conductive nanocomposites it is crucial to optimize each step of the latex-based process. In particular this is applicable to the first step, which is the exfoliation and dispersion of a nanofiller in water. In Chapter 5 optimum conditions for the exfoliation and dispersion of graphene obtained by thermal reduction of graphite oxide at a concentration of 1 mg/ml using conventional surfactants such as sodium dodecylbenzene sulfonate (SDBS), SC, PSS and Tween-80 are demonstrated. The obtained dispersions were used for the preparation of nanocomposites. The composites prepared from dispersions stabilized with ionic surfactants all exhibit the same percolation threshold and the same final conductivity values, which means that graphene possesses the same degree of exfoliation in all the systems and the dispersion conditions had been optimized for the used surfactants. When preparing nanocomposites using Tween-80-stabilized graphene dispersions, higher percolation thresholds and lower conductivities in comparison with the systems utilizing SDBS, SC and PSS were observed. This is probably due to a large amount of the bulky surfactant present on the graphene surface which stabilizes the dispersion by a steric effect, but which acts as a kind of insulating layer between the graphene platelets in the final composite.

It was demonstrated that the introduction of a highly conductive polymeric surfactant (poly(3,4-ethylenedioxythiophene):poly(styrene sulfonate) (PEDOT:PSS)) in the water dispersion step and finally into graphene/PS nanocomposites can significantly lower the percolation threshold and increase the ultimate conductivity. By using Scanning Electron Microscopy (SEM) and replacing a

highly conductive PEDOT:PSS by a low conductive one, an idea of the possible morphology of the graphene/PEDOT:PSS system was obtained. It was shown that the use of a low conductive PEDOT:PSS can decrease the percolation threshold but by breaking the contacts between the highest conductive particles in this system, namely the graphene platelets, can also decrease the conductivity values above the percolation threshold due to the “shielding” of the graphene. It looks as if graphene is covered with this conductive polymer. The higher the coverage is, the lower the contribution of graphene to the conductivity of the composite becomes.

In Chapter 6, the cooperative nature of the two conductive fillers in multiwalled carbon nanotubes (MWCNTs)/PEDOT:PSS/PS composites with the focus on the contribution of the CNTs to the overall composite conductivity was investigated. For that the CNTs were replaced by non-conductive fillers with an almost identical aspect ratio, namely cellulose whiskers, and the two systems MWCNTs/PEDOT:PSS/PS and cellulose/PEDOT:PSS/PS, were compared. It was demonstrated that even at relatively low loadings of the conductive polymer the polymer plays the main role in the determining the overall conductivity of the corresponding composites. The role of the CNTs, on the other hand, seems to be that of forming a percolating template on which the conductive PEDOT:PSS adsorbs, which means that the CNTs can in fact be replaced in this case by the cheap and most abundant natural material, *i.e.* cellulose. By replacing the CNTs in the composites by cellulose nanowhiskers using the four-step latex technology utilizing conductive surfactant, PEDOT:PSS, cellulose-based PS composites with an extremely low percolation threshold of the conductive polymer were developed. The percolation threshold of 2.2 wt % of PEDOT:PSS for PEDOT:PSS/PS composites was lowered to 0.4 wt % by adding 0.8 wt % of the cheap cellulose whiskers.

Acknowledgements

My staying at SPC has come to an end and now it's time to say good-bye. During past four years spent in Eindhoven I met many wonderful people. For their help in completion of my thesis and in daily life I want to thank these people.

Firstly I want to thank my promoter Prof. Cor Koning for giving me the chance to do my PhD here. Cor, thank you very much for your efforts, patience, always positive attitude and great support. An atmosphere during our project meetings was fantastic, we discussed not just work but also some football and life in general. I really enjoyed a lot working with you!

The reading committee consisting of Prof. Paul van der Schoot, Prof. Rene Janssen, Prof. Ton Peijs and Prof. Dick Broer are thanked for their contribution to the final acceptance of the thesis and being my core defense committee. Prof. Alex van Herk and Prof. Bert de With are thanked for joining the extended defense committee. The Dutch Polymer Institute is thanked for the financial support of this work.

I would like to thank people without whom many results presented in the thesis wouldn't have been achieved. Marcos, thanks a lot for your daily help in this project! We were discussing everything, writing reports together, you were measuring my samples with different techniques and so on and so on... It was not just a serious work but also a lot of fun. Despite the fact that our countries are very far from each other and one could expect a big difference in culture, in reality it wasn't the case and we could understand each other perfectly. I enjoyed working with you a lot! Ronald and Paul, thank you very much for your cooperation, many fruitful discussions and your theoretical contribution. You broadened my view on many things in this project. Paul, you were bringing not just bright ideas and explanations but also a lot of humor to our "big project meetings". Sasha A., thank you very much for measuring C-AFM and good advices. Rinske Knoop and Joachim Loos are thanked for many samples analyzed with SEM and TEM. Joachim, I'd like to thank you also for your cooperation and contribution to this work during first two years of my PhD. I would like to thank my student Stefan van Berkel for the fantastic work he did within this project, which resulted in a patent application.

Many and many thanks go to all my nice colleagues in SPC! My special thanks go to MC, who was teaching me everything about nanocomposites when I just started my PhD. MC, thank you very much for that and also for your help with other different things, which helped me to adapt to this project and

also to the new country. Many thanks go to my officemates! Inge, you were helping me and our office in general with everything. I don't remember any problem/question where you couldn't help or didn't know something. Without you our office wouldn't survive. You were translating all the letters I was receiving from different organizations here and explaining what I had to do to solve different problems. Thank you very much for everything! Hectorinho, I want to thank you for many good advices you gave me during my stay here. And thank you for a very nice atmosphere in the office and a lot of fun you were bringing to us. Wouter, thank you very much for your help with many different things during my first year in the Netherlands, without you my first months here would be much more difficult. Erik, I enjoyed our football discussions and many many other discussions we had. Thank to us and Hector now Inge knows much more about football than she knew before. Gijs, you also were helping me a lot giving good advices and explaining what and how works here. By making a lot of jokes and strange sounds together with Inge you contributed to the fantastic atmosphere we had in sto 1.32. Julien and Shaneesh, special thanks to you for being very nice officemates and your help when I needed something. Pleunie and Caroline, thank you for arranging everything that was needed. Hans, Rob and John, thank you for discussions and signing my safety forms without any questions. Lots of thanks to my other very nice colleagues: Lidia (amazingly kind and helpful girl; also spoke a little bit of Russian to me), Martin O (always has time when someone has a question), Roxy (always had time for me), Raf (could answer any question from any field of chemistry; explained different aspects of rugby to me), Maurice (I enjoyed watching FC Eindhoven with you man), Pooja (was making the UV machine measure for me when it didn't want to measure anything), Gemma (our speaking proper English girl), Lyazzat, Bart, Seda, Gozde, Bahar, Dogan (your Russian is very good), Sandra, Monique, Timo, Fabian, Ece, Dirk, Jey, Hemant, Jerome, Camille, Joris, Miloud, Rutger, Syed, Martin F (thanks for making me clean my lab table, otherwise it would become a mess; sometimes it became still.. but better than could be), Mark B, Mark P and many many others.... Donglin, I want to specially thank you. It's difficult to overestimate your help, especially during last couple of months of my PhD. We also enjoyed a lot of drinks together at our cluster meetings. Some things like "beer for everybody", "rum for the lady", "I'm not gonna be a gentleman for nothing" I will never forget. Thank you!

My dear Spartak SPC mates, it was fantastic to play with you, I was happy to be part of such a team! Marcos, Donglin, Maurice, Hector, Niels, Sjoerd, Mark B, Joris, Ard, Joost, Tom, Benjamin, Bas, Mark P, Miloud, thank you all!

Acknowledgements

My SMG friends... Marcos, Sasha K, Sasha A, Isabelle, Vlado, Ana, Camille, Mark B, Baris, Delei, Benjamin (not SMG but...) we had great drinks and a lot of fun. I'll never forget this.

My Russian (Seva, Vika and Anya) and slightly Russian (Thijs, Niek) friends I met in Eindhoven, thank you for your help in daily life, advices and great drinks.

И самое главное. Моя особая, самая большая благодарность, моей дорогой семье- моим родителям, сестренке, Ане, моим дедушкам и бабушкам, тем, кто со мной, и тем, кто ушел. Вы, каждый по-своему, сделали это все возможным, и каждому из вас принадлежит частичка этой работы. Дорогие родители, вы всегда поддерживали меня во всех аспектах жизни и особенно много в годы моего пребывания в Нидерландах. Спасибо вам большое за все! Анечка, твой вклад в эту работу так же трудно переоценить, особенно в последние полгода. Ты оградила меня от всего, дав мне возможность полностью сконцентрироваться на работе. Спасибо! Дорогие бабушки и дедушки, каждый из вас многому научил меня. Спасибо!

List of Publications

Evgeniy Tkalya, Marcos Ghislandi, Ronald Otten, Mustafa Lotya, Alexander Alekseev, Paul van der Schoot, Jonathan Coleman, Bert de With, Cor Koning. “Experimental and theoretical study of the influence of dispersion state of graphene on the percolation threshold of conductive graphene/polystyrene nanocomposites”. *To be submitted.*

A. Alkseev, D. Chen, E. E. Tkalya, M. G. Ghislandi, Yu. Syurik, O. Ageev, J. Loos, G. De With, “Local organization of graphene network inside graphene/polymer composites”. *Adv. Funct. Mater.* Accepted.

Evgeniy Tkalya, Cor Koning, “Process for the preparation of conductive polymer composition”, patent of Dutch Polymer Institute. *Submitted.*

Evgeniy Tkalya, Stefan van Berkel, Cor Koning. “Polymer composition”, patent of Dutch Polymer Institute, application number EP10005170.5, international application number PCT/EP2011/002444.

Evgeniy Tkalya, Cor Koning, “Conductive polymer composition”, patent of Dutch Polymer Institute, EP2216358, international number WO2010/086176.

Evgeniy Tkalya, Marcos Ghislandi, Alexander Alkseev, Cor Koning, Joachim Loos, “Latex-based concept for the preparation of graphene-based polymer nanocomposites”. *J. Mater. Chem.*, 2010, 20, 3035–3039.

Curriculum Vitae

Evgeniy Tkalya was born on the 24th of February 1982 in Podolsk, Moscow Region, Russia. After finishing his high school education in Troitsk (Moscow Region) in 1999 he started his bachelor at the Lomonosov Moscow State Academy of Fine Chemical Technology. In 2003 he graduated with a B.Sc in Chemical Technology and Biotechnology. Subsequently he started his master studies in Chemical Technology and Biotechnology at the Department of Chemistry and Technology of High-molecular Compounds of Lomonosov Moscow State Academy of Fine Chemical Technology. In September 2004 he started his graduation project with title "Polymer microspheres as bioligands carriers for the diagnostic test-systems" under supervision of Prof. I. A. Grickova. He graduated in July 2005. From August 2005 till January 2007 he worked at the Research Institute of Physicochemical Medicine (Ministry of Public Health of Russian Federation, Moscow, Russia) on polymer synthesis for phagocytosis study. From February 2007 till September 2007 he worked at the University of Basel on synthesis of sugar-based block-copolymers for drug delivery. In November 2007 he was employed as a PhD-student at the Eindhoven University of Technology in the polymer chemistry group under guidance of Prof. dr. C. E. Koning.